

Galaxies and Black Holes in the First Billion Years

Richard S Ellis^a

^aUniversity College London, Department of Physics & Astronomy, Gower Street, London WC1E 6BT, UK

© 20xx Elsevier Ltd. All rights reserved.

Abstract:

I present written notes from three lectures given at the 54th Saas-Fee Advanced Course of the Swiss Society of Astrophysics and Astronomy in January 2025 entitled *Galaxies and Black Holes in the First Billion Years as seen by the JWST*. I focused my lectures on progress in studies of cosmic reionisation, the properties of galaxies in the reionisation era, topics related to the redshift frontier and the search for Population III stars. The lectures were given to graduate students in astrophysics and cover both pedagogical material as well as observational results from the first two and half years of JWST science operations. The pace of discovery with JWST is, of course, rapid and so my lectures discuss long-term goals, the analysis methods and their assumptions and limitations in the hope that the underlying material will retain some value in the near future. In this written version, the visual material is that presented at Saas-Fee but I have provided updates on progress from the literature up to August 2025. The material is aimed at early career researchers and should not be considered as a scholarly review of the entire JWST literature on high redshift galaxies.

Preface

It was a pleasure to give these lectures on the progress being made by the James Webb Space Telescope (JWST) in understanding the formation and early evolution of galaxies at the beautiful location of Saas-Fee in the Swiss Alps in January 2025. The timing of the meeting was perfect. Two and a half years after science operations began, Early Release Observations, Cycles 1 and 2 General Observer and most of the Guaranteed Time programmes had been completed. The JWST archives were full of rich imaging and spectroscopic datasets and there were over 500 scientific articles to digest. The participants were at the beginning of their graduate careers and full of enthusiasm!

The pace of discovery with JWST is, of course, rapid and I was mindful how quickly my lectures and their written record might become out of date. Therefore, in addition to summarising the state-of-the-art in our understanding of the JWST observations, I decided to focus also on the long-term goals, the analysis methods, their assumptions and limitations, hoping that the underlying material will retain some value in a few years' time. However, there is no way to avoid the fact that much of the material presented herein has a "time stamp" of January 2025. In this write up, I decided to keep the visual material I presented at Saas-Fee but have provided brief updates and references in the text of relevant articles up to August 2025.

The Saas-Fee series has provided an invaluable record of the progress in astrophysics for over 50 years. It was amusing to revisit my earlier lectures on the high redshift universe given at Saas-Fee in 2006! I'm hoping the present notes will continue this tradition. They are intended primarily for early career researchers and should not be considered as some form of scholarly review of the entire JWST literature.

I thank the organisers, Pascal Oesch, Romain Meyer and Michaela Hirschmann for inviting me once again to Saas-Fee. Their support, guidance and hospitality has been wonderful. I also thank my many former students and postdocs who have kept me on the straight and narrow in this topic over many years. I particularly thank Yuichi Harikane, Koki Kakiichi, Romain Meyer, Kimihiko Nakajima, Tucker Jones, Guido Roberts-Borsani, Aayush Saxena, Dan Stark and Mengtao Tang who answered many of my questions on the latest results.

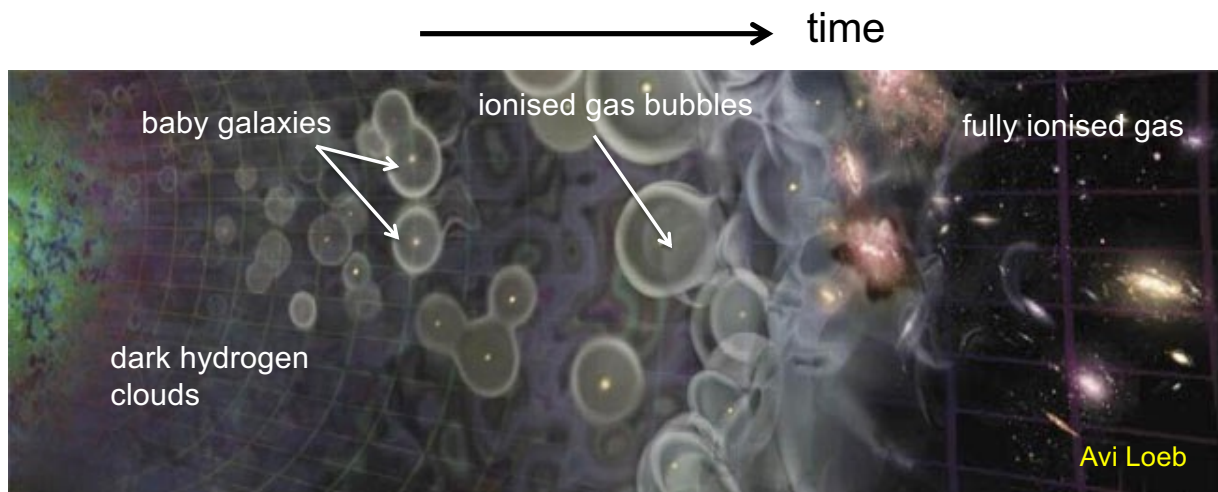
Finally, and above all, it was inspiring to meet such an enthusiastic group of students at Saas-Fee. I wish them all the very best in their careers. We can certainly agree that, with JWST, the future is very bright!

Lecture 1: Cosmic Reionisation

1 Introduction

It is an exciting time for those of us studying early galaxies given the unprecedented opportunities now possible using NASA's James Webb Space Telescope (JWST). In these lectures, I will attempt to digest the astonishing progress made in the space of only two and half years since science operations began in July 2022. Although it is inevitable that many of the details discussed will soon become outdated, I hope by covering both the progress made and the challenges remaining, my lecture notes will still be of value, particularly to the graduate students attending this Saas-Fee course who are very fortunate to be witnessing this unique period in the history of extragalactic astronomy.

In my first lecture I will cover the topic of cosmic reionisation: the period during which hydrogen in the intergalactic medium (IGM) transitioned from a neutral to ionised state. The cartoon in Figure 1 shows a possible timeline. At recombination, corresponding to $z=1100$ some 370,000 years after the Big Bang, the primordial plasma has cooled so that the hydrogen atom formed for the first time. At this point, free electrons were no longer available to scatter the thermal glow and we see this moment as the last scattering surface in the cosmic microwave background. Dark hydrogen clouds coalesced under gravity aided by non-baryonic dark matter halos which fractionated from the cosmic expansion at an earlier era. The clouds became Jeans unstable and collapsed raising the temperature sufficient to ignite nuclear burning from the first stars, possibly by $z \approx 15-30$ some 150-200 Myr later - an epoch often romantically referred to as 'cosmic dawn.' Devoid of heavy elements at this stage, these stars are likely to be more massive than those in the present universe due to the absence of metal cooling at the time of collapse. Additionally there will be no metal line blanketing in their stellar atmospheres. For both reasons these early stars emitted copious amounts of ultraviolet photons which created local ionised gas bubbles. As time progressed the bubbles expanded and became more numerous, eventually overlapping until the entire IGM was fully ionised by $z \approx 5.3$, just over 1 Gyr after the Big Bang. Of course the cartoon is a possible scenario. It assumes cosmic reionisation was driven mostly by star-forming galaxies. But it does emphasise the importance of this reionisation era by positing an association with the birth of galaxies and the commencement of nuclear processing in stellar nuclei which, of course, eventually led to our own existence.



$t = 3.7 \cdot 10^5$ yr, $z = 1100$:	Recombination & formation of H atom
$t \sim 200$ Myr, $z \sim 20-30$:	Hydrogen clouds drawn to DM & collapse
$t \sim 250$ Myr, $z \sim 15-20$:	Nuclear ignition – cosmic dawn
$t \sim 250$ Myr – 1 Gyr $15 < z < 5.3$:	UV photons from galaxies (+ AGN?) reionise IGM

Fig. 1 Illustrative timeline of the first billion years of cosmic history. From left to right: the thermal glow from the Big Bang and last scattering surface when the hydrogen atom first formed (370,000 yrs, $z=1100$). Dark hydrogen clouds clump under gravity aided by dark matter becoming Jean unstable and collapse. The gas temperature rises igniting nuclear fusion and the universe is bathed in starlight (150-200 Myr, $z \approx 20-30$). Hot massive stars, free from metals, emit copious amounts of UV photons that reionise the local surroundings. Such ionised bubbles expand and become more numerous, eventually overlapping to fully ionise the intergalactic medium (1.1 Gyr, $z \approx 5.3$) (Courtesy: Avi Loeb).

The big questions we aim to address in studying this era with JWST include: when did reionisation begin and end; which sources were responsible and can we recognise a primordial stellar system first emerging from darkness. The last topic is reserved for Lecture 3.

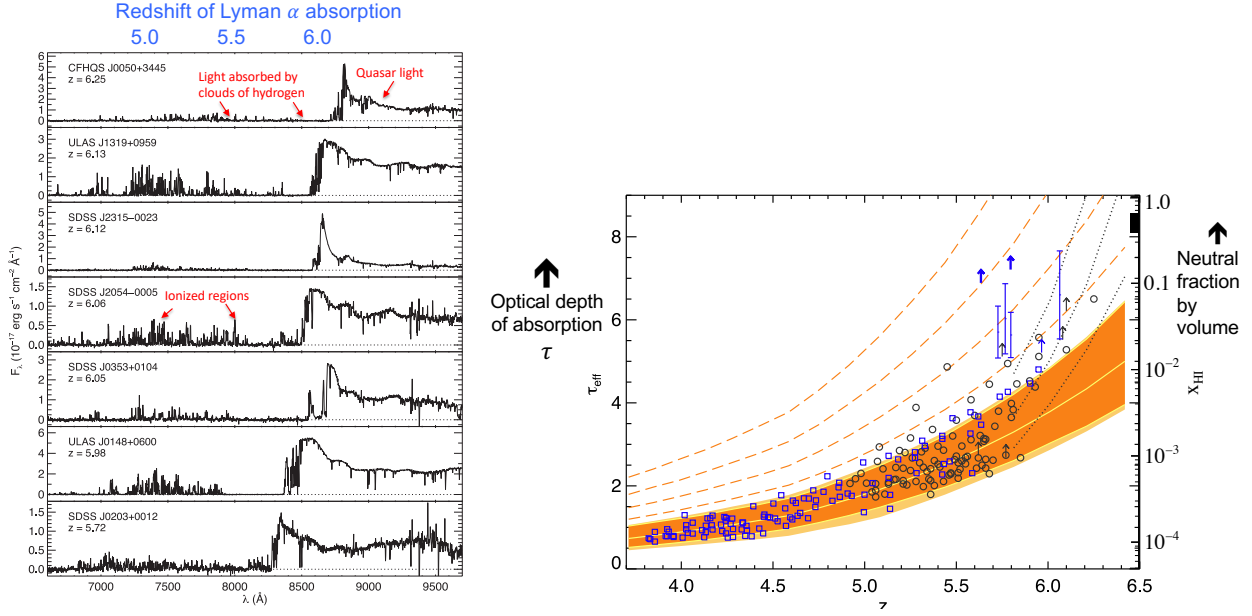


Fig. 2 Quasar absorption spectroscopy determines the end of cosmic reionisation: (Left) Selection of spectra of $z \geq 6$ quasars. The depth of absorption shortward of Lyman α emission line traces the line of sight, redshift-dependent, opacity of neutral hydrogen (HI). Occasional transmission spikes indicate localised ionised regions. (Right) The fractional volume density of neutral hydrogen x_{HI} derived from the optical depth τ of Lyman α absorption for a large sample of quasar spectra. The noticeable upturn at redshifts $z > 5.5$ corresponds to entering the partially neutral reionisation era. The scatter at a given redshift is an important indication of the patchiness of the reionisation process (Bosman et al., 2018)

2 Quasar Absorption and the End of Reionisation

Let's begin with some important astronomical history. Astronomers have known the intergalactic medium is fully ionised today since 1965. When luminous quasars were discovered in the early 1960s, redshift records were rapidly broken. By 1965, using the Palomar telescope, Martin Schmidt was able to secure a spectrum of the radio source 3C9 at $z=2.0$ providing, for the first time, a glimpse at the rest-frame ultraviolet continuum and the prominent Lyman α emission line at 1216 \AA . The absence of any foreground absorption blueward of this emission was interpreted by Gunn and Peterson (1965) as evidence for a low value for the density of neutral hydrogen. They speculated that at some point in earlier cosmic history the IGM had been fully ionised. It wasn't until 2001 that astronomers secured their first indication of when this earlier period of cosmic reionisation occurred. The Sloan Digital Sky Survey (SDSS) was used to locate the first meaningful sample of quasars at a redshift $z \approx 6$ (Becker et al 2001). Contrary to the situation at $z \approx 2$, the spectra showed significant absorption blueward of Lyman α emission indicative of an increased opacity from neutral hydrogen. This was an early indication that we had reached a look-back time sufficient to detect neutral gas in the IGM and could begin probing the so-called reionisation era.

Absorption line spectroscopy has given us the most precise indication of when reionisation ended. The left panel of Figure 2 shows some recent spectra from a sample of over 70 $z \approx 6$ quasars. We can quantify the Lyman α opacity via an optical depth τ using the observed continuum flux $I(\lambda)$ viz.

$$I(\lambda) = I_0 \exp(-\tau) \quad (1)$$

where the unattenuated continuum flux I_0 is determined from an average rest-frame quasar spectrum at lower redshift when there is minimal hydrogen absorption. For low column densities of neutral hydrogen n_{HI} , the opacity is related via

$$\tau = \frac{\pi e^2}{m_e c} f_{\alpha} \lambda_{\alpha} H(z)^{-1} n_{\text{HI}} \quad (2)$$

where f is the oscillator strength of Lyman α and $H(z)$ is the Hubble constant. Each quasar spectrum enables a measurement of $\tau(z)$ over a range in redshift, corresponding to the fluctuating signal in the Lyman α forest. Measures along different quasar sightlines then trace the patchiness of the signal. To trace the reionisation history, it is usual to quote the neutral gas fraction by volume $x_{\text{HI}} = n_{\text{HI}}/n_{\text{H}}$. The right panel of Figure 2 shows a recent compilation of opacities and neutral fractions from Bosman et al. (2018) where the scatter among different quasars at a given absorption redshift is evident. The most important feature, however, is a distinct upturn in the opacity at $z > 5.5$ consistent with entering the partially neutral era.

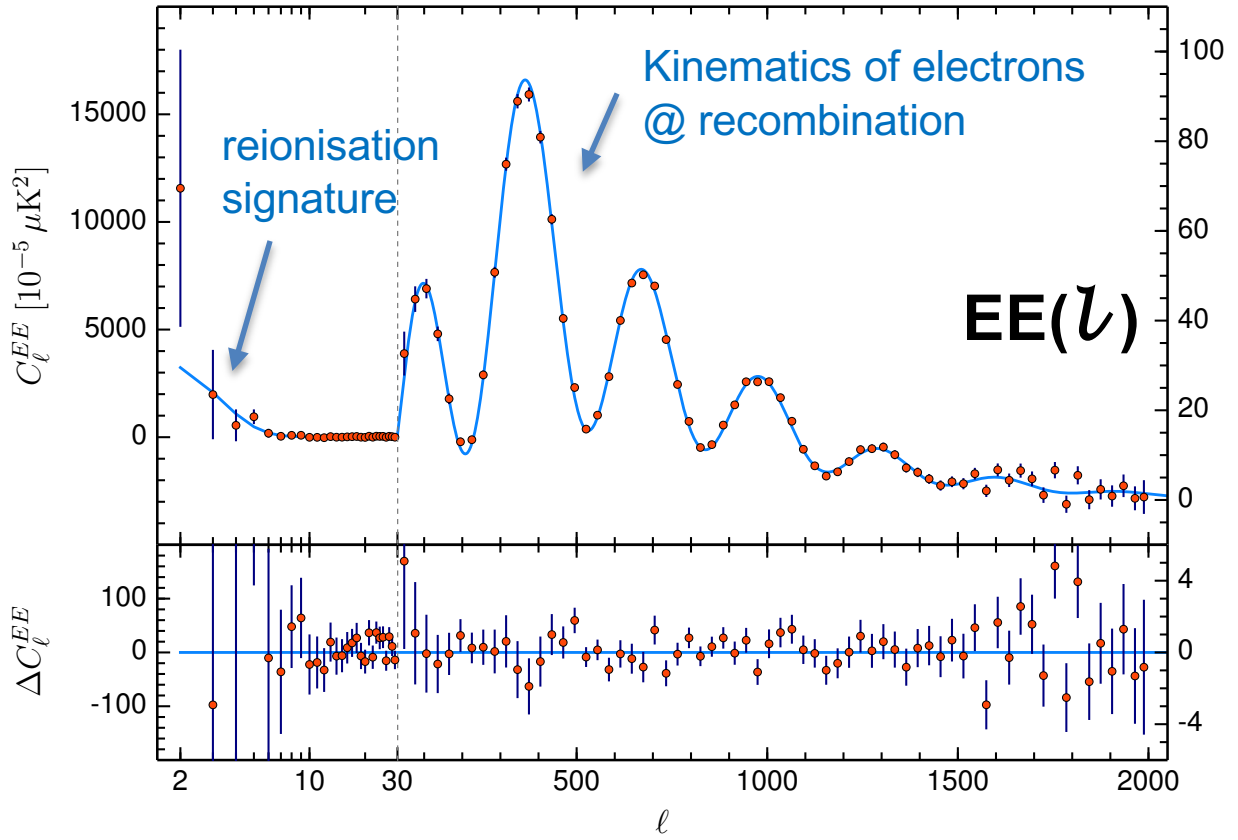


Fig. 3 Angular power spectrum of the polarisation or E-mode of the cosmic microwave background. The signal arises from Thomson (electron) scattering along the partial and fully-ionised intergalactic medium down to the present epoch. The optical depth τ is determined primarily from the upturn at large angular scales or low multipoles (Planck Collaboration et al., 2020).

Such spectroscopic analyses have been very productive in charting the end of reionisation because, over the redshift range $5 < z < 6$, they provide direct measures of the neutral fraction x_{HI} . However, the Lyman α opacity method cannot easily be applied at higher redshift since only a modest neutral fraction ($x_{HI} \sim 10^{-3}$) saturates the absorption and eliminates any measured flux. Other methods, such as exploiting the effect of damped absorption on the Lyman α emission profile, are discussed in the reviews by Fan et al. (2006) and Fan et al. (2023). Regardless of the methods used, a basic limitation however is the scarcity of quasars beyond a redshift $z \approx 7$.

Recently, through the remarkable efficiency of JWST’s spectrographs, it has become observationally feasible to study the Lyman α forest at $z \approx 5-6$ in the spectra of *background galaxies* (Meyer et al., 2025; Umeda et al., 2025). This important development will enable many more IGM sightlines to be explored, and to higher redshift given the increased statistics will also enable studies of the Lyman β absorption which saturates earlier in cosmic time than Lyman α .

3 Cosmic Microwave Background Constraints

NASA’s WMAP and ESA’s Planck satellites have provided valuable constraints on the duration and median redshift of reionisation through polarisation measures of the cosmic microwave background (CMB). Readers will be familiar with the angular power spectrum of temperature fluctuations $TT(l)$ where l is the angular multipole moment at the surface of last scattering. This anisotropic radiation field suffers electron (Thomson) scattering by the integrated column of electrons along the line of sight starting from the commencement of reionisation down to the present day. The polarisation signal is commonly referred to as the E- or gradient mode and its angular power spectrum is $EE(l)$.

Reionisation also damps $TT(l)$ by an amount that is degenerate with its intrinsic amplitude. Fortunately this degeneracy can be broken since reionisation also produces an unique $EE(l)$ signal on large angular scales (>30 arcmin, $l < 200$, Figure 3). In practice cosmologists use the combined TT, EE and TE correlations to constrain the *optical depth of Thomson scattering* τ which was first detected by WMAP

and whose value was considerably refined by Planck. Formally

$$\tau = \langle n_H \rangle c \sigma_T \int_0^{\infty} x_e(z) (1+z)^2 H(z)^{-1} dz \quad (3)$$

so a larger τ implies an earlier period of reionisation. As an integrated measure τ constrains the median redshift z_{mid} and duration of reionisation, but not the redshift-dependent neutral fraction $x_{HI}(z)$.

The first WMAP results in 2003 gave $\tau=0.117 \pm 0.055$ suggesting the start of reionisation might even be beyond reach of JWST. However, these results were significantly affected by Galactic foreground emission and over the next decade both the WMAP mission (2003-2013) and Planck (2009-2013) consistently lowered their estimates of τ . The final Planck value $\tau=0.057 \pm 0.007$ (Planck Collaboration et al., 2020) implies a mid point of the reionisation era at $z_{mid}=7.7 \pm 0.7$, with parametric fits to the EE, TT and TE data that suggest reionisation began at $z \approx 10$ -12 and ended at $z \approx 6$. Subsequent reconsiderations of the polarisation calibrations indicate a modest *increase* to $\tau=0.063 \pm 0.005$ (de Belsunce et al., 2021).

Regarding the beginning of cosmic reionisation and, by possible implication, the timing of “cosmic dawn”, the Planck team were fairly confident “disfavouring any major contribution to the ionised fraction that could form as early as $z > 15$ ”. However, as mentioned, these conclusions were based on parametric models. Subsequent analyses in the context of Λ CDM cosmology taking into account the Planck τ plus secondary anisotropies induced by bulk motions of electrons (the so-called “kinetic Sunyaev-Zeldovich effect”) indicated that earlier ionised regions could exist to redshifts $z \approx 16$ and beyond (Greig and Mesinger, 2017). Although we are unlikely to learn substantially more on the timing of reionisation from CMB studies until the launch of the Japanese Litebird mission (currently ≈ 2032), Planck clearly played a very significant role in demonstrating that the reionisation era can be explored in considerable detail by JWST.

4 Probes of Lyman alpha emission

Returning to constraints relating to the end of reionisation, while recognising the limitations arising from saturation of Lyman α absorption in the spectra of quasars, in the late 2000s ground-based astronomers turned to probes based on *Lyman α emission*. Hot gas in H II regions heated by young stars shines via recombination in Lyman α emission (Dijkstra, 2014). As a resonant transition of hydrogen from $n=2$ to 1, the line is readily scattered by neutral hydrogen. Consequently if a galaxy lies in a neutral IGM, the line intensity will be significantly attenuated. Alternatively, if the galaxies lies in an ionised bubble, Lyman α photons can travel freely without hindrance through the bubble and will be redshifted out of resonance by the cosmic expansion at the bubble surface. A straightforward observational probe is to measure the fraction of galaxies at a given redshift that reveal Lyman α emission, $X_{Ly\alpha}(z)$. As we approach the neutral-dominated era, even though the intrinsic line emission will be present, $X_{Ly\alpha}(z)$ should decrease to zero.

To apply this method, galaxies were selected in photometric redshift slices using the Lyman break technique (Steidel et al., 1995) and the fraction $X_{Ly\alpha}$ showing line emission above a limiting equivalent width determined. Keck (Stark et al., 2011; Schenker et al., 2014) and VLT (Pentericci et al., 2011, 2014) surveys indicated an increase in the fraction from $z \approx 4$ to 6 (due to increased star formation and/or reduced dust attenuation) but revealed a marked decline in a short time interval earlier at $z > 6$. With much uncertainty, the data suggested neutral fractions as high as $X_{HI} \approx 0.4$ at $z=7$ and $X_{HI} \approx 0.65$ at $z=8$.

However, this Lyman α fraction method has several uncertainties. Using ground-based telescopes, the spectroscopic redshift of a galaxy often cannot be determined if there is no Lyman α emission line. Such non-emitting sources could therefore be lower redshift interlopers. Their inclusion in sample would act to incorrectly reduce the inferred value of $X_{Ly\alpha}$ mimicking a more neutral IGM. Moreover if a galaxy has outflowing hot gas its relative velocity will reduce the effect of resonant scattering making Lyman α visible even in a neutral IGM. To allow for such outflows would require a systemic redshift derived from another (usually weaker) emission line usually beyond reach of ground-based telescopes. Finally, early results were based on observations in a few independent sightlines and thus suffered from cosmic variance (see Treu et al. (2013)).

To understand the complexity of deriving the IGM neutral fraction from the visibility of Lyman α emission, the various processes that affect the intensity and profile of Lyman α emission are shown in Figure 4 (Mason et al., 2018). Even in a fully ionised IGM, Lyman α photons can be scattered and attenuated by neutral gas in the interstellar medium (ISM) or circumgalactic medium (CGM) of the host galaxy. Photons propagating directly to the observer may lead to the blueward wing of the intrinsic line being eliminated. Likewise the peak intensity would be reduced in proportion to the combined ISM+CGM+IGM neutral components. In contrast, IGM attenuation will be *diminished* if the Lyman α emission has a significant outflowing velocity Δv relative to the local IGM. Finally, line emission will be affected by any dust present within the galaxy.

Mason et al. (2018) attempted to model these effects by evaluating the change in the equivalent width distribution of Lyman α emission across the transition in the ionisation state between $z \approx 7$ and $z \approx 6$. The authors also adopted an empirical correlation between the UV luminosity of a galaxy and its Lyman α velocity offset Δv , using systemic redshifts from other lines in the spectra of a large sample at $z \approx 2$ -3. Finally, to estimate the ISM neutral hydrogen content n_{HI} , they adopted a correlation with halo mass from simulations. As the state of the art calculation prior to JWST, they applied the model to 68 $z \approx 7$ galaxies of which 12 had ground-based spectroscopic detections of Lyman α , and derived $x_{HI}(z=7) = 0.59 \pm 0.13$ (Figure 4). The result was the most convincing estimate of x_{HI} in the reionisation era using Ly α emission prior to the arrival of JWST.

JWST has greatly improved the prospects of tracing neutral and ionised gas in the reionisation era via its extended infrared wavelength coverage compared to both ground-based telescopes and HST. The most significant feature is spectroscopic access with NIRSpec to other

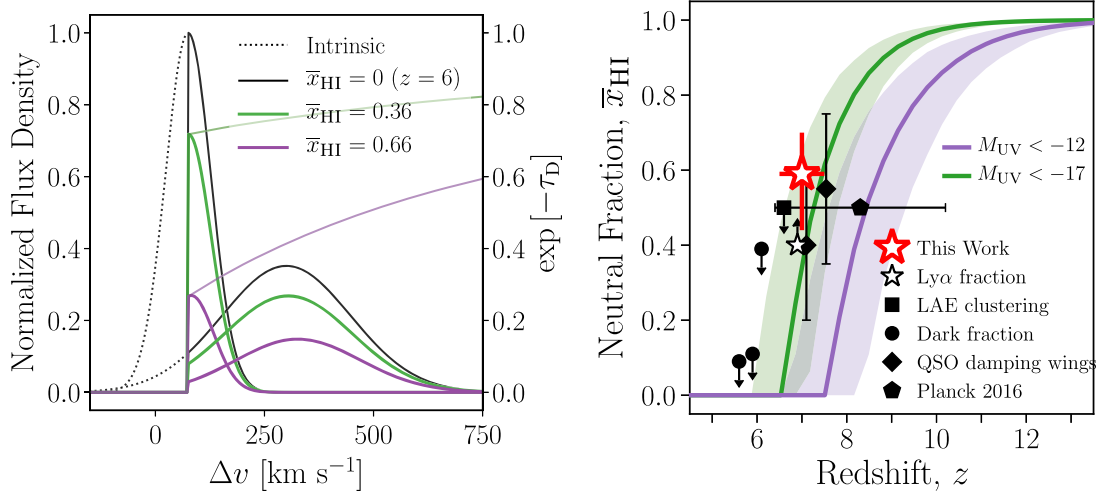


Fig. 4 The complexity of interpreting Lyman α emission. (Left) The intrinsic Gaussian line profile can be affected by HI scattering in any of the ISM, CSM and IGM such that the blueward wing is eliminated and the overall line flux diminished. However, if the emitting gas has a velocity offset Δv , this can reduce the effect and render an otherwise extinguished line observable. (Right) By assuming the correlation between Ly α velocity and luminosity observed at lower redshift, pre-JWST data on 68 $z \approx 7$ galaxies was used to infer a neutral fraction at $z=7$ (red star), well into the neutral era (Mason et al., 2018).

hydrogen lines such as H α (to $z \approx 6.6$) and H β ($z \approx 9.2$). As the Balmer series lines are unaffected by resonant scattering, it becomes possible to estimate the intrinsic Lyman α flux. Assuming Case B recombination for a star-forming region with a typical electron density $n_e = 100 \text{ cm}^{-3}$ and temperature $T_e = 10^4 \text{ K}$, $\text{Ly}\alpha/\text{H}\alpha = 8.2$ thus the escape fraction of Lyman alpha $f_{\text{esc}}(\text{Ly}\alpha) = L(\text{Ly}\alpha)/8.2 \cdot L(\text{H}\alpha)$. Similar calculations can be made at higher redshift using the combination of H β and Lyman α .

The two panels in Figure 5 show an early derivation of the declining escape fraction of Lyman α with redshift from Saxena et al. (2024) (see also Napolitano et al. (2023)). While these trends give much credence to the tentative deductions made prior to JWST, redshift-dependent selection effects may still be present. Clearly only Lyman α emitting galaxies can be used in such analyses and these may lie in regions of lower than average x_{HI} .

The more recent JWST analysis undertaken by Tang et al. (2024) (see a similar analysis by Kageura et al. (2025)) follows the initiative taken by Mason et al discussed earlier by making reference to a comparison sample of Lyman α demographics in the fully-ionised era. The comparison sample utilises data from the JADES, FRESCO and Keck/VLT samples and comprises 79 spectra that reveal both H α and Ly α . Probability distributions of equivalent widths, escape fractions and velocity offsets are constructed as a function of luminosity and UV continuum slope. The reionisation sample then comprises 210 $6.5 < z < 13$ spectra from taken JADES, the Early Release Science (ERS) campaigns and various General Observer programmes. 33 of these reveal Lyman alpha emission over $6.5 < z < 10.5$.

This approach enables comparisons of the Lyman α demographics over a range of redshifts, taking into account biases that would otherwise occur due to observational limitations. The analysis reveals a convincing decline in the Lyman α emission fraction to $z \approx 10$ and the first meaningful estimate of the evolving neutral fraction $x_{\text{HI}}(z)$ using one method through most of the reionisation era (Figure 6).

Tang et al also provide a glimpse of the future possibilities of IGM tomography. It is reasonable to assume that the escape of Lyman α can be used as a proxy for escaping radiation capable of ionising the IGM, i.e. the Lyman continuum (see next section) and hence for tracing ionised bubbles. They use the spatial distribution of [O III] emitters from FRESCO's NIRCcam grism survey to trace overdensities in both GOODS fields. In the resulting 3-D map of the sample (Figure 7) some Lyman α emitters are found in clustered regions whose members may have collectively ionised the local region. Others are isolated examples which may be solely capable of ionising their surroundings. This work highlights by direct 3-D mapping, the role that galaxies play in cosmic reionisation (see Chen et al. (2025) for an update of this tomographic approach).

In summary, both Lyman α absorption and emission techniques have been useful in delineating the history of the redshift-dependent neutral fraction $x_{\text{HI}}(z)$ over $5 < z < 10$ consistent with the coarser constraints from the CMB. We can also see evidence for the patchiness of the process and ultimately we can hope to be able to connect ionised bubbles with the sources responsible - a question we will return to later. Perhaps the most exciting development from JWST is the emerging evidence from Lyman α tomography (Tang et al., 2024; Chen et al., 2025) that galaxies are likely responsible for creating local ionised regions and thus play a dominant role in the overall process.

5 The Reionisation Budget

In order to determine which sources governed the reionisation process we first need to understand the balance between the rate of ionising photons \dot{n}_{ion} and the recombination time for neutral hydrogen t_{rec} . If the volume-averaged fraction of ionised hydrogen at a given time is

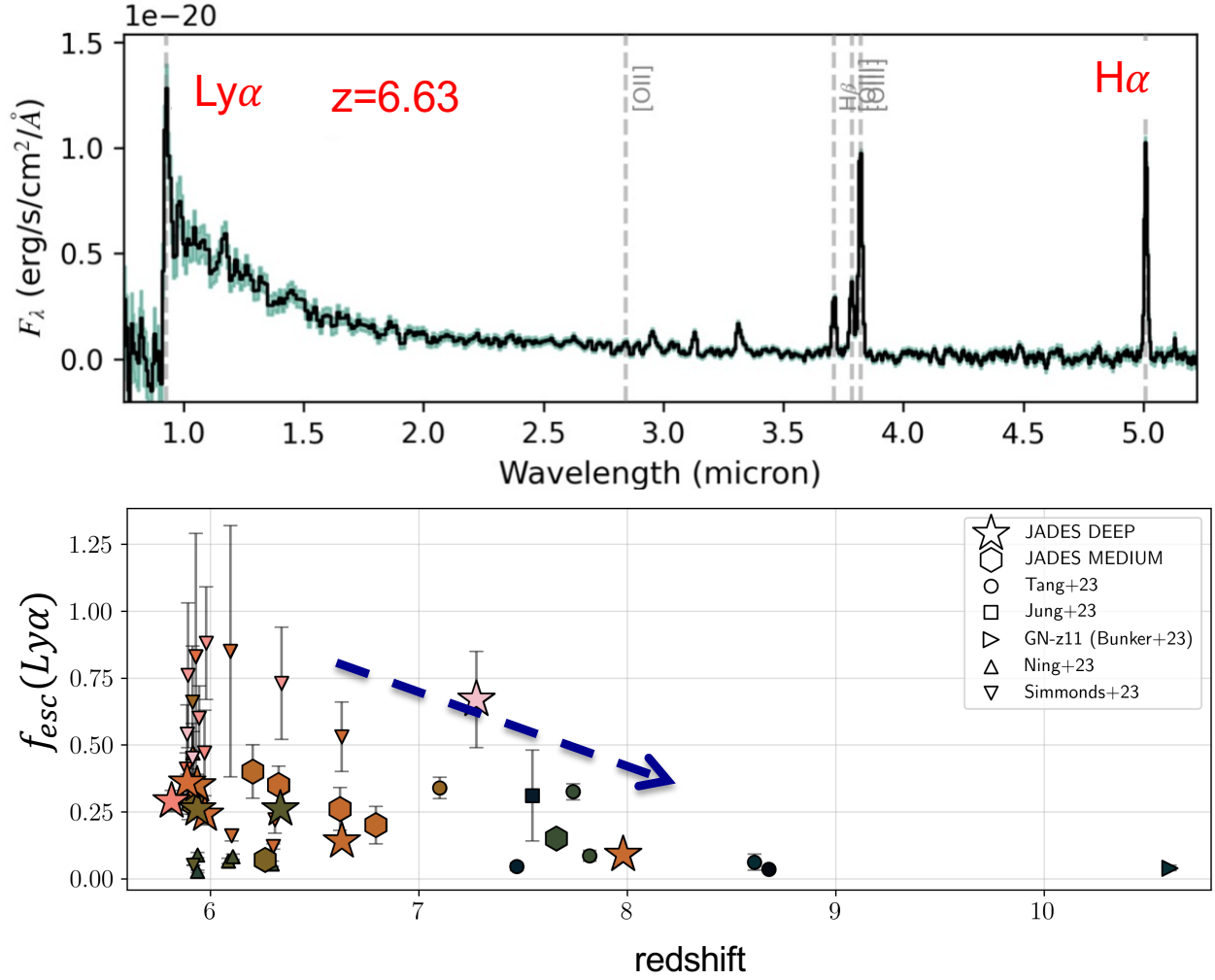


Fig. 5 JWST has significantly improved the prospects for constraining the IGM neutrality in the reionisation era using line emission measures. (Top) Spectrum of a $z=6.63$ galaxy revealing both Ly α and H α which, assuming recombination physics, permits determining the escape fraction of Ly α . (Bottom) Early confirmation of the declining visibility of Ly α with redshift well into the reionisation era (Saxena et al., 2024).

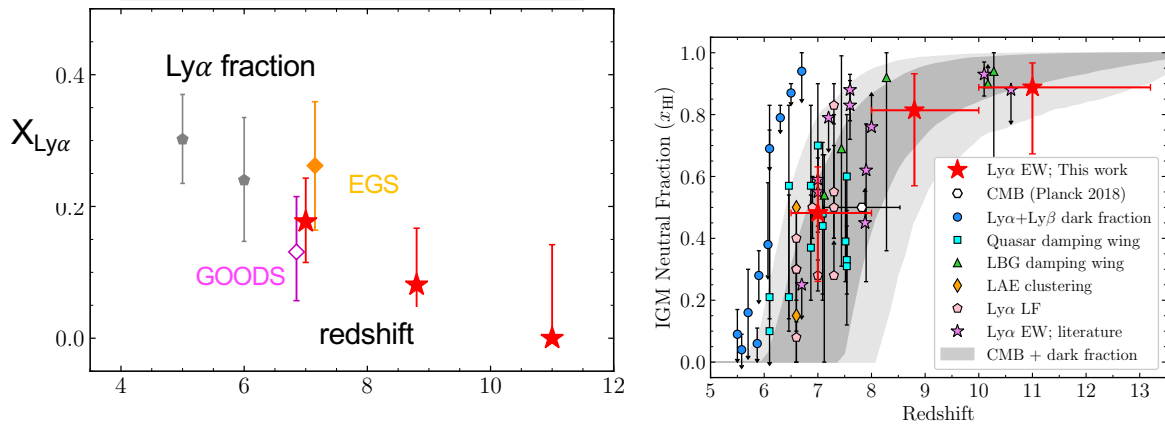


Fig. 6 (Left) Declining visibility of Ly α with redshift from over 200 $z > 6.5$ JWST spectra and a controlled comparison sample in the fully-ionised era. (Right) Inferred history of the neutral fraction from Ly α is shown by the red points and represents the first self-consistent determination of x_{HI} using one method through the bulk of the reionisation era (Tang et al., 2024).

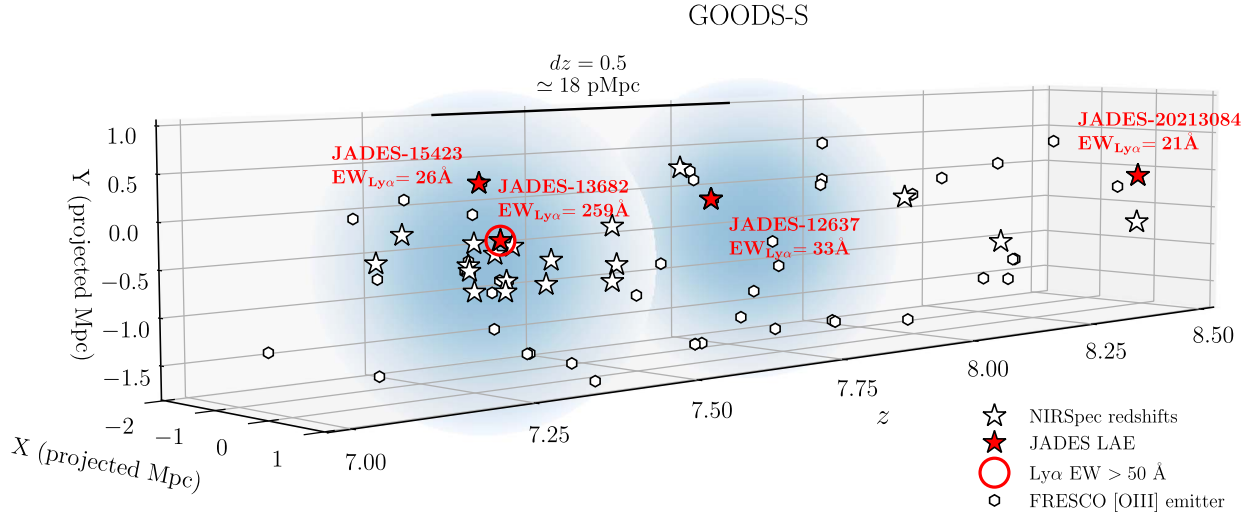


Fig. 7 Spatial distribution of $\text{Ly}\alpha$ emitters (red) with respect to non-emitters in GOODS-S from the analysis of Tang et al. (2024). Whereas many emitters lie in clustered regions suggesting such associations may be responsible for the ionised regions (indicated in blue), there are also isolated examples.

Q_{HII} , then its evolutionary change with time is given by e.g. (Madau, 2000; Miralda-Escudé et al., 2000) :

$$\dot{Q}_{\text{HII}} = \frac{\dot{n}_{\text{ion}}}{\langle n_{\text{H}} \rangle} - \frac{Q_{\text{HII}}}{t_{\text{rec}}} \quad (4)$$

where the recombination time depends on the IGM temperature T_{IGM} through a recombination coefficient $\alpha(T_{\text{IGM}})$ and a dimensionless clumping factor

$$C = \frac{\langle n^2 \rangle}{\langle n \rangle^2} \quad (5)$$

For Case A recombination, corresponding to the optically thick case

$$t_{\text{rec}} = [n_{\text{H}} \alpha(T_{\text{IGM}}) C]^{-1} \quad (6)$$

Simulations of large scale structure generally indicate the clumping factor is in the range $C \simeq 1-6$ and not a crucial ingredient in changing the transition from a neutral ($Q_{\text{HII}} = 0$) IGM to one that is fully ionised ($Q_{\text{HII}} = 1$). If so, the pace of reionisation and the dominant sources are determined by understanding the ionisation rate \dot{n}_{ion} .

In the absence of a detailed picture, it has become customary to break the problem into three manageable components (Robertson et al., 2010) :

$$\dot{n}_{\text{ion}} = \rho_{\text{UV}} \xi_{\text{ion}} f_{\text{esc}} \quad (7)$$

See Figure 8 for an illustration.

Taking each component in turn:

- ρ_{UV} is the integrated abundance (per comoving volume) of the chosen class of sources, across all luminosities. This is derived by integrating the associated luminosity function down to some fiducial absolute magnitude, often $M_{\text{UV}} = -17$.
- ξ_{ion} is the intrinsic production rate of photons capable of ionising hydrogen (i.e. with energies > 13.6 eV). It is defined as the number of such photons per second $N(H^0)$ divided by the UV luminosity in ergs at a longer wavelength, traditionally ≈ 1500 Å. It is usually presented as a logarithmic quantity in units of Hz erg^{-1} . This quantity can be estimated by diagnosing the stellar population from fits to the spectral energy distribution, or using nebular emission lines to gauge the hardness of the radiation field. However, several assumptions must be made regarding the nature of the stellar population e.g. whether stellar binaries make a major contribution to the radiation field and the nature of the stellar initial mass function.
- f_{esc} is the fraction of ionising photons that manage to escape the source into the IGM, often quoted as a percentage. This is very

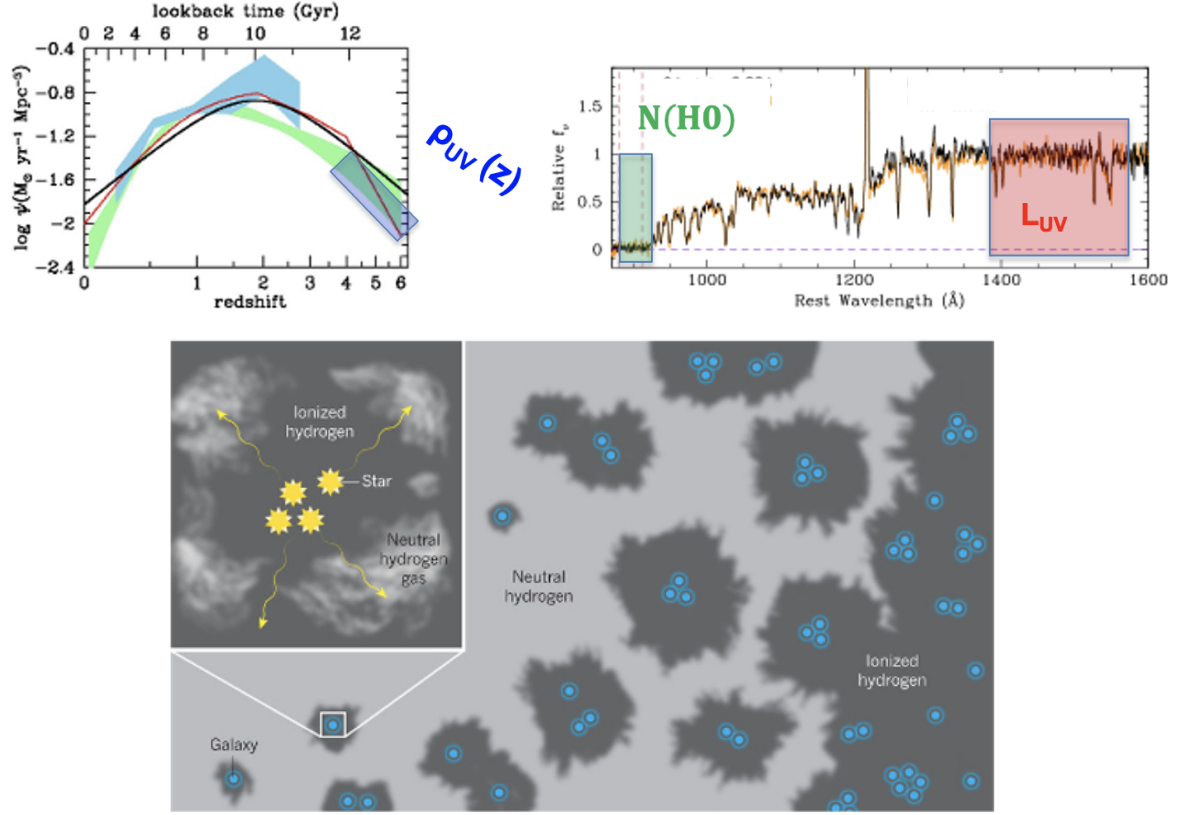


Fig. 8 A simple illustration of the three components of the reionisation rate \dot{n}_{ion} (Left:) ρ_{UV} is the redshift-dependent integrated UV luminosity density. (Right:) ξ_{ion} is the intrinsic production rate of Lyman continuum photons $N(H^0)$ per UV luminosity L_{UV} . (Lower:) The escape fraction f_{esc} is the fraction of Lyman continuum photons that can reach the IGM (Courtesy: Mark Dickinson, Chuck Steidel & Dawn Erb).

challenging to measure beyond a redshift $z \approx 4$ due to line of sight hydrogen absorption. Direct measures of the Lyman continuum “leaking radiation” are only possible at redshifts $z \leq 3$ which has led to searches for “analogues” of reionisation-era galaxies in order to make progress.

Before discussing the latest JWST results, it’s worth issuing some cautionary remarks on this simplistic view of the overall ionisation rate. Star-forming galaxies represent an enormously diverse population in terms of size, luminosity and stellar activity. It would seem naive to apply single values of ξ_{ion} or f_{esc} to an entire population, as was the standard practice prior to JWST. Moreover, simulations suggest that both parameters may increase with redshift. Lower metallicities will increase ξ_{ion} and radiation pressure from energetic star formation in compact sources at higher redshift will create porous channels in the ISM increasing f_{esc} . Finally, although rarer, AGN may contaminate the galaxy population and make a significant contribution to the ionisation process, particularly at later times.

5.1 UV luminosity density

Let us discuss what is known about each of these 3 ingredients from both pre-JWST and JWST data.

The UV luminosity density ρ_{UV} is derived by integrating the redshift-dependent UV luminosity function. This is a simpler task than estimating the physically more important integrated star formation rate density ρ_{SFR} commonly quoted (Madau and Dickinson, 2014) because it avoids understanding the SFR-UV calibration which depends on metallicity, star formation histories, the initial mass function and contributions from dust-obscured sources.

The galaxy luminosity function (LF) is traditionally expressed in terms of the Schechter function (Schechter, 1976)

$$\Phi(L) \frac{dL}{L^*} = \Phi^* \left(\frac{L}{L^*} \right)^{-\alpha} \exp\left(-\frac{L}{L^*}\right) \frac{dL}{L^*} \quad (8)$$

The seemingly complex function is simply a power law with a faint end slope of α multiplied by an exponential for the portion more luminous than a characteristic luminosity, L^* . The integrated luminosity density is then:

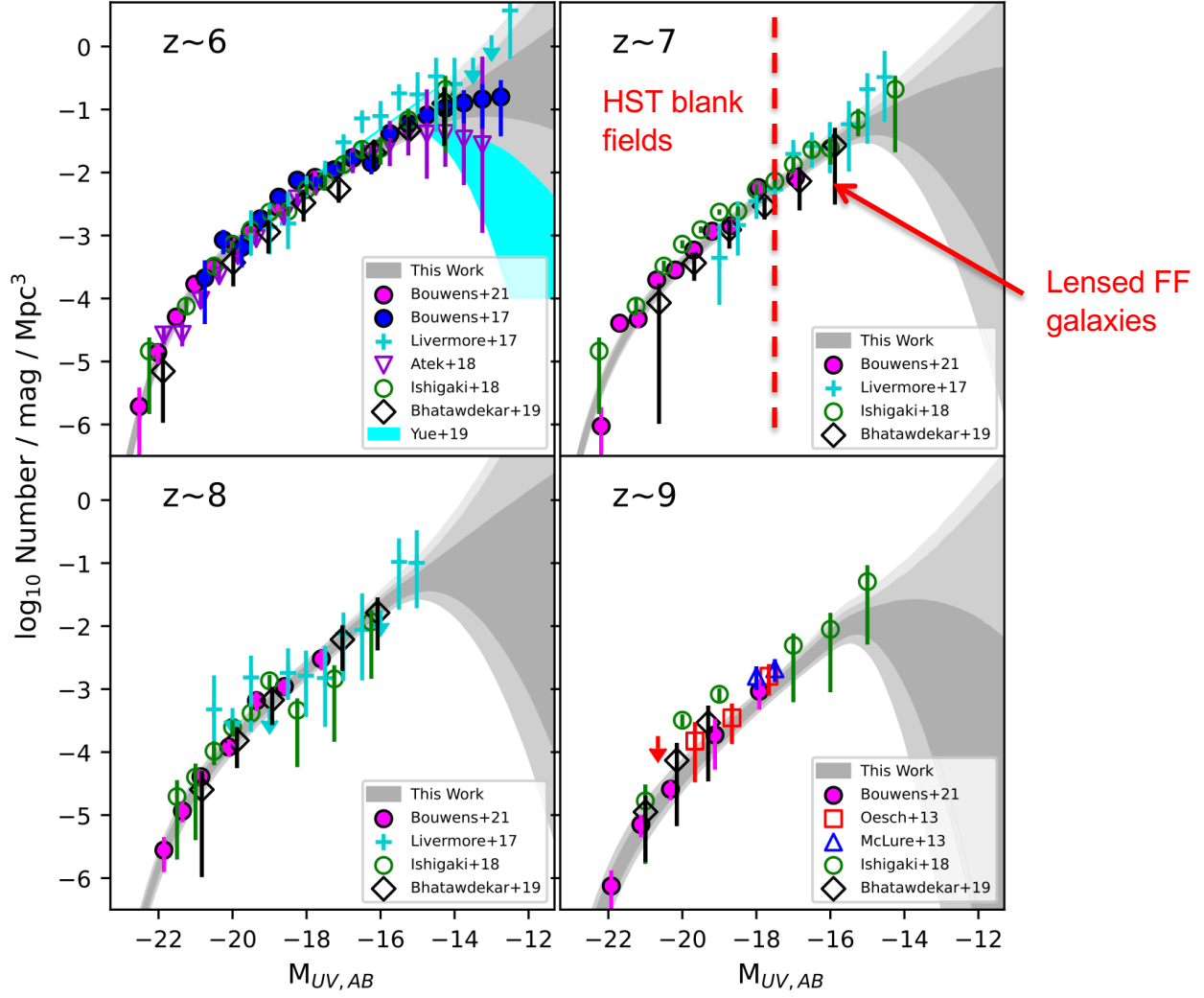


Fig. 9 Redshift-dependent UV luminosity function of galaxies combining HST’s deep fields and the six lensing Frontier Field Clusters (Bouwens et al., 2022). The red dashed line indicates the luminosity limit of the deep fields, fainter than which the contribution analysed via imaging through lensing clusters is crucial. Since the Schechter faint end slope α [Eqn 8] is steeper than -2 in this redshift range, the integrated ρ_{UV} would be divergent so a faint limit to the integration must be chosen. The grey shaded areas illustrates there is not yet any statistically-significant evidence of a decline to $M_{UV} = -13$.

$$\rho_L = \int \Phi(L) L dL = \Phi^* L^* \Gamma(\alpha + 2) \quad (9)$$

For galaxies, the observed UV LF has a faint end slope that steepens from $\alpha \simeq -2$ at intermediate redshift to -2.4 in the reionisation era (Bouwens et al., 2022). Not only do intrinsically faint galaxies dominate the integral but, for $\alpha \leq -2$, the integral above diverges unless the faint end of the LF turns down at some point as theorists predict could be the case due to reionisation feedback effects.

Perhaps surprisingly, the current best estimate of $\rho_{UV}(z)$ still comes from HST observations, at least to redshifts $z \simeq 9$. This is because HST has observed galaxies in several deep fields as well as through the six Frontier Field lensing clusters, thereby mitigating cosmic variance effects. However, JWST does probe the LF to higher redshift. Figure 9 shows the most recent LF measures over $6 < z < 9$ and highlights the important contribution from lensed sources as well as the constraints on any possible turn-down in the LF down to a luminosity of $M_{UV} = -13$ (Bouwens et al., 2022). To this limit the UV luminosity density is known to better than 20% (making it the most accurately determined of the three components introduced above!)

5.2 Ionising Productivity ξ_{ion}

Ionising radiation could be thermally produced from hot, young stars, or non-thermal radiation from active galactic nuclei (AGN). In the past, ξ_{ion} was mostly determined by using stellar population synthesis (SPS) models to fit to the spectral energy distribution (SED) compiled

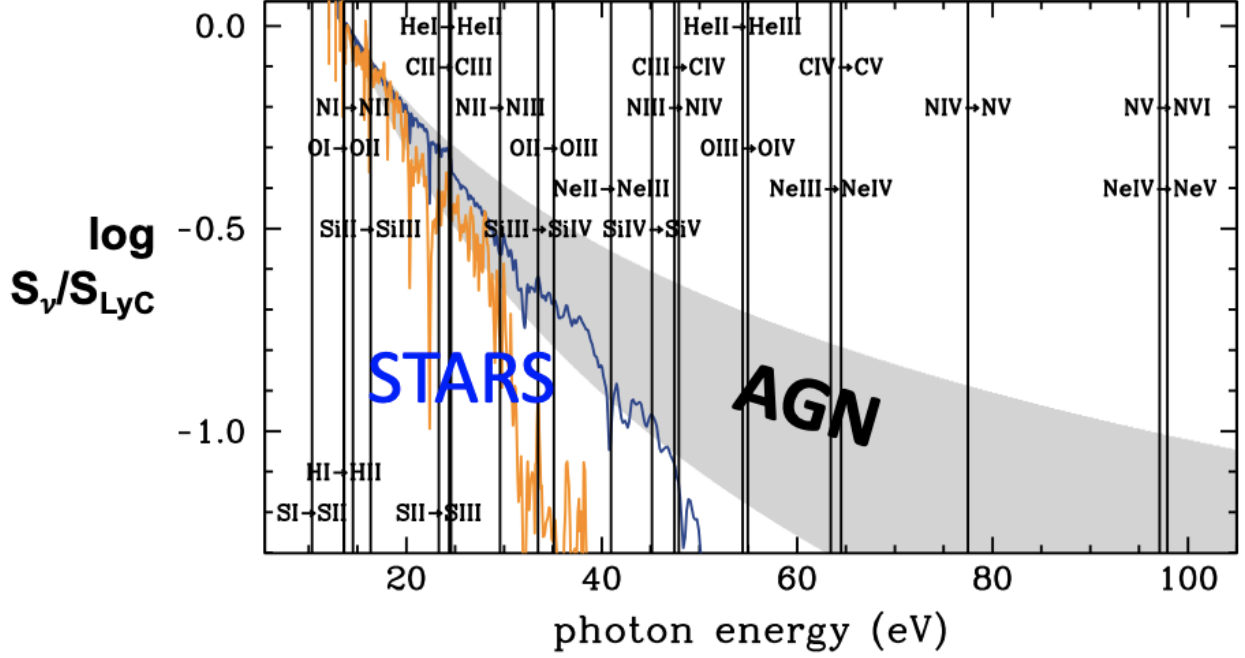


Fig. 10 Intrinsic spectral energy distributions S_ν (in terms of that at the Lyman limit S_{LyC}) versus photon energy (eV) for stars with 3% (orange) and 0.1% (blue) solar metallicities, compared with AGN (the grey shaded area) with a range of likely power law indices. Vertical lines indicate the ionising energies of ions of different species. The visibility and ratios of such ionic spectrum lines can be used to gauge the hardness of the radiation (Feltre et al., 2016).

from broad-band photometry or even from more basic data such as the UV continuum slope calibrated by such models.

The advent of JWST has led to an increased awareness of using spectroscopic data and two techniques are now in common use.

Balmer lines and recombination physics: For an ionisation-bounded nebula, the ionisation and recombination rates are equal. The ionisation rate can therefore be derived from the dust-corrected luminosity of $H\alpha$ emission, via

$$L(H\alpha) = C(T, n_e)N(H^0) \quad (10)$$

Unfortunately, this leads to a degeneracy with the escape fraction f_{esc} , such that

$$\xi_{\text{ion}} = \frac{N(H^0)}{L_{\text{UV}}} (1 - f_{\text{esc}}) \quad (11)$$

An impressive example of this method is the analysis of 670 $1.4 < z < 2.6$ Lyman break galaxies (LBGs) in the Keck MOSDEF survey (Shivaei et al., 2018). These authors determined $N(H^0)$ from Balmer line measures of $H\alpha$ and $H\beta$ and L_{UV} from SED fits to 3D-HST photometry. Depending on the adopted UV extinction law, they find

$$\log \xi_{\text{ion}} = 25.0 - 25.3 \text{ Hz erg}^{-1}$$

Rest-UV metal lines of high ionisation potential: Photoionisation models of stellar populations of different metallicities or AGN can predict the expected line ratios for metals in various ionisation states. An illustrative figure from Feltre et al. (2016) in Figure 10 shows how key emission lines such as CIII], CIV and NV with associate high ionisation potentials can be used to diagnose the hardness of the radiation field.

An example of this method followed VLT rest-UV spectra of ≈ 100 metal-poor, relatively dust-free Lyman α emitting galaxies (LAEs) at $z \approx 3$ considered to be better analogues of $z > 7$ galaxies than Lyman break galaxies (LBGs) discussed above (Nakajima et al., 2018). These authors found:

$$\log \xi_{\text{ion}} = 25.5\text{-}25.7 \text{ Hz erg}^{-1}$$

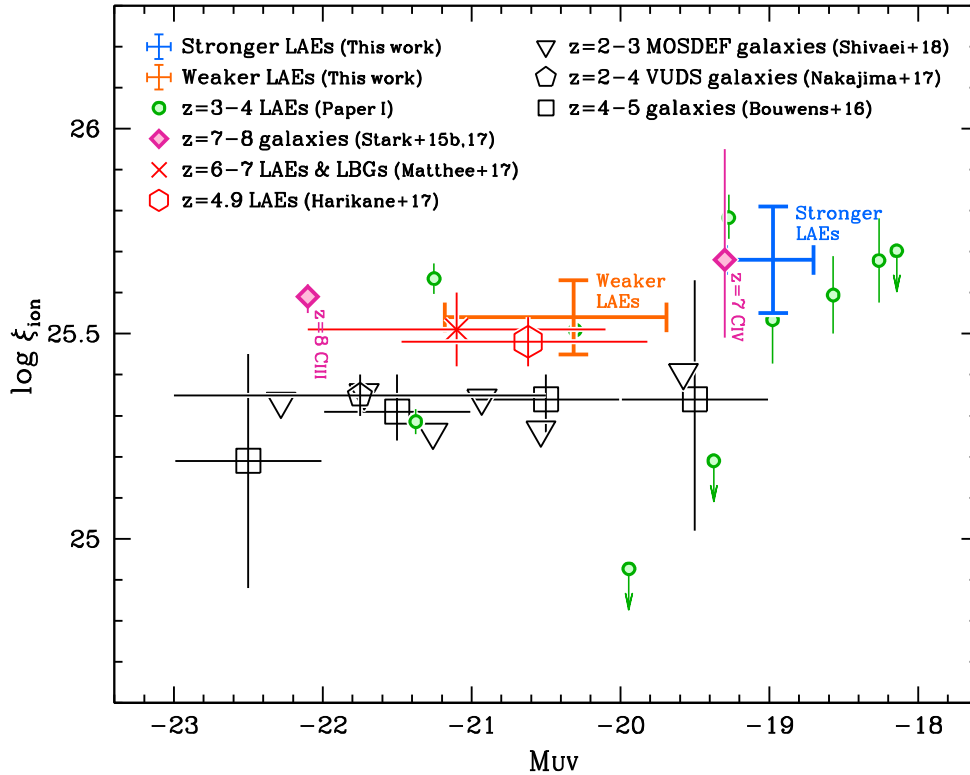


Fig. 11 Intrinsic ionising production rate ξ_{ion} derived from photoionisation models for a sample of $z \approx 3$ Ly α emitters of various UV luminosities (orange and blue points) compared to a coeval population of Lyman Break galaxies (open symbols). LAEs have a harder radiation field and are better analogues of galaxies in the reionisation era (Nakajima et al., 2018).

i.e. a harder radiation field than for LBGs (see Figure 11). Very limited pre-JWST samples of star-forming galaxies at $z > 7$ (Stark et al., 2017) revealed high ionisation lines consistent with those seen in intermediate redshift LAEs.

The infrared capability of JWST means it is now possible to extend the first of the two methods introduced above into the reionisation era for the first time. There is a marked distinction between those adopting a *photometric approach* - using excess fluxes seen in key broad and medium band filters to infer Balmer and other line strengths - and those focusing on genuine spectroscopy. This is a recurring theme in JWST studies of the reionisation era. Photometric measures of galaxy properties offer the advantage of larger samples probing to higher redshift and perhaps permitting a selection method free from any bias. Spectroscopic measures are usually more precise but more limited in redshift range and, when applied to the merged database of many different JWST campaigns, there's naturally a greater likelihood of biases e.g. to systems with stronger line emission.

The JEMS imaging survey (Simmonds et al., 2024) analyses 677 $4 < z < 9$ LBGs using NIRCcam medium and broad-band photometry sensitive to the presence of H α and [O III] 5007 Å (the latter used as a proxy for H α at higher redshift). They find a modest increase in ξ_{ion} with redshift. By contrast, Saxena et al. (2024) using JADES spectra of 16 LAEs found no convincing increase with redshift with $\log \xi_{ion} = 25.6$ very similar to that found for LAEs at $z \approx 3$. Differences have also been found between the photometric and spectroscopic analyses in claimed trends with absolute magnitude M_{UV} and UV continuum slope. An enlarged spectroscopic survey of 167 galaxies to $z \approx 6.7$ from JADES and CEERS samples now finds weaker trends with redshift and only marginally harder radiation fields for luminous galaxies, possibly indicating the presence of AGN (Pahl et al. (2024), see also Llerena et al. (2024)). Summarising, it seems likely that galaxies in the reionisation era may have radiation fields uniformly stronger than Lyman break galaxies at intermediate redshift. Any trends with luminosity would be very important, particularly in understanding the relative contribution of intrinsically faint or luminous galaxies to reionisation. If star formation is stochastic, it is likely that ξ_{ion} would be lower in sub-luminous sources observed during a down-turn in activity (Stark et al., 2025).

5.3 Escape Fraction f_{esc}

This final parameter presents the greatest challenge in understanding the process of reionisation for two very different reasons. Firstly, hydrodynamical simulations suggest that young star-forming galaxies are complex systems and that any emerging Lyman continuum radiation would be highly time-dependent due to bursty star formation and anisotropic due to the irregular distribution of porous regions in the ISM (Wise et al. (2014); Trebitsch et al. (2017); Barrow et al. (2020), see Figure 12). A second problem is that the attenuation of the

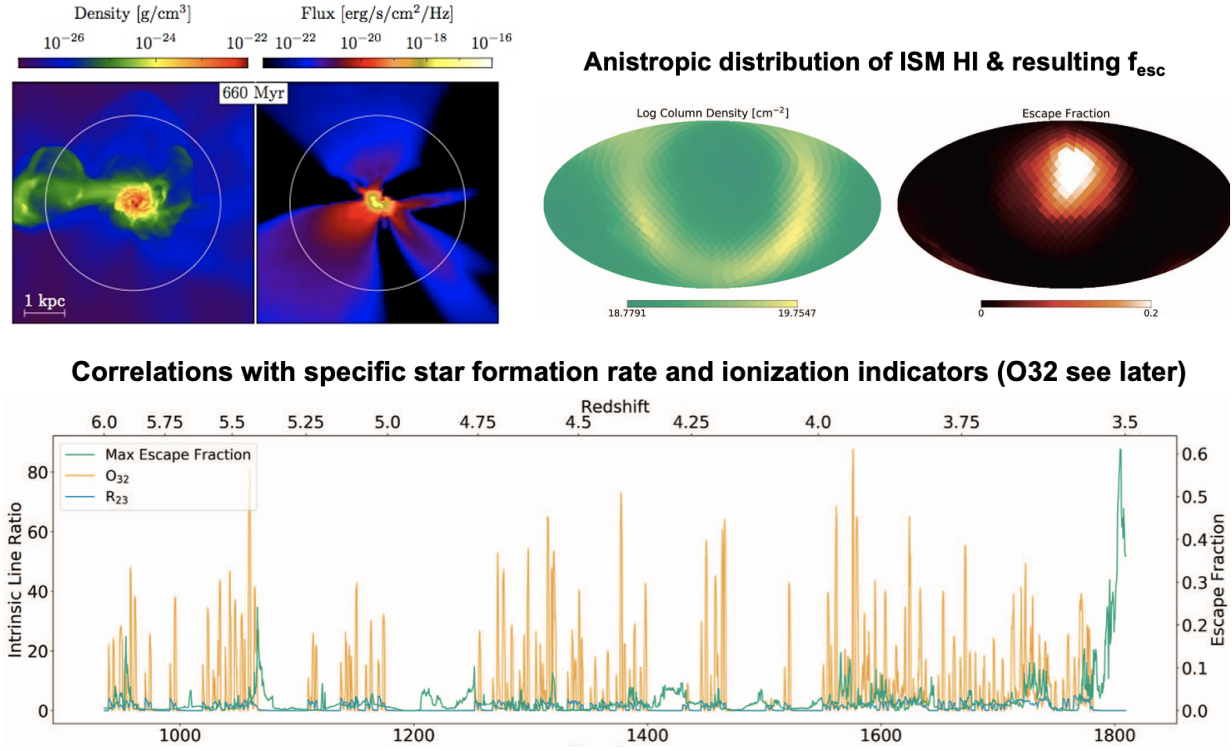


Fig. 12 Numerical simulations of the leaking Lyman continuum from star-forming galaxies (Wise et al., 2014; Barrow et al., 2020). (Top) Evidence for anisotropic leakage whereby radiation pressure creates specific channels through the inhomogeneous neutral gas. (Bottom) Demonstration of how stochastic star formation influences the leakage and correlates with observable diagnostic line ratios (R23 and O32, see text)

IGM increases beyond $z \approx 4$ (Inoue et al., 2014) which means direct measures of f_{esc} are restricted to redshifts $z \leq 3$ where lower redshift “analogues” of reionisation era systems can be studied.

First some definitions. The “ideal” definition of f_{esc} would be the fraction of the intrinsic number of ionising photons that escape into the IGM without being absorbed by neutral hydrogen in the ISM/CGM. In practice however, we don’t observe the intrinsic rate so the ideal value is sometimes referred to as the (unobservable) *absolute value* $f_{\text{esc}}^{\text{abs}}$. Observers usually refer instead to a *relative value* based on observations below and above the Lyman continuum limit at 912 Å

$$f_{\text{esc}}^{\text{rel}} = \frac{(f_{900}/f_{1500})_{\text{obs}}}{(L_{900}/L_{1500})_{\text{int}}} \quad (12)$$

where the intrinsic (int) ratio is determined from a stellar synthesis model.

Direct methods at very low redshifts ($0.2 < z < 0.4$) have naturally provided the most detailed information but nonetheless some puzzles have arisen. So-called “Green Pea” galaxies are compact low redshift galaxies with intense [O III] 5007 Å emission. HST’s UV-sensitive Cosmic Origins Spectrograph (COS) often reveals non-zero fluxes below the Lyman limit indicating, in some case, f_{esc} values as high as 20-40% (Izotov et al., 2016, 2022). Various correlations have been presented between f_{esc} and the strength of Lyman α , Mg II and the line ratio O32 (= [O III] 5007/[O II] 3727 Å). However, HST COS also recently undertook a systematic survey of 66 low metallicity galaxies chosen to sample a wider range of UV continuum slopes, O32 ratios and star formation rates (Flury et al., 2022). Although the mean escape fraction for this sample is $\approx 10\%$ and a subset has $f_{\text{esc}} > 20\%$, there is surprisingly little difference in the above physical properties between the Lyman continuum (LyC) leakers and non-leakers. A recent study of the Lyman Alpha and Continuum Origins Survey finds leakers have more compact Ly α cores suggesting both LyC and Ly α photons are emerging through sightlines cleared by central starbursts (Saldana-Lopez et al., 2025). This further suggests that whether a galaxy is a leaker or not depends not only on recent star formation but also on the viewing angle.

Direct LyC detections can be sought for large samples at redshift $z \approx 3$ which represents a “sweet spot” in terms of redshift since the Lyman limit enters the optical range of ground-based multi-object spectrographs yet the IGM opacity is still modest. Even so, the LyC signal is mostly too faint to be detected in individual galaxies. Only 12 galaxies reveal individual LyC detections in the comprehensive Keck spectroscopic survey of 124 LBGs by Steidel et al. (2018). That analysis is largely based on stacked spectra yielding average values of $f_{\text{esc}} \approx 6\text{-}9\%$ depending on various modelling assumptions. Contamination of the LyC stacked signal from lower redshift sources along the sight line may inadvertently lead to an overestimated average f_{esc} . Such contaminants might be undetected in ground-based imaging

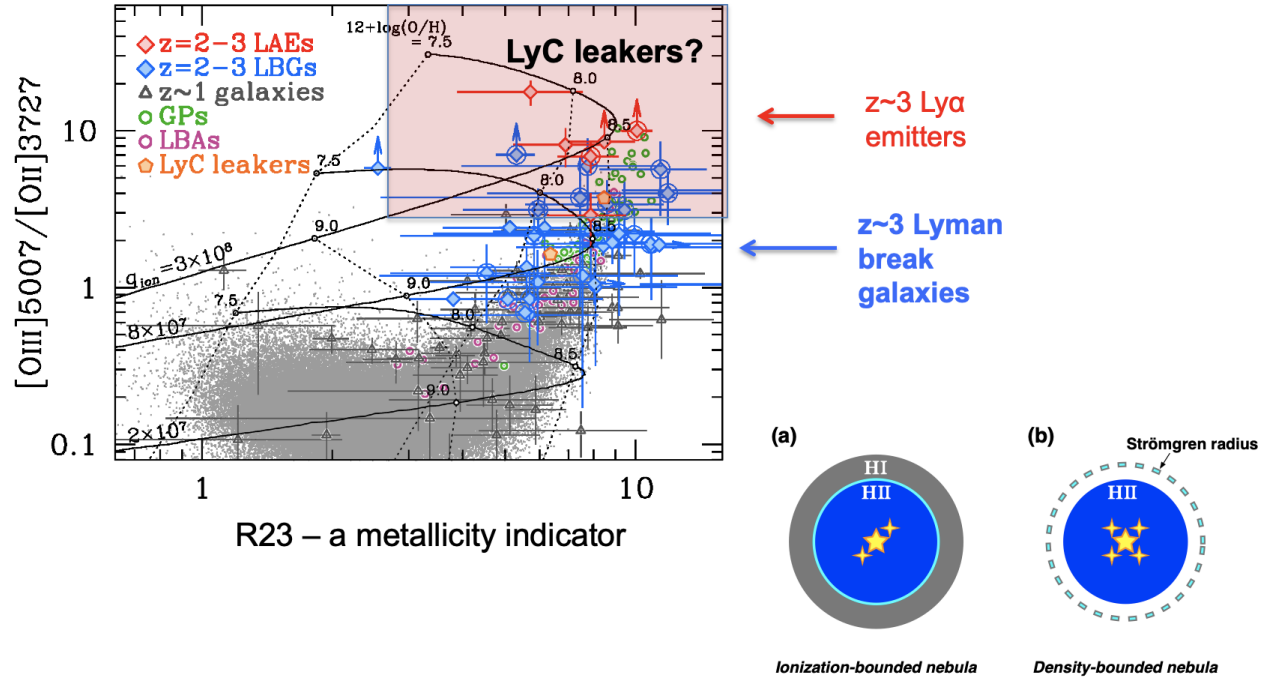


Fig. 13 Lyman α emitters at $z \approx 3$ (red lozenges) and local “Green Pea” galaxies (green) have a larger O32 line ratio than Lyman break galaxies (blue). Nakajima and Ouchi (2014) postulate such extreme line ratios may arise from density-bound (rather than ionisation-bound) HII regions (see lower right inset) which implying a higher escape fraction.

and reveal no associated spectroscopic features.

Nakajima and Ouchi (2014) proposed that high O32 line ratios are inconsistent with traditionally-assumed *ionisation-bound* nebulae (a.k.a. Strömgren spheres) and may reflect *density-bound* H II regions with larger escape fractions. They demonstrate (Figure 13) that $z \approx 3$ LAEs have systematically higher O32 values than LBGs and thus may represent better analogues of reionisation-era galaxies. Following this suggestion, Fletcher et al. (2019) undertook deep (20 orbit) HST WFC3 F336W imaging of 61 $z \approx 3$ LAEs with associated HST/Subaru broad-band imaging and Keck/VLT spectroscopy. Fitting the SEDs enabled the authors to predict the intrinsic Lyman continuum flux in the F336W filter. Comparing with the observed flux and correcting for IGM absorption provides the likelihood distribution of f_{esc} . Although 20% of the sample showed significant F336W detections with f_{esc} value ranging from 15-50% (right panel of Figure 14), fully half the sample showed no detections at all implying individual values of $f_{\text{esc}} < 1.5\%$. As with the lower redshift HST COS samples, demographically the non-leaker population seems no different to the leaker population. Remarkably, even a F336W stacked image of the non-leakers reveals no signal suggesting an average $f_{\text{esc}} < 0.3\%$. Once again, it seems Lyman continuum radiation is either observed or not at all.

Even with the superlative image quality of HST, foreground contamination remains a major concern for direct imaging measures of f_{esc} . Earlier claims of Lyman continuum detections based on ground-based narrow-band data were subsequently shown by improved HST imaging to arise from unassociated foreground sources (see left panel of Figure 14, Mostardi et al. (2015)). JWST is even revisiting earlier claimed HST detections and apparently uncovering confusion between Lyman continuum signals and foreground galaxies (Schaerer, priv. comm.)

The situation regarding escape fractions prior to the launch of JWST was critically summarised by Naidu et al. (2020). In addition to measures based on direct spectroscopy or UV imaging, less direct probes include measures of the covering fraction of neutral gas derived from high signal/noise absorption line spectra (Jones et al., 2012, 2013; Leethochawalit et al., 2016) and studies of double-peaked Lyman alpha emitters where the velocity separation V_{sep} between the peaks relates to the size of the ionised regions (Verhamme et al., 2015; Michel-Dansac et al., 2020). Izotov et al. (2018) show a convincing anti-correlation between V_{sep} and f_{esc} (Figure 15) but, to date, there are very few reionisation-era galaxies with such double-peaked Lyman α profiles (one is shown in the lower right of Figure 15, Matthee et al. (2018)). As Naidu et al discuss, although the literature is rich in analyses of individual galaxies with high f_{esc} there may be a natural bias against publishing negative results. Despite heroic observational efforts, prior to JWST there was little consensus on the average value for star-forming galaxies typical of those in the reionisation era.

Given the difficulty of inferring f_{esc} for sources in the reionisation era, theorists have tried to correlate the escape fraction seen in simulations with other properties observable at high redshift (e.g. Choustikov et al. (2024)). The results are somewhat inconclusive at the present time. Clearly f_{esc} is a complex quantity that fluctuates according to irregular star formation histories and geometrical anisotropies, and so a better approach is to statistically correlate the IGM opacity inferred from quasar absorption spectra of the Lyman α forest with

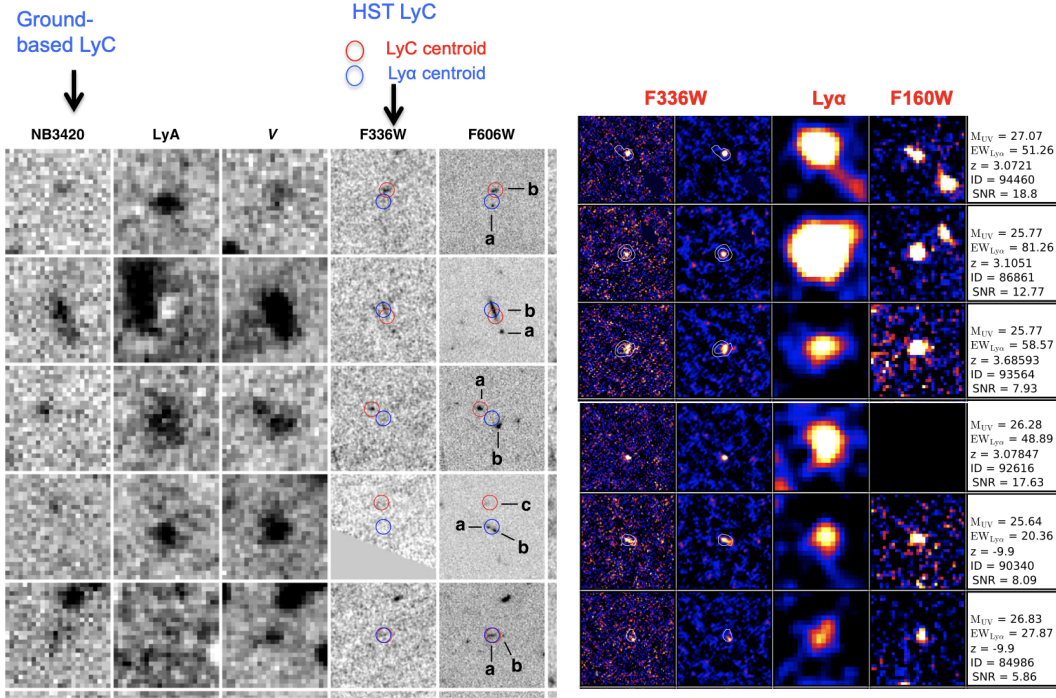


Fig. 14 Deep UV imaging of $z \approx 3$ Lyman α emitters as a probe of leaking radiation. (Left) While ground-based narrow-band 3420 Å imaging revealed promising candidates, subsequent HST imaging in F336W demonstrates offsets between the putative LyC leakage (red circles) and Lyman α emission (blue circles) indicating likely foreground contamination (Mostardi et al., 2015). (Right) A selection of promising candidates from a similar HST-based F336W campaign (Fletcher et al., 2019). Over half this sample shows no discernible detections even when stacked, suggesting anisotropic leakage is the cause of such wide variations in f_{esc} .

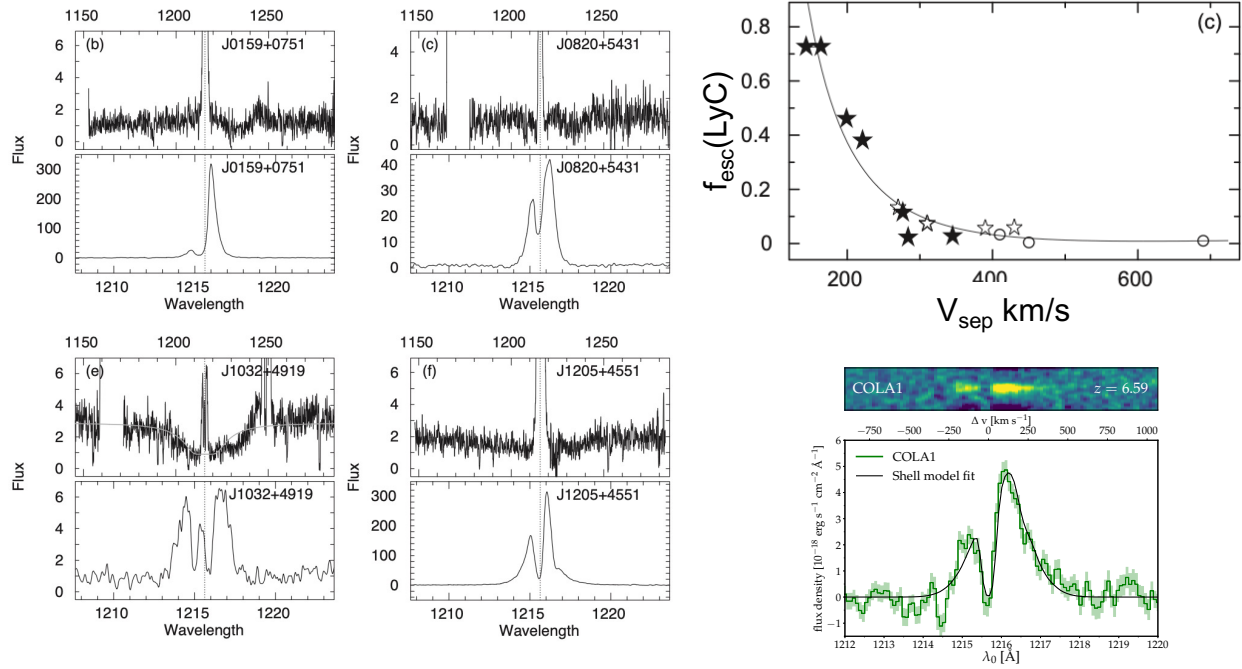


Fig. 15 Double-peak Lyman α emitters as a promising probe of f_{esc} . The main display shows high quality HST COS line profiles of selected $z \approx 0.03 - 0.06$ SDSS galaxies with high O32 (Izotov et al., 2018) and a convincing anti-correlation between the derived f_{esc} and the peak separation V_{sep} which is the principal of the method (upper right). A convincing example of a double-peaked LAE in the reionisation era is shown in the lower right (Matthee et al., 2018).

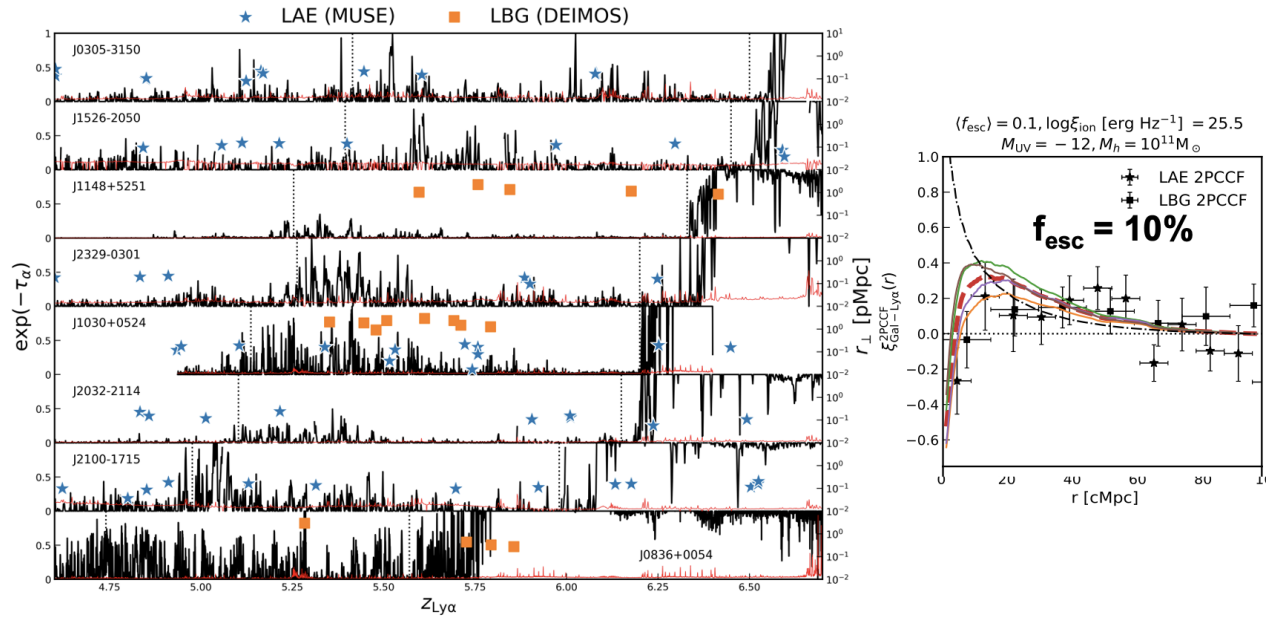


Fig. 16 Estimating f_{esc} via direct spatial correlations between galaxies and the fluctuating transmission in the Lyman α forest as first proposed by Kakiichi et al. (2018). Absorption spectra of 8 $z > 6.5$ quasars sample the IGM over the redshift range $4.8 < z < 6.1$. Keck and VLT redshift surveys locate galaxies and measure their distance to each sightline. The right panel shows the cross-correlation which is fit by a model which accounts for the likely clustering of sub-luminous galaxies beyond the spectroscopic limit of the galaxy survey. An average escape fraction of $\approx 10\%$ is a reasonable fit to the data (Meyer et al., 2020).

the proximate presence of associated galaxies. First proposed as a proof-of-concept by Kakiichi et al. (2018), Meyer et al. (2020) applied the method to the sightlines of eight $z \approx 6.5$ quasars securing Keck+VLT redshifts for 60 galaxies within the same cosmic volume as that probed by the Lyman α forest over $4.6 < z_{\text{abs}} < 6.6$ (Figure 16). The positive cross-correlation over 10-50 comoving Mpc is consistent with an average $f_{\text{esc}} \approx 10\%$ assuming the typical galaxy has an intrinsic production rate $\log \xi_{\text{ion}} = 25.5 \text{ erg Hz}^{-1}$. One limitation of this promising method is that ground-based redshift surveys can only trace the most luminous galaxies at such high redshifts and so the associated population of intrinsically fainter sources which also contribute to the ionising flux must somehow be accounted for.

The JWST ASPIRE programme (PI: F. Wang) is adopting a similar strategy using NIRCcam F356W slitless spectra to locate [O III] emitters associated with 25 $z > 6.5$ quasar sightlines. A preliminary analysis based on the first 5 quasars and 50 [OIII] emitters detects a positive cross-correlation suggesting a similar result to that of Meyer et al (Kakiichi et al., 2025). Likewise the EIGER survey (Kashino et al., 2025) has correlated [O III] emitters with the Ly α forest in 6 QSO sightlines and examines how the cross-correlation evolves over $5 < z < 7$ suggesting that the influence of the background radiation field becomes important at higher redshift.

Kakiichi and colleagues have proposed a further refinement of their method. As high redshift quasars are sparsely distributed on the sky and the above technique is limited to a number of 1-D sightlines, it is seriously affected by cosmic variance. Harnessing the unique wide field prime focus of the Subaru telescope, the new idea is to undertake deep narrow-band imaging to reveal photometrically the depth of Lyman α absorption at one selected redshift for all the background galaxies. The same narrow-band filter can also simultaneously locate Lyman α emitters at this redshift and thus undertake the cross-correlation. This provides a significant increase in the number of cross-correlated galaxy absorber pairs! The challenging requirements include ultra-deep Subaru narrow-band imaging which becomes progressively more demanding at higher redshifts and spectroscopic redshifts for all the background galaxies so there is no confusion regarding the origin of the absorption signal. This project is now being undertaken in the COSMOS-3D survey, a Cycle 3 Treasury Programme (PI: Kakiichi) where the redshifts are being determined using NIRCcam F444W slitless spectroscopy.

Finally, two further intriguing ideas have emerged since the Lectures that bypass the inability to measure f_{esc} directly beyond $z \approx 4$ due to IGM absorption. The first is to study galaxies lying in the ionised “proximity zones” created by luminous quasars. Yue et al. (2025) apply this method to 15 $z \approx 6-7$ galaxies lying within 2500 km sec^{-1} of a quasars and find significant flux blueward of Ly α compared to a control sample of galaxies not associated with any quasars. Their inferred escape fraction for Ly α emission is consistent with a LyC $f_{\text{esc}} \approx 10\%$. The second utilises topics I discuss in Lecture 2 that relate to the UV continuum slope and the contribution made by the nebular continuum emitted by young galaxies with hot stars (Lecture 2, Section 3.5). This nebular continuum is redder than its stellar counterpart and is naturally anti-correlated with f_{esc} ; if $f_{\text{esc}} = 1$, there is zero nebular contribution to the UV continuum. Giovanazzo et al. (2025) apply this idea to a large spectroscopic database and find a non-zero f_{esc} for only 5% of their sample. Nonetheless, they claim an average value overall of $\approx 10\%$.

Summarising, the escape fraction from typical star forming galaxies in the reionisation-era remains a fundamental challenge to con-

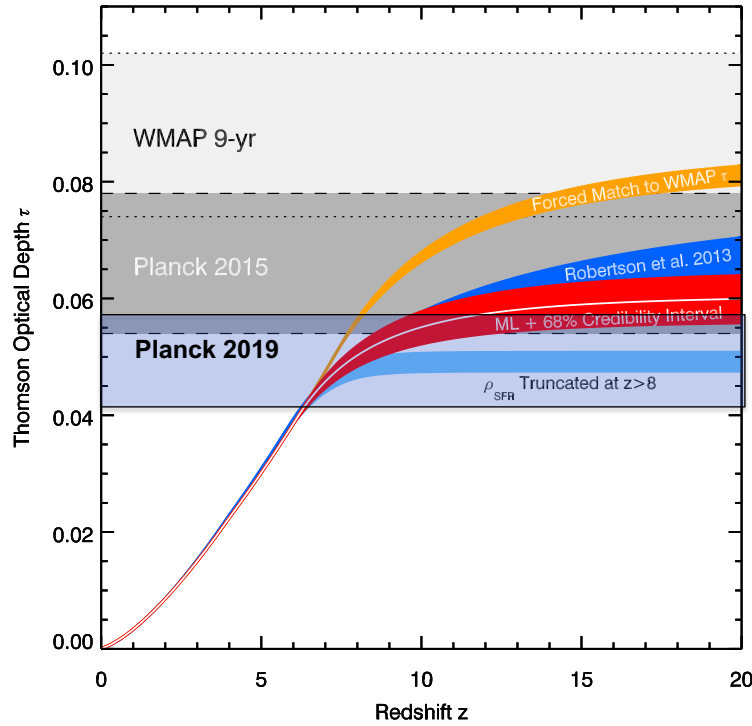


Fig. 17 Reconciling the demographics of galaxies determined with HST with the Planck optical depth τ to Thomson scattering (Robertson et al., 2015). The figure shows the integrated contribution of IGM electrons produced by leakage from star-forming galaxies to τ as redshift increases assuming $\log \xi_{\text{ion}} = 25.5$ cgs and $f_{\text{esc}} = 10\%$ irrespective of luminosity and redshift as well as an option for a steeper rate of declining ρ_{UV} beyond $z=8$ (blue curve). The unlabeled red curve is a reasonable match to τ assuming galaxies emerged in the redshift range $15 < z < 20$.

firming that cosmic reionisation is primarily driven by galaxies. I suspect the only reliable way forward is to secure statistical correlations between galaxies and the opacity of HI in local IGM, either via the methods being adopted by ASPIRE, EIGER and COSMOS-3D, or ultimately via matching JWST sources with 21cm tomography using the Square Kilometre Array (Lecture 3).

6 Constraining the Reionisation History

Let's now attempt to make sense of the observational constraints on the ionising budget noting again the simplistic assumption that the ionisation rate \dot{n} can be broken into three constituent ingredients, which may themselves vary with redshift and galaxy luminosity. Of particular importance is the degeneracy between ξ_{ion} and f_{esc} since it is often only the product that is constrained observationally.

We begin with the popular view that galaxies dominate the process of reionisation. In this case, a simple question is whether the demographics of galaxies, as probed by the redshift-dependent UV luminosity density $\rho_{\text{UV}}(z)$ can be reconciled with the Planck optical depth τ when we adopt universal values for the other two ingredients ξ_{ion} and f_{esc} . Following Robertson et al. (2015) who adopted $\langle \log \xi_{\text{ion}} \rangle = 25.5$ Hz erg⁻¹ and $\langle f_{\text{esc}} \rangle = 10\%$ for all star-forming galaxies, the integrated contribution to τ is shown in Figure 17. To the accuracy this is possible, with the exception of escape fraction adopted, the cumulative optical depth is satisfactorily matched with Planck's final value $\tau = 0.063$ by a redshift $z \approx 11-15$.

But does this agreement exclude a contribution from AGN? In terms of pre-JWST constraints, Naidu et al. (2020) pointed out that Robertson et al.'s simplistic model fails to match the rapidly declining neutral fraction suggested by various quasar absorption probes and the fraction of Lyman α emitters (right panel of Figure 6). At the time this article was written, there was conflicting information on whether ξ_{ion} varies with luminosity. The rapid decline in $x_{\text{HI}}(z)$ for $z < 8$ could be matched by assuming luminous sources played a more significant contribution, perhaps due to the onset of AGN activity.

In Lecture 2 I will discuss the growing body of evidence from JWST that low luminosity AGN are more numerous in the latter half of the reionisation era than suggested by earlier data. Noting the absence of persuasive evidence for a uniformly significant value ($\approx 10-20\%$) for the escape fraction from star-forming galaxies, this has led some to propose a dominant role by AGN. Madau et al. (2024) have presented a AGN-dominated model which can also satisfy the integrated Planck τ and updated constraints on the redshift-dependent neutral fraction $X_{\text{HI}}(z)$. However, the model has some very debatable assumptions. It assumes 15% of galaxies (over all redshifts and luminosities) contain AGN whose escape fraction is greater than 80%. This fraction is not yet justified given many AGN candidates claimed from JWST

observations are hotly debated (see Lecture 2). A further dubious assertion is that, for those galaxies hosting AGN, at least 50% of the UV luminosity arises from a non-thermal component. This cannot be justified across the entire UV luminosities at all epochs. Hopefully as further evidence for AGN activity in the reionisation era is gathered, the extreme views of "all done by galaxies" and "all done by AGN" will be compromised!

In concluding, Pahl et al. (2024) take their modest dependencies of ξ_{ion} on redshift and luminosity and find a reionisation history very similar to that based on Robertson et al's simple model. A key issue is the question of whether there is an unacceptably rapid decline in x_{HI} for $z < 8$ which might indicate an AGN contribution. Unfortunately, as Pahl et al discuss, the uncertainties remain quite large. In Lecture 3 we will briefly explore the promise of using the 21cm line as a tracer of the ionisation state of the IGM. This can be via emission line tomography revealing the location of ionised bubbles as well as in line of sight absorption in spectra of background radio galaxies. Sims et al. (2025) use current upper limits on the 21cm power spectrum from SKA pathfinders and incorporate it into a reionisation history that is quite similar to that of Pahl et al.

7 Summary

In this first lecture, we have addressed two fundamental questions:

1. **When** did reionisation begin and end and, ideally can we constrain the evolving neutral fraction $x_{HI}(z)$? A reminder we'll further address the beginning of reionisation in Lecture 3.
2. **How** was it accomplished, i.e. by which sources, luminous or feeble galaxies and/or AGN?

In addressing **when**: the quasar Lyman α forest shows a declining HI opacity down to $z = 5.3$. As it was often assumed reionisation ended at $z = 6$, the quasar observers are keen to point out their data requires neutral gas at this epoch. However, at some point defining an "end" corresponding to a precise $x_{HI} \equiv 0$ does seem somewhat arbitrary.

Regarding the beginning of reionisation, analyses of Planck and other data in the context of Λ CDM permits some level of ionisation in the IGM beyond $z = 12$. A particularly significant development is the discovery of a Lyman α emitting galaxy at a redshift $z = 13.0$ (Witstok et al., 2024) which implies the early existence of an ionised region.

In addressing **how**: the absence of strong luminosity trends in ξ_{ion} would suggest that feeble galaxies dominate the process, although a fundamental limitation remains our understanding of the escape fraction. As we will see in Lecture 2, while JWST observations suggest a much-increased number of AGN, most calculations suggest they still only provide a minor contribution to the reionisation budget. While the rapid change in x_{HI} below $z < 8$ makes an appealing case for a late AGN contribution, the uncertainties in many of these x_{HI} measures remain significant.

However, to end on a positive note, the continued increase in JWST spectroscopy will significantly improve the statistics of ξ_{ion} and its dependence on luminosity as well as claims for AGN activity in the overall galaxy population. Likewise projects like COSMOS-3D, EIGER and ASPIRE promise much improved statistics on how galaxies contribute to the ionised state of their local IGM. Finally, as discussed in Lecture 3, the Square Kilometre Array will contribute further to the galaxy-IGM connection via tomography of the 21cm line of hydrogen.

8 Recommended Reading on Cosmic Reionisation

Major Review Articles:

1. Loeb and Barkana (2001) - a classical theoretical review
2. Fan et al. (2006) - early quasar data and CMB discussion
3. Madau and Dickinson (2014) - classic article on galaxy demographics
4. Dijkstra (2014) - Lyman alpha emission as a probe of reionisation
5. Stark (2016) - galaxies in first billion years
6. Ouchi et al. (2020) - analyses of Lyman alpha emitters
7. Fan et al. (2023) - updated review of quasars and IGM

Pre-JWST articles

1. Robertson et al. (2015) - HST galaxy demographics in context of Planck CMB
2. Planck Collaboration et al. (2020) - final constraints on reionisation
3. Greig and Mesinger (2017) - fits to Planck in context of Λ CDM
4. Naidu et al. (2020) - proposes special role of luminous sources
5. Garaldi et al. (2022) - *THESAN* radiation-hydro simulations

JWST review articles (so far)

1. Adamo et al. (2024) - review written by selected attendants at ISSI Breakthrough Workshop held in Bonn, March 2024
2. Stark et al. (2025) - review by Stark, Topping, Endsley & Tang submitted to Encyclopaedia of Astrophysics, November 2024

Lecture 2: Galaxies in the Reionisation Era

1 Introduction

Following my introduction in Lecture 1, it is worth understanding how we arrived at this remarkable period in observational astronomy where it has become possible to secure spectra of such quality that we can contemplate measuring the history of chemical enrichment in the universe back to the emergence of the first stellar systems. Over my own career (1974 to the present), I have witnessed the subject of galaxy evolution transition from simply counting faint galaxies on photographic plates without any statistically-sound information on their redshifts (late 1970s), through the first spectroscopic surveys probing barely to a redshift $z \approx 1$ (late 1980s), the launch and repair of Hubble Space Telescope (HST) (1990-93), the development of 8-10 metre class telescopes (late 1990s - early 2000s) to the promise of mid-infrared and sub-mm facilities such as the Spitzer Space Telescope, the James Clerk Maxwell telescope and ultimately the Atacama Large Millimetre Array (ALMA). JWST represents the final chapter in this remarkable revolution in observational capability and, some might argue, the largest single leap in performance over this dramatic half century of progress.

Underpinning this story is one common factor - technological development. Focusing on a few of these technical revolutions that, in my opinion, transformed the field, I begin with the *Charge Coupled Device (CCD)* which arrived on 4 metre class telescopes in the early 1980s. The initial examples were humble devices in a 256×256 pixel format but with sensitivities ≈ 30 -50 times that of hyper-sensitised photographic emulsions. This led to a major revolution in photometric measures of faint galaxies. One ultimate example of this development is the HyperSuprimeCam imaging system on the 8.2 metre Subaru telescope (Miyazaki et al., 2018) comprising a mosaic of 116 2048×4096 CCDs which has completed an exquisite deep survey of 1500 deg^2 (Figure 18). The CCD era may soon be over as the number of manufacturers is limited and most commercial imaging systems now use lower noise Complementary Metal-Oxide-Semiconductor (CMOS) detectors.

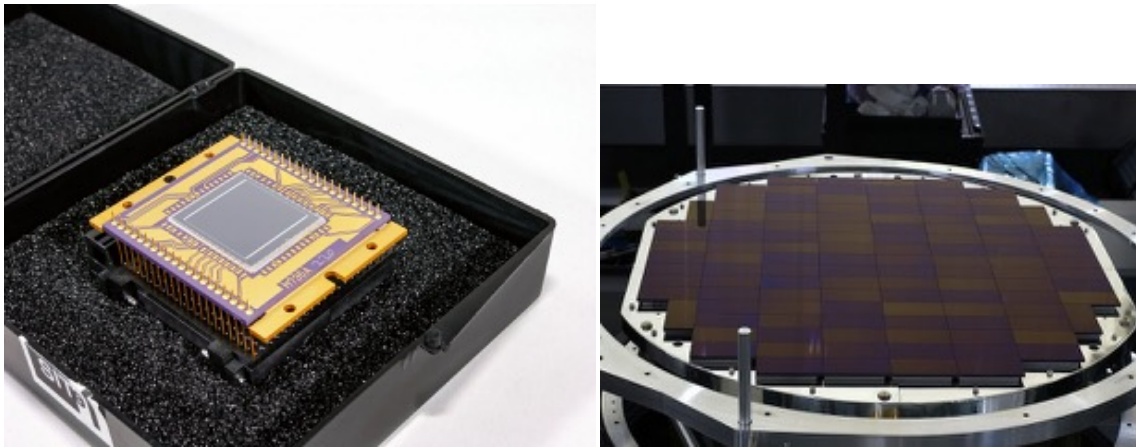


Fig. 18 *The revolution in astronomical detectors. (Left) A Charge Coupled Device (CCD) of modest format from the early 1980s. Such digital detectors have quantum efficiencies 30-50 times those of the earlier hyper-sensitised photographic plates. (Right) The Hyper-Suprime Camera on the 8.2 metre Subaru telescope (Miyazaki et al., 2018). This remarkable 870 Megapixel camera comprises a mosaic of 116 CCDs and can capture the entire Andromeda spiral galaxy in a single exposure.*

My second major development is *multi-object spectroscopy* (see Figure 19). The pioneering work to chase the cosmic expansion history using clusters of galaxies with the venerable 200-inch Hale telescope on Mount Palomar involved long slit spectroscopy on single targets, often with multiple night exposures. Multi-object spectroscopy using fibre optic couplers and machine-milled multi-slit masks in the telescope focal plane emerged in the mid-1980s. The former led to major discoveries in large scale structure via the Sloan Digital Sky Survey (SDSS) conducted on a dedicated 2.5 metre telescope and the 2 degree Field Redshift Survey on the Anglo-Australian Telescope; the latter demonstrated the power and efficiency of a robotic positioner with 400 fibres for the first time. Multi-slit masks can also be fabricated for imaging spectrographs providing resolved spectroscopy and improved sky subtraction for fainter sources. The final example of this revolution is the integral field unit (IFU) whereby a spectrum is produced for every point in a (typically) restricted field of view. This has been very effective in discovering line emitting galaxies without any prior imaging survey. A highly-readable account of the development of the IFU is given by Bacon (2024) who pioneered the MUSE instrument on ESO's VLT. Unlike HST, JWST's instrumentation suite was developed to take advantage of the progress that followed the use of multi-object facilities on ground-based telescopes, e.g. in NIRSpec's Micro-Shutter Assembly (MSA) which represents an automated version of the multi-slit mask, and integral field capabilities on NIRSpec and MIRI.

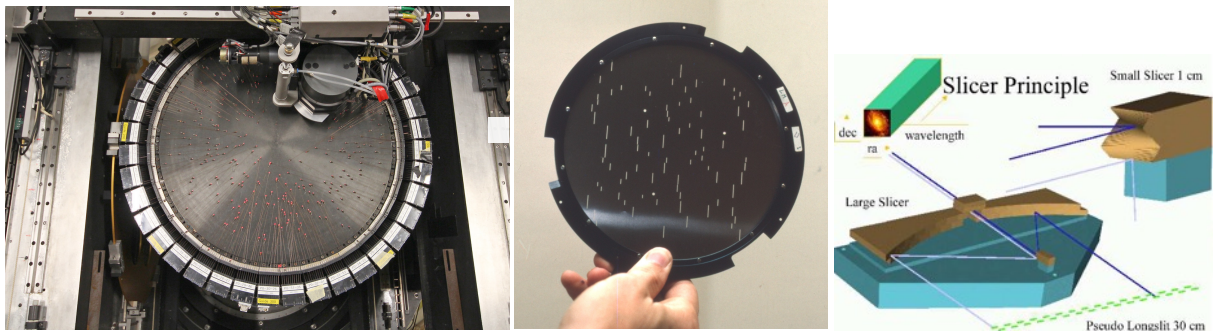


Fig. 19 Technologies for multi-object spectroscopy: (Left) The automated 400 fibre positioner for the 2 degree field facility at the prime focus of the Anglo-Australian Telescope. (Centre) A multi-slit mask for a ground-based imaging spectrograph. (Right) The image slicer concept for the MUSE integral field spectrograph on ESO's Very Large Telescope.

The final major development that greatly contributed to progress was the construction of 8-10 metre class telescopes in the 1990s. Alongside the development of large monolithic primary mirrors with active support (e.g. for the twin Gemini and four Unit Telescopes comprising ESO's Very Large Telescope) was the pioneering concept of a large segmented primary at the Keck observatory which demonstrated the way forward for ESO's Extremely Large Telescope, a 39 metre facility now nearing completion. The addition of laser guide star based adaptive optics led to angular resolutions better than HST which, when coupled with larger aperture and integral field spectrographs, led to resolved kinematics of $z > 2$ galaxies.

Of course, powerful facilities are not, by themselves, sufficient to guarantee progress. New ideas and scientific intuition are essential for discoveries. In this category I have selected three developments that accelerated our understanding of galaxy evolution. The first is the demonstration and subsequent application of the *Lyman break technique*. Although championed very effectively by Chuck Steidel and colleagues (Steidel et al., 1995, 1996), the idea of using the Lyman continuum discontinuity to provide a redshift indicator can be traced to discussions of the "faint blue galaxy problem" by Tyson and Guhathakurta (Guhathakurta et al., 1990). The photometric drop-out method has been extraordinarily effective in pre-selecting galaxies for spectroscopic study and providing redshift-dependent measures of the galaxy luminosity function and star-formation rate density. It spawned the entire field of photometric redshift determination and SED fitting from multi-colour broad band imaging which was not originally anticipated as a goal of HST imaging.

A second development worthy of note was the first *Hubble Deep Field (HDF)* proposed by Bob Williams, Director of the Space Telescope Science Institute, in 1996. Williams had the ambitious vision of creating a very deep publicly-available multi-colour dataset that would galvanise and inspire the extragalactic community. Despite concerns from respected senior colleagues that such an image would waste a large amount of observing time so soon after the embarrassment of HST's mis-shaped primary, it was a huge success and spawned an international effort with the Keck telescope to secured redshifts for hundreds of faint galaxies (Figure 20). This HDF led to a sequence of several further deep fields in the 2000s and similar programmes with JWST. The HDF story is described in detail in Williams' popular account which can be found online¹

The final scientific advance worth highlighting is when *strong gravitational lensing* became a standard tool of the observational astronomer. Lensing was an obscure field of study until 1988 when Genevieve Soucail and colleagues in Toulouse used the Canada France Hawaii Telescope (CFHT) to demonstrate that the puzzling arc-like feature in the $z=0.37$ cluster Abell 370 was a galaxy at a redshift $z=0.72$ distorted and magnified by the foreground cluster (Soucail et al., 1988); see also a review of the early history by Treu and Ellis (2015). HST's improved image quality revealed numerous examples of morphologically similar, multiply-imaged, lensed galaxies in other clusters and the development of mass models for the lensing clusters sufficiently precise they could even be used to estimate redshifts based purely on their geometrical positions (Kneib et al. (1996); Ebbels et al. (1998), Figure 21). Strong lensing not only magnifies distant galaxies enabling probes of the galaxy luminosity function to fainter luminosities (Lecture 1) but also enlarges them enabling resolved kinematic studies with integral field spectrographs. As a result, the phenomenon has contributed significantly to our understanding of early galaxy formation and evolution. During 2013-16, HST conducted the Frontier Fields Survey (Lotz et al., 2017), an ambitious programme of multi-band imaging through six lensing cluster to exploit this phenomenon. Cluster lensing has also featured prominently in Early Release Science programmes with JWST, e.g. the GLASS survey (Treu et al., 2022).

2 Pre-JWST results confirmed by JWST

The most basic observable for probing the reionisation era is the redshift-dependent comoving abundance of star-forming galaxies. Through the succession of HST deep fields and the Frontier Field Survey discussed in Lecture 1, the evolving rest-frame UV luminosity function was derived using Lyman break selection to redshift $z \approx 10$ (Bouwens et al., 2022). Although the deep field and lensing searches, when

¹<https://iopscience.iop.org/book/mono/978-0-7503-1756-6.pdf>

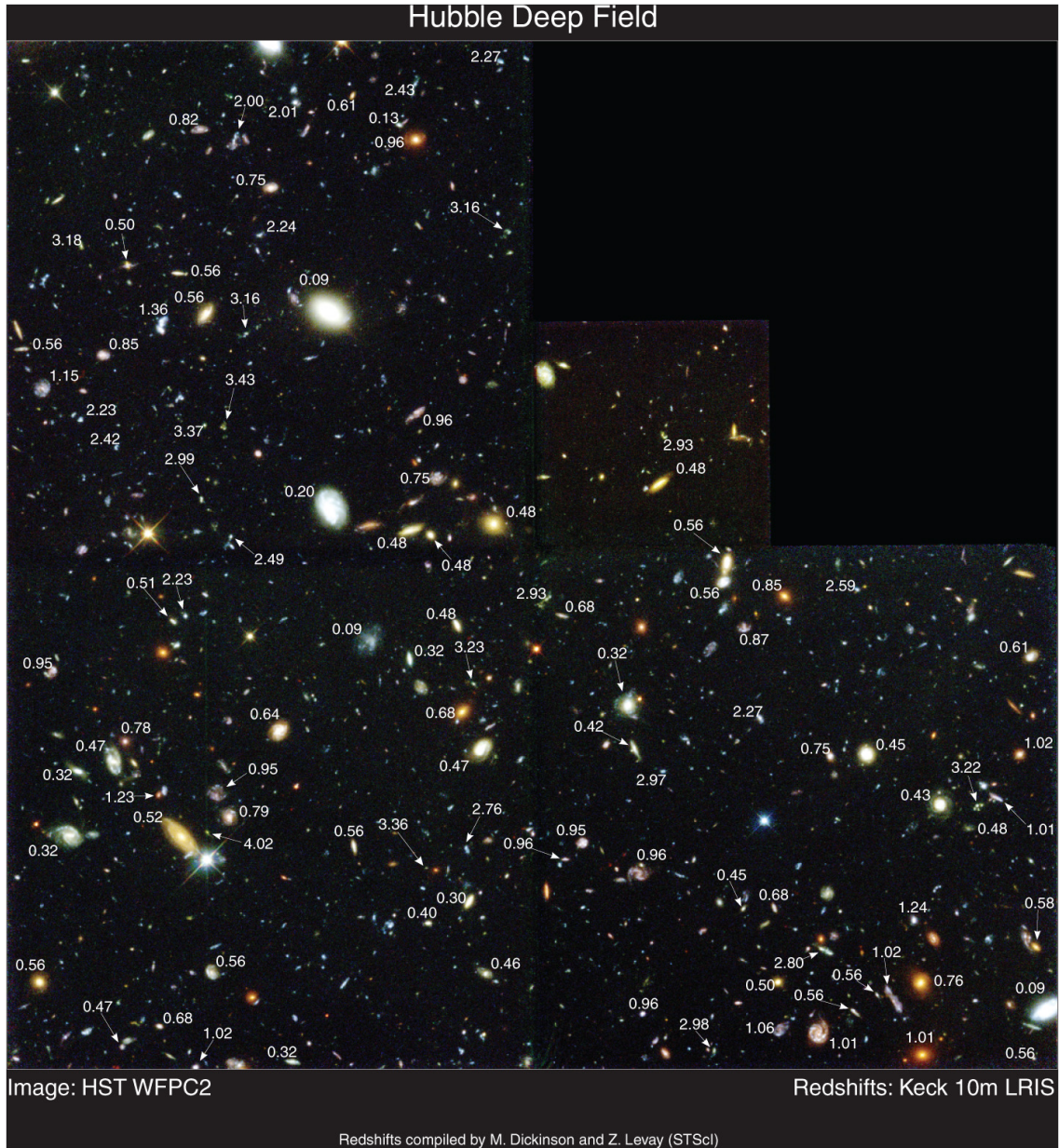


Fig. 20 *The Hubble Deep Field (HDF) taken in 1996 following the initiative of Bob William, Director STScI at the time. The public release of this spectacular WFPC2 multi-band image led to cooperation amongst Keck observers in securing spectroscopic redshifts for a large sample of galaxies. HDF also led to a pattern of subsequent deep fields taken with HST imaging cameras. (Courtesy of Mark Dickinson & Zolt Levay).*

considered independently, gave consistent results, there was debate in the community about the rate of decline in abundance beyond a redshift $z \approx 8$ (Figure 22). Models of galaxy assembly in standard Λ CDM cosmology together with a star formation rate (SFR) proportional to the baryon fraction in each dark matter halo predicted a steep decline in the SFR density over $8 < z < 10$. Oesch et al. (2018) argued this was consistent with the limited number of galaxies seen at redshifts $z \approx 9-10$ at the time. However, McLeod et al. (2016, 2021) predicted a continuous decline rate $\propto (1+z)^{-4.2}$ at variance with most theoretical models. The difference was surprising given both teams were using more or less the same observational data, disagreeing only on individual photometric redshifts and how the counts should be binned. The implications were important for JWST given the significant difference in the number of galaxies expected beyond $z \approx 10$.

Of course spectroscopic data is crucial, even if only at the most basic level to confirm the photometric redshifts. After over a decade of heroic efforts using Keck's MOSFIRE, VLT's X-shooter, the WFC3 grism on HST and ALMA, a total of only ≈ 60 spectroscopic redshifts was secured beyond a redshift $z=6$ collectively by the community. Such observations were usually taken at low spectral resolution and with low signal to noise in regions badly affected by intense airglow emission lines. Figure 23 contrasts the situation pre-JWST with a recent compilation of 1300 JWST spectroscopic redshifts. As we will discuss in Lecture 3, JWST soon resolved the earlier debate on the question

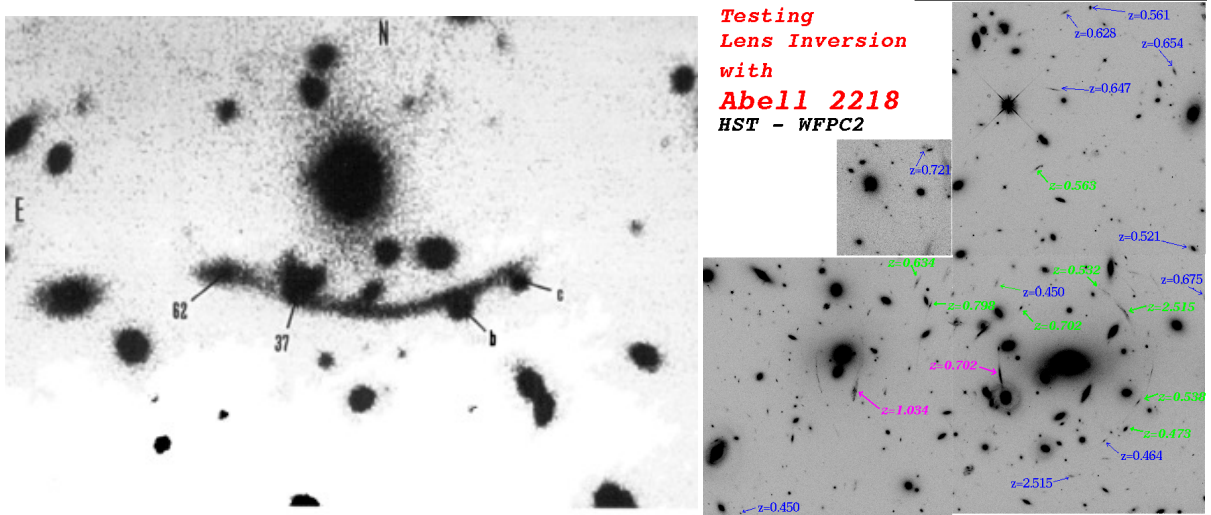


Fig. 21 The early promise of strong gravitational lensing. (Left) CFHT image of the giant arc in the cluster Abell 370 ($z=0.37$) which was spectroscopically confirmed to be a magnified and distorted image of a background $z=0.72$ galaxy by Soucail et al. (1988). HST image of the lensing cluster Abell 2218. HST's improved resolution enabled the recognition of multiple images of the same background source improving mass models sufficiently that their redshifts could be estimated geometrically and later verified spectroscopically e.g. Ebbels et al. (1998).

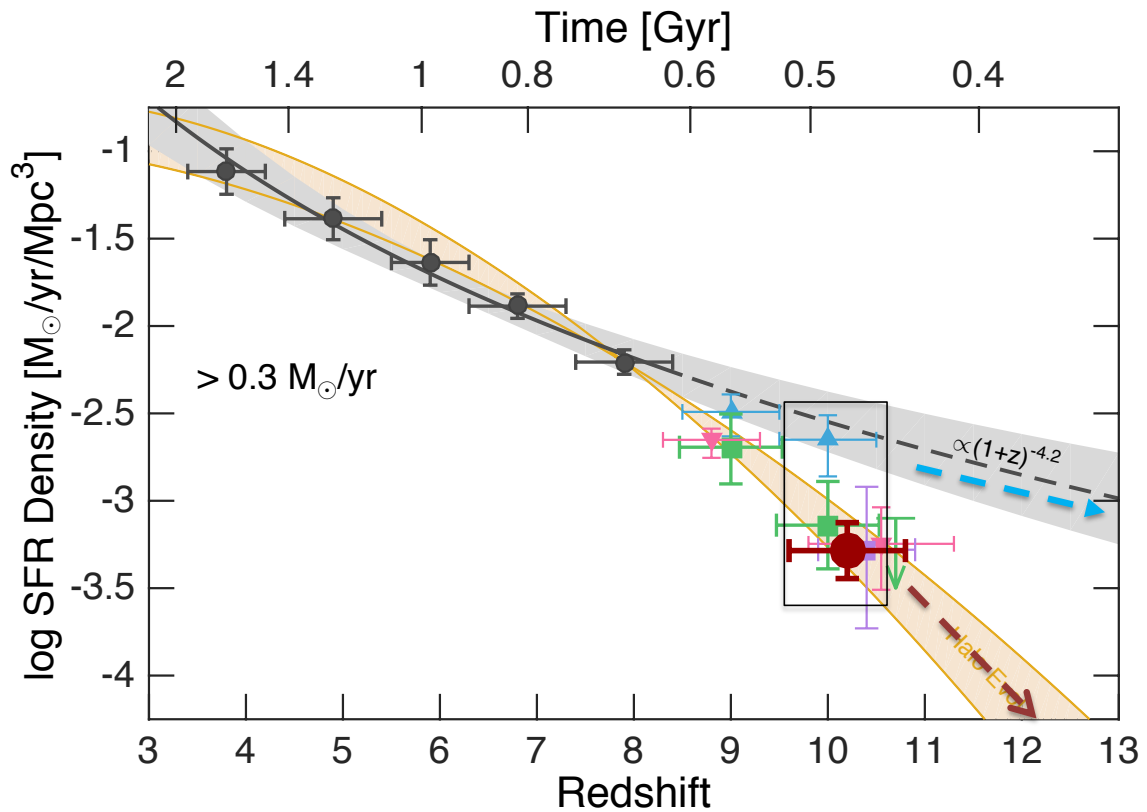


Fig. 22 A pre-JWST census of the redshift-dependent comoving star formation rate density of galaxies derived from rest-frame UV luminosities in all HST deep fields and the lensing Frontier Field clusters (Oesch et al., 2018). The maroon arrow indicates the declining density proposed by Oesch et al. (2018) which matched a theoretical prediction based on a constant star formation efficiency (see text and Lecture 3). The blue arrow indicates a more gradual decline rate proposed by the analysis of McLeod et al. (2016). Clearly the difference in the inferred decline at $8 < z < 10$ made a considerable difference in predicting what JWST would find beyond a redshift $z \approx 10$.

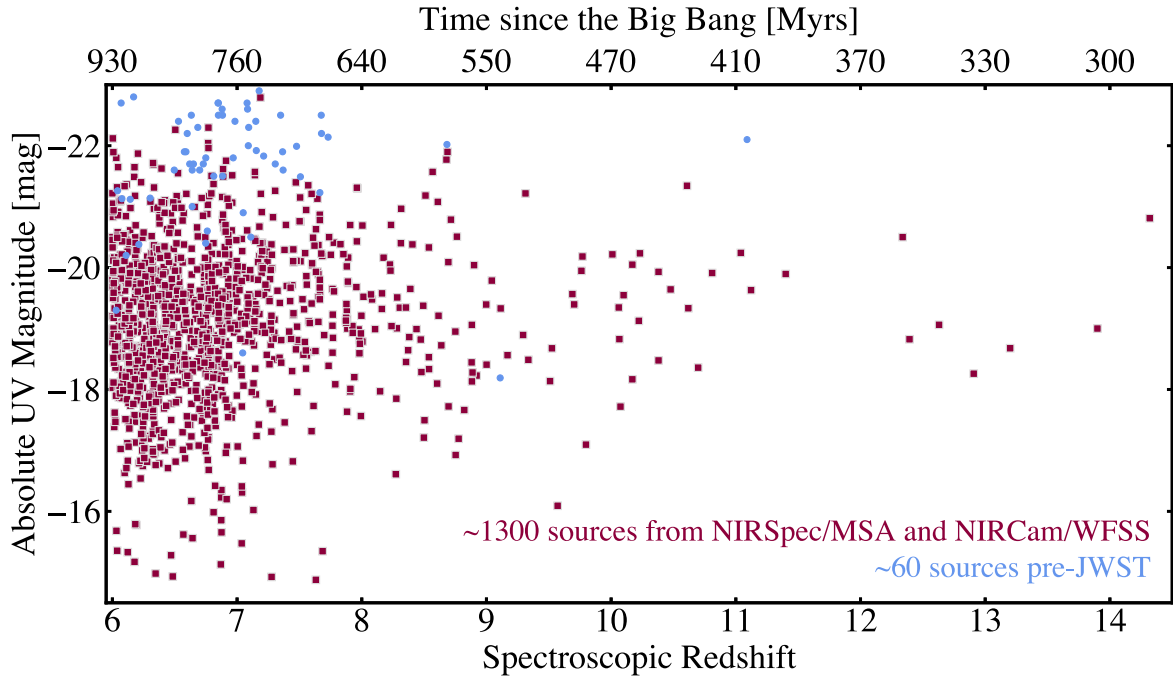


Fig. 23 The dramatic improvement in the $z > 6$ spectroscopic redshift dataset from pre-JWST observations (blue dots) to JWST (maroon) as of January 2025. Note also the wider range in luminosity probed within the late reionisation era $z \approx 6-8$ (Courtesy of Guido Roberts-Borsani).

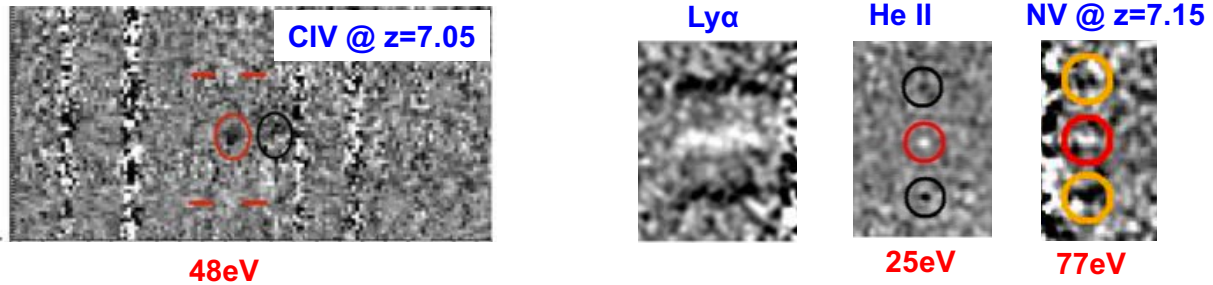


Fig. 24 Evidence for hard radiation fields from high ionisation emission lines and possible AGN from broad $\text{Ly}\alpha$ emission at $z > 7$ in the reionisation era based on challenging observations with Keck prior to JWST (Stark et al., 2015, 2017; Laporte et al., 2017). Characterising the role of AGN in the reionisation era remains a major JWST activity (see Section 5).

of the $z > 10$ census by locating sources to $z = 14$ and beyond.

Given the vastly improved quality of present-day JWST spectroscopy, it might be tempting to disregard all early pre-JWST articles as inconsequential but, in fact, important results emerged which have stood the test of time. Despite the observational challenges, ground-based spectra revealed emission lines indicative of hard radiation fields and the possible presence of active galactic nuclei at $z > 7$. Figure 24 shows examples of emission in high ionisation lines from CIV (48 eV), NV (77 eV) as well as broad $\text{Ly}\alpha$ (Stark et al., 2015, 2017; Laporte et al., 2017) using ground-based telescopes.

A second important result was the early use of broad-band photometry to trace the presence of intense [O III] emission at redshifts $z \approx 7-9$ using Spitzer $4.5\mu\text{m}$ photometry. Four such candidate [O III] emitters were located in the CANDELS fields. Whilst [O III] was beyond spectroscopic reach with both HST and ground-based telescopes, spectroscopic redshifts were nonetheless secured for all four revealing Lyman α emission (Roberts-Borsani et al., 2016) (Figure 25). This is surprising given the IGM should be substantially neutral at these redshifts and, as discussed in Lecture 1, Lyman α should be highly attenuated by resonant scattering. The implication is that each [O III] emitter has, either on its own or together with nearby clustered sources, created a local ionised bubble enabling $\text{Ly}\alpha$ photons to propagate. Both results that demonstrated hard radiation fields and ionised regions in the heart of the reionisation era have been confirmed with subsequent JWST data.

It is also encouraging how the most distant known sources based on challenging observations made with HST and ground-based telescopes have been confirmed by JWST. Figure 26 compares the HST and JWST spectra of GNz-11, the brightest $z > 10$ Lyman break source

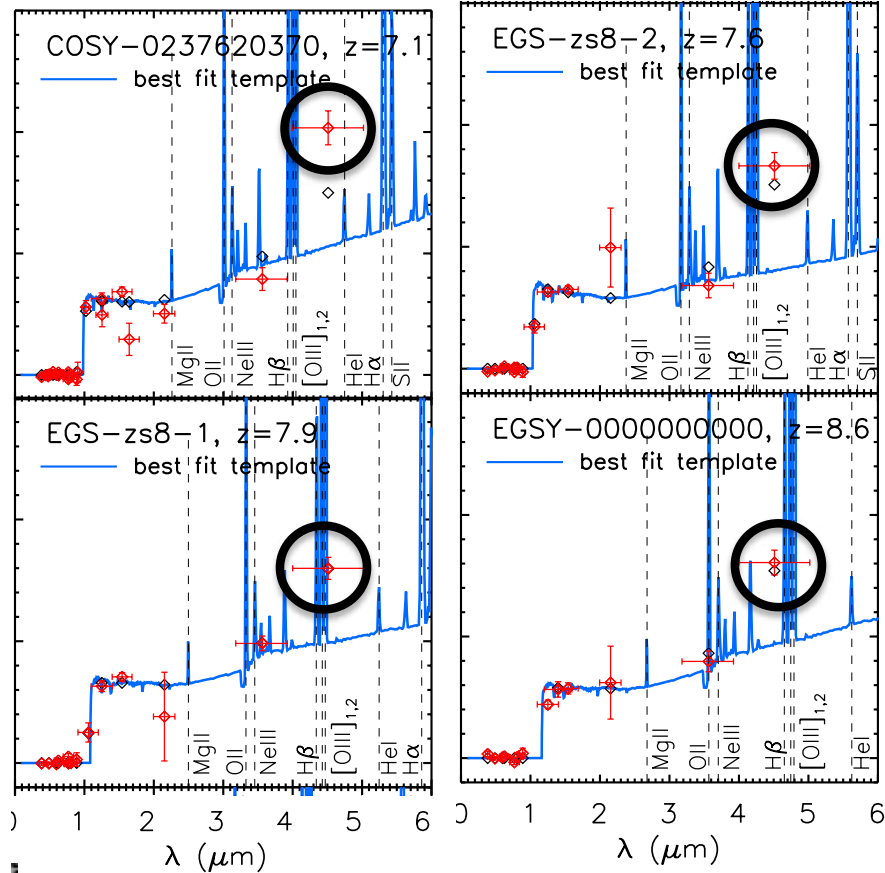


Fig. 25 The discovery of four intense $[O\ III]$ -emitting galaxies at $7 < z < 9$ via an excess flux (black circles) seen in the Spitzer $4.5\mu\text{m}$ band in their spectral energy distributions (Roberts-Borsani et al., 2016). Subsequent Keck spectra revealed all four show $\text{Ly}\alpha$ emission indicating they have created ionised bubbles in an otherwise neutral IGM. This work paved the way for comprehensive surveys of charting ionised bubbles using $\text{Ly}\alpha$ emission seen in JWST spectra e.g. Tang et al. (2024).

in the CANDELS field. Originally claimed to have a photometric redshift of $z=10.2 \pm 0.4$, a heroic 12 hour HST WFC3 grism observation proposed a spectroscopic redshift $z = 11.1 \pm 0.1$ (Oesch et al., 2016). A Keck spectrum suggested a similar redshift based on what transpired to be unlikely emission lines (Jiang et al., 2021). The 6.9 hour NIRSpect prism spectrum demonstrates dramatically the progress now possible with JWST revealing a prominent Lyman break at a redshift $z=10.603$ intermediate between Oesch et al’s photometric and spectroscopic claims (Bunker et al., 2023). An even more remarkable confirmation has been achieved for the most distant claimed source in the Ultra Deep Field (Ellis et al., 2013). This source was only seen in the F160W filter and its absence in the F140W led to two possible explanations - either a Lyman break within the narrow portion of the broad F140W filter transmission that is not covered by the F160W filter, or an unusually strong emission line in the F160W filter e.g. $\text{H}\alpha$ at $z \sim 1$. Naturally the claim for a photometric redshift of $z=11.9 \pm 0.3$ based on a detection in a single filter was viewed with some skepticism! However, JWST has confirmed a spectroscopic redshift $z=11.1$, making this retrospectively the most distant source detected by HST.

3 Physical Properties

We will first introduce the methods in common use to derive the most important physical characteristic for galaxies in the reionisation era and then discuss the results in the context of the emerging picture of galaxy evolution.

3.1 Stellar Population Synthesis Models

At the heart of most analyses of galaxy properties is the *stellar population synthesis (SPS) code* whose goal is to fit the spectral energy distribution and/or spectrum of a galaxy in the context of a model which incorporates theoretical tracks or “isochrones” of how stars evolve on the Hertzsprung-Russell diagram according to an assumed initial mass function and metallicity for various star formation histories (SFH). The foundation of this method was established by Beatrix Tinsley (1941-81) and her contribution can be found in a remarkably detailed

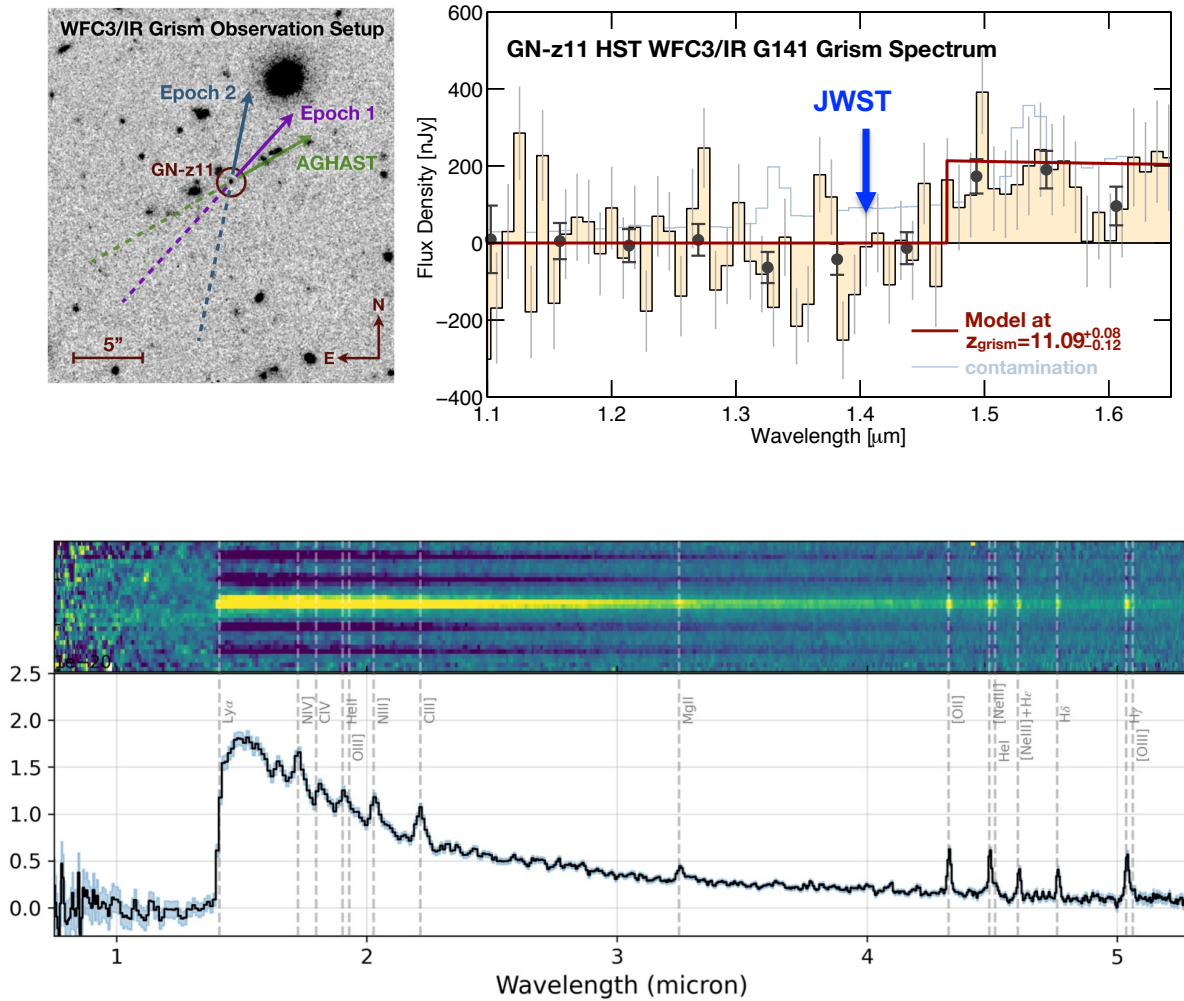


Fig. 26 A comparison of the HST grism and JWST NIRSpect spectrum of the $z=10.603$ galaxy GNz-11, dramatically illustrating the remarkable progress possible with JWST. The sole feature in the 12 hour HST grism spectrum is the Lyman break, which offers a crude redshift indicator ($z=11.1 \pm 0.1$) because of the uncertainty of a Lyman damping wing (Oesch et al., 2016). By contrast the 6.9 hour JWST spectrum locates an abundance of diagnostic emission lines yielding a precise redshift of $z=10.603$. (Bunker et al., 2023).

article (Tinsley, 1980a) which, although in a rather obscure journal, has conveniently been resubmitted on the archive².

Popular variants of this basic method in common use include (NB: not an exhaustive list):

1. *Bruzual & Charlot* - (Bruzual A. and Charlot, 1993): A series of empirical models developed from 1980 with regularly updated stellar spectra predicting integrated colours and spectra for various SFHs including single bursts (a.k.a. simple stellar populations, SSP), constant SFR (so-called “c-models”), exponentially-declining SFRs (so-called “ τ models” with $\text{SFR} \propto e^{-\tau}$).
2. *Conroy & Gunn* - (Conroy and Gunn, 2010): The Flexible Stellar Population Synthesis (FSPS) code predicts SSPs for various stellar initial mass functions (IMF) and metallicities. The user can then combine these appropriately to create various SFHs. The allied code *Prospector* derives physical parameters from fits to observational data.
3. *BAGPIPES* - (Carnall et al., 2018): Analyses spectral energy distributions using the Bruzual & Charlot library of stellar spectra including nebular data from the *CLOUDY* code (Ferland et al., 2017) with Bayesian nested sampling to fit parameters from observations.

Conroy (2013) provides an excellent review of recent progress in SPS models. In Figure 27 I reproduce a figure from his review that nicely summarises how the input parameters (IMF, isochrones, library of stellar spectra) can be used to deliver a range of composite stellar populations which are fitted to the observational data (spectral energy distributions and/or spectra) to yield physical parameters including star formation rates, stellar masses, metallicities, measures of dust extinction and potentially star formation and chemical enrichment histories.

Whilst these codes represent a considerable investment of effort following decades of work assembling stellar spectra for the full range of masses, ages and metallicities and, as a consequence, are now standard tools in the literature, new researchers may be tempted to use them

²<https://arxiv.org/abs/2203.02041>

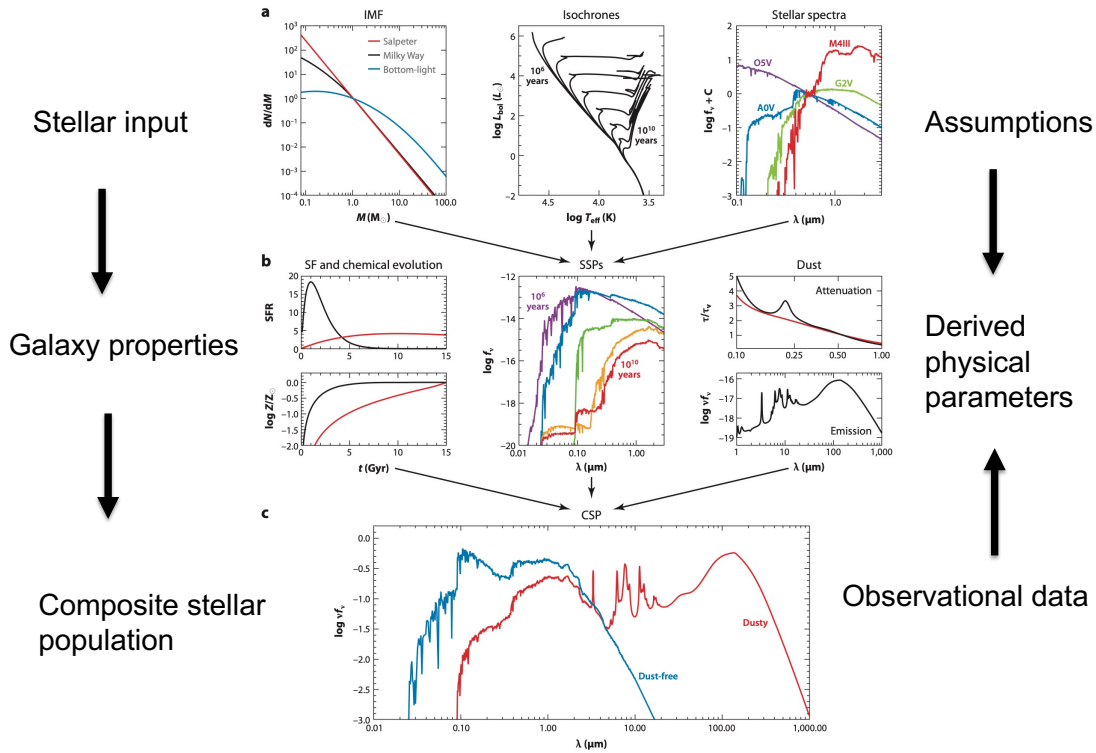


Fig. 27 A succinct summary of a process by which galaxy properties may be inferred from observations using stellar population synthesis models (Conroy, 2013). The input properties of stars include their initial mass function, isochrones which predict their luminosity and colour evolution for a given stellar mass and composition, plus observed spectra for the full range of masses, metallicities and ages. A range of star formation and chemical enrichment histories are then adopted that yield a large array of possible composite stellar populations and their spectra and SEDs. Associated codes optimally derive the various parameters by fitting the observations.

as a “black box” without fully appreciating the basic physics. So in what follows, I try to simplify the discussion so the key observational requirements and uncertainties are more apparent.

3.2 Star Formation Rates

Although in the local universe there are many independent probes of the star formation rate (SFR) of a galaxy including probes of radio emission from Type II supernova remnants and far-infrared measures arising from dust heated by young hot stars, in practice radio probes cannot yet be applied to meaningful samples at high redshift. The two main probes remaining are Balmer emission lines, notably $H\alpha$, and the rest-frame UV continuum (Kennicutt, 1998; Madau and Dickinson, 2014). $H\alpha$ emission in galaxies normally arises from gaseous HII regions heated by O stars whose main sequence lifetimes are less than 20 Myr. Accordingly it gives a near-instantaneous measure of the SFR. By contrast, the UV continuum luminosity (typically measured at 1500 \AA) arises from a broader range of stars whose main sequence lifetimes extend to ≈ 100 Myr. Both measures are affected by dust attenuation although that can be estimated using the Balmer decrement, $H\alpha/H\beta$. The UV continuum also depends on the stellar initial mass function and stellar metallicity which induces line blanketing at UV wavelengths. Comparisons of both $H\alpha$ and UV continuum-based measures in local samples reveal a scatter which can be used to infer the stochasticity of the star formation history (Sullivan et al., 2001).

3.3 Stellar Masses

For those of us studying high redshift star-forming galaxies, it is tempting to focus mostly on the rest-frame UV which, as we discussed above, has featured almost exclusively in constructing the census of early galaxies because detailed measures at longer wavelengths were beyond reach at high redshift with HST and ground-based observatories. However, low mass stars are far more abundant in all stellar populations and since they have long main sequence lifetimes, for extended star formation histories they accumulate over cosmic history thereby contributing significantly to the overall galaxy stellar mass. For a galaxy of a given stellar mass, the K-band ($2 \mu\text{m}$) brightness is largely independent of how that mass was assembled and so, to first order, is a reasonable proxy for the stellar mass. This is in marked contrast to the UV and optical colours which reflect only the younger stars (Kauffmann and Charlot, 1998). To accurately determine the stellar mass of galaxy it is thus very important to have observational data at rest-frame infrared wavelengths. At very high redshifts being probed by JWST, the rest-frame K band shifts to $10\text{--}20 \mu\text{m}$ which is only accessible with MIRI.

The technique for inferring stellar masses M_* in galaxies follows the approach discussed in Brinchmann and Ellis (2000). The spectral

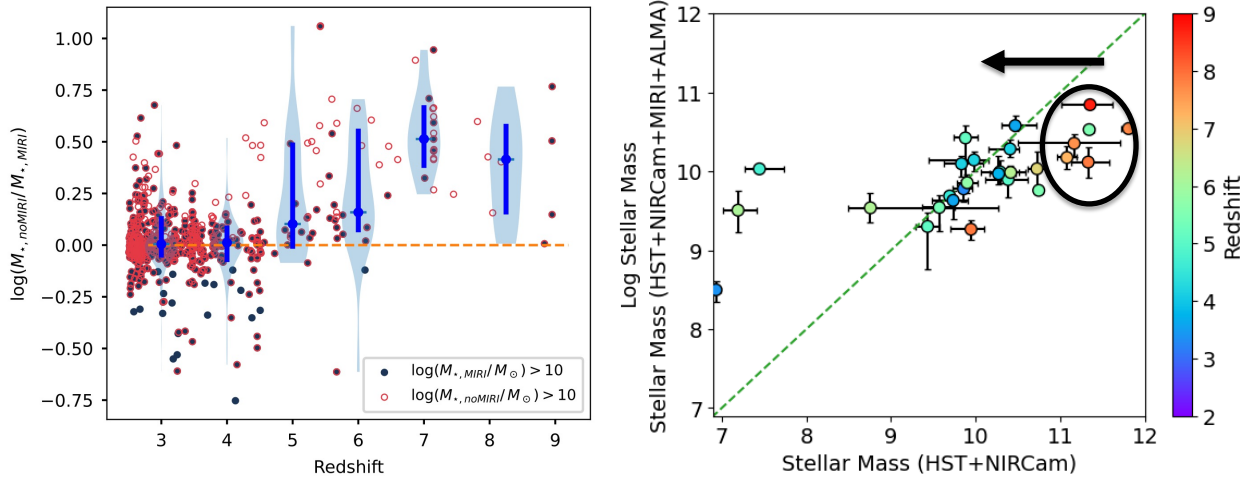


Fig. 28 The importance of MIRI photometry in estimating stellar masses in the reionisation era. (Left) The logarithmic difference between masses determined without and including MIRI as a function of redshift from Wang et al. (2024b). (Right) A direct comparison of MIRI+NIRCam and NIRCam-only masses from Williams et al. (2024). Due to an inability to break the degeneracy of SED fitting between age and dust content, NIRCam-only stellar masses at $z > 7$ can be overestimated by factors of $\times 3$ -5.

energy distribution (SED) is fit with SPS models to derive a mass/light ratio of the overall stellar populations e.g. for the K band this would be $(M_*/L)_K$. Given the redshift of the galaxy, the K-band luminosity L_K is known and hence the stellar mass can be determined. Despite the well-established importance of ensuring the rest-frame infrared is incorporated in SED fits, much of the recent literature on JWST stellar masses is still primarily derived only from NIRCam photometry. At $z > 7$ this corresponds to an upper rest-frame wavelength of only $\lambda < 6000 \text{ \AA}$. The dangers of not including MIRI data for galaxies beyond $z \approx 5$ have been illustrated by Wang et al. (2024b); Williams et al. (2024). Without MIRI data, masses are overestimated since, over the restricted rest-frame coverage available with NIRCam, there is a degeneracy between the effects of age and dust. As shown in Figure 28, this can amount to overestimates as large as a factor of $\times 3$ -5.

3.4 Stellar Ages

The age of a stellar population is naturally similarly affected if the underlying older, redder stars cannot be adequately probed. Numerous articles in the recent JWST literature have claimed $z \approx 7$ -8 galaxies are “young” with ages $< 10 \text{ Myr}$ but this likely represents the “outshining” effect whereby at rest-optical wavelengths the contribution to the SED is dominated by such young stars. Although it pre-dates the JWST era, this outshining effect was nicely illustrated for a sample of $z \approx 6.6$ -6.9 Lyman break galaxies using Spitzer $4.5 \mu\text{m}$ photometry (Whitler et al., 2023). Only by incorporating the Spitzer photometry is it possible to distinguish between a mean stellar age of 10 and 250 Myr. In this particular sample, 25% of the population has stellar ages greater than 250 Myr consistent with formation at redshifts $z \approx 9$ and earlier (Figure 29). A comprehensive demonstration of the dangers of outshining in analysing JWST photometry in the case of bursty star formation is given by Wang et al. (2025).

This is not to diminish the importance of age-related signatures in rest-frame optical spectra. The most significant feature of importance is the Balmer break which is most prominent for A-type stars whose ages are $< 500 \text{ Myr}$. The physical basis of this age-indicator is that hydrogen absorption in the outer atmospheres of stars is highly dependent on the star’s mass. At low stellar masses with cooler temperatures, the principal source of opacity is the negative hydrogen ion H^- , whereas in the most massive hot stars, the hydrogen is fully ionised. Only in the intermediate mass stars with lifetimes of several 100 Myr is this Balmer break visible. Again, it is easily diluted if there has been residual star formation within the last few Myr and even if the break is located it only provides a lower age limit for the stellar population.

High quality spectra are needed to locate and accurately measure this Balmer break. The interpretation of its strength from broadband photometry alone is often challenging due to contamination from rest-frame optical emission lines e.g. [O II]. The RUBIES JWST programme has demonstrated the presence of Balmer breaks in several reionisation-era galaxies and derived past SFHs extending to $z \approx 10$ and earlier (Figure 30, Wang et al. (2024a), see also Kuruvanthodi et al. (2024); Roberts-Borsani et al. (2024)).

3.5 UV continuum slopes and nebular contributions

The UV continuum slope is a further important diagnostic than can be derived either photometrically or spectroscopically. It is not only sensitive to the age of the actively star-forming population in high redshift galaxies, but also to the stellar IMF, dust content, metallicity and the ionising production rate (ξ_{ion} , see Lecture 1). Traditionally the slope β is measured between 1250 and 2600 \AA according to the following relation:

$$f_\lambda \propto \lambda^{-\beta} \quad (13)$$

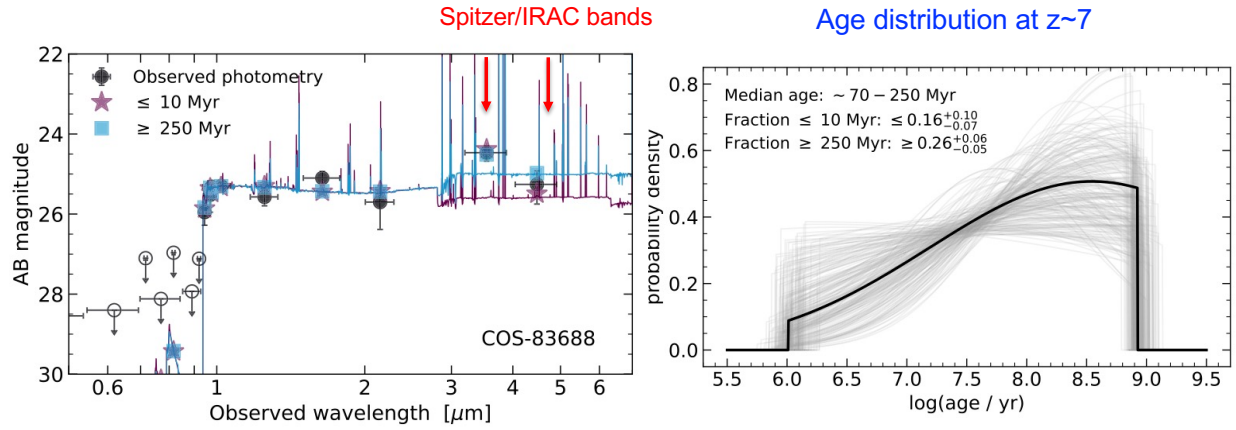


Fig. 29 Pre-JWST illustration of the important role of rest-frame infrared photometry in detecting old stars in actively star-forming galaxies at high redshift (Whitler et al., 2023). (Left) The SED of a $z=6.6$ galaxy where the Spitzer/IRAC 3.6 and 4.5 μm photometry indicates an excess flux which cannot arise from known emission lines and thus represents the continuum radiation from a population of old stars. Ages as diverse as 10 and 250 Myr cannot be distinguished from SED fits to the shorter wavelength data. (Right) Incorporating the Spitzer data for a sample of $6.6 < z < 6.9$ galaxies, the inferred star formation history indicates less than 16% are truly young (< 10 My) whereas at least 26% have ages > 250 Myr corresponding to redshifts of formation as high as $z \approx 9$.

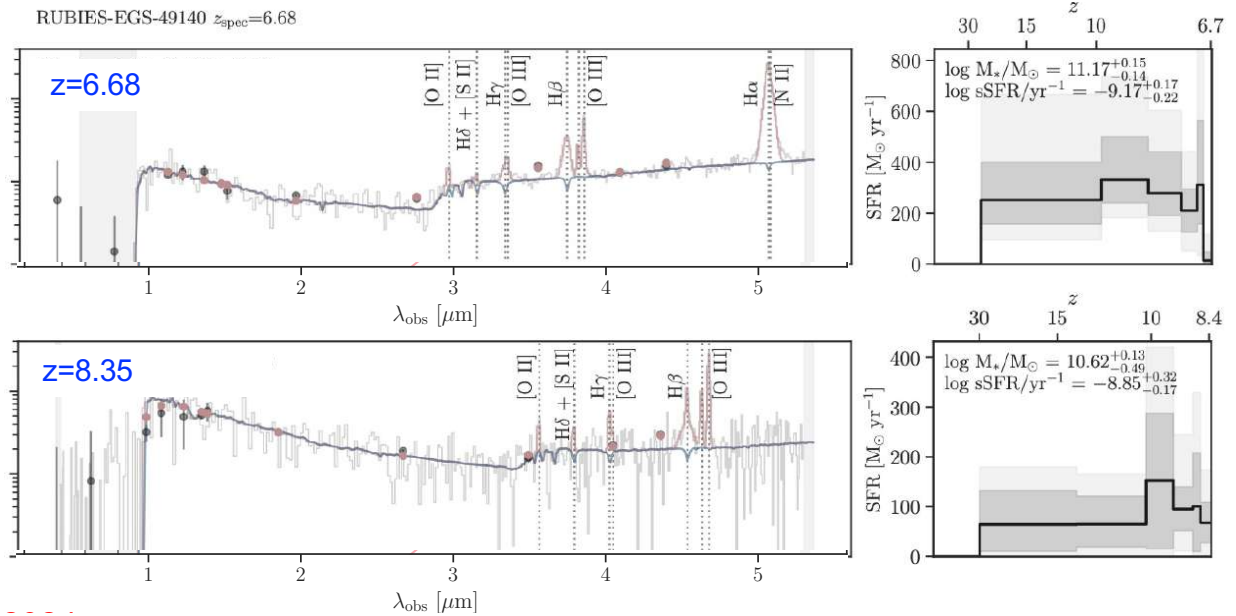


Fig. 30 The Balmer break as an age diagnostic (Wang et al., 2024a). (Left) Spectra and SED for two galaxies from the RUBIES programme which show clear evidence of both a photometric and spectroscopic Balmer break seen at $3 \mu\text{m}$. The feature arises only in stars with main sequence ages of several 100 Myr and thus can be used as a lower limit for the age of the stellar population. (Right) Inferred star formation histories for both galaxies indicating possible contributions beyond $z \approx 10$. (The sensitivity to activity at yet higher redshifts is limited.)

such that steeper UV slopes correspond to more negative values of β .

Stellar population synthesis models for an instantaneous burst of low metallicities predict $\beta > -3.0$ for a standard IMF. However, as young massive stars are capable of heating up the surrounding gas the slightly redder nebular continuum may also contribute, and when included the instantaneous limit becomes $\beta > -2.6$ (see Figure 31). First encountered astrophysically in planetary nebulae, hot stars can induce free-bound, free-free and two-photon continuous emission in gaseous hydrogen. Its presence can be distinguished from starlight via a negative Balmer jump and a UV downturn at 1400 \AA arising from two-photon emission (Katz et al., 2024). In the latter case two photons are emitted from the 2s to 1s data with a combined energy equivalent to the Lyman α transition (see centre right panel of Figure 31). The importance of the nebular continuum follows from its sensitivity to a top-heavy IMF which some believe may be a signature of Population III stars (Lecture 3). Convincing examples of galaxy spectra revealing nebular continuum emission are shown in the lower panel of Figure 31. Model fits to such spectra suggest the fractional contribution from nebular emission at 1500 \AA can be as high as 60%. Although a dominant

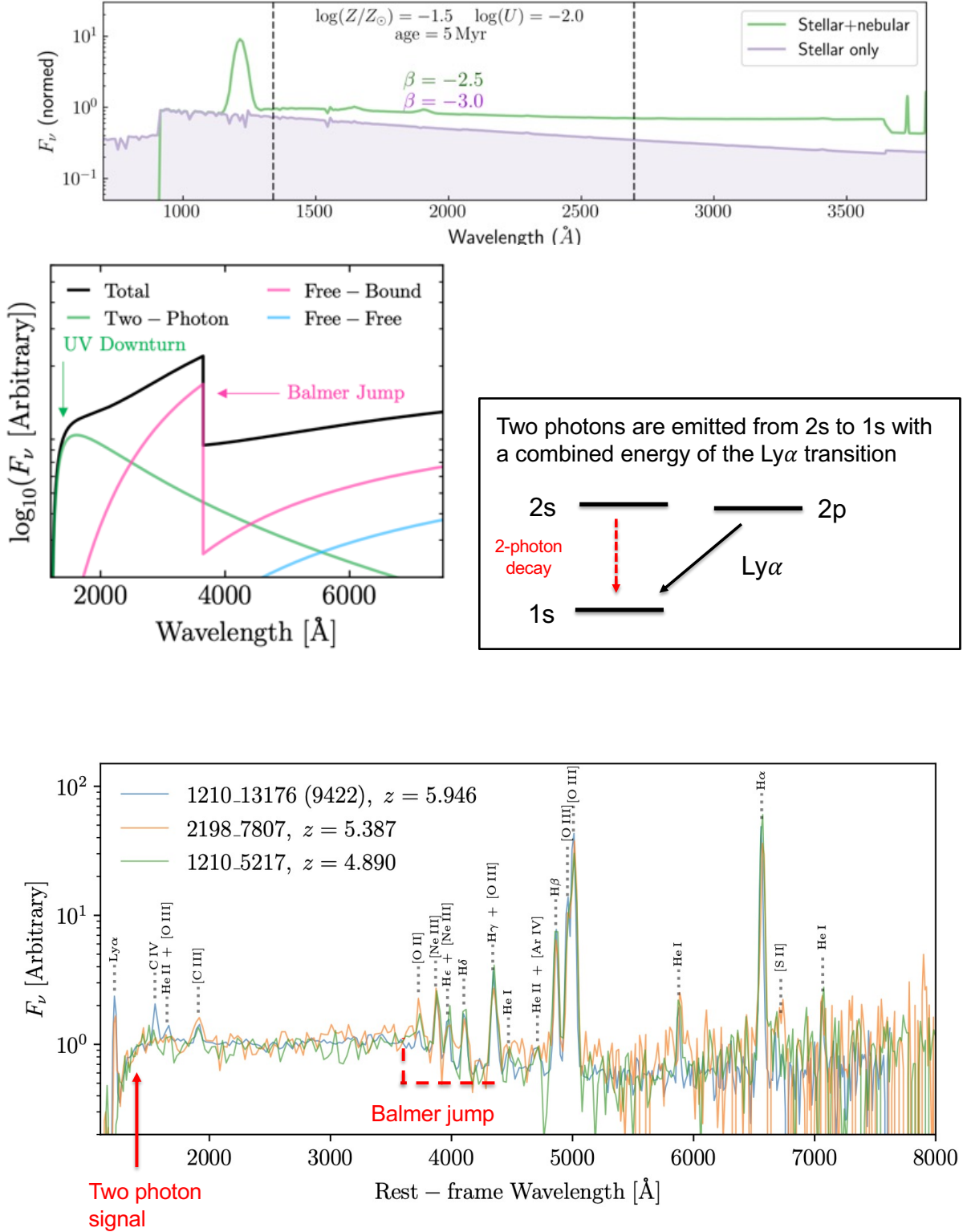


Fig. 31 Aspects of the UV continuum slope. (Top) Model UV spectrum for a instantaneous starburst illustrating the steepest UV slope β possible for a stellar only and stellar + nebular contribution (Saxena et al., 2024). (Centre left) Components of the nebular continuum which arise from free-free, free-bound and two-photon emission. The key observational features are a strong negative Balmer jump arising from free-bound emission and a UV downturn longward of Ly α arising from two-photon emission (Katz et al., 2024). (Centre right) Physical origin of two-photon decay. Two photons are simultaneously emitted from the 2s to 1s state of hydrogen which can break the normal selection rule if their combined energies equals that of Lyman α (2p to 1s). (Bottom) Spectra for three galaxies showing the negative Balmer jump and two-photon UV downturn (Katz et al., 2024).

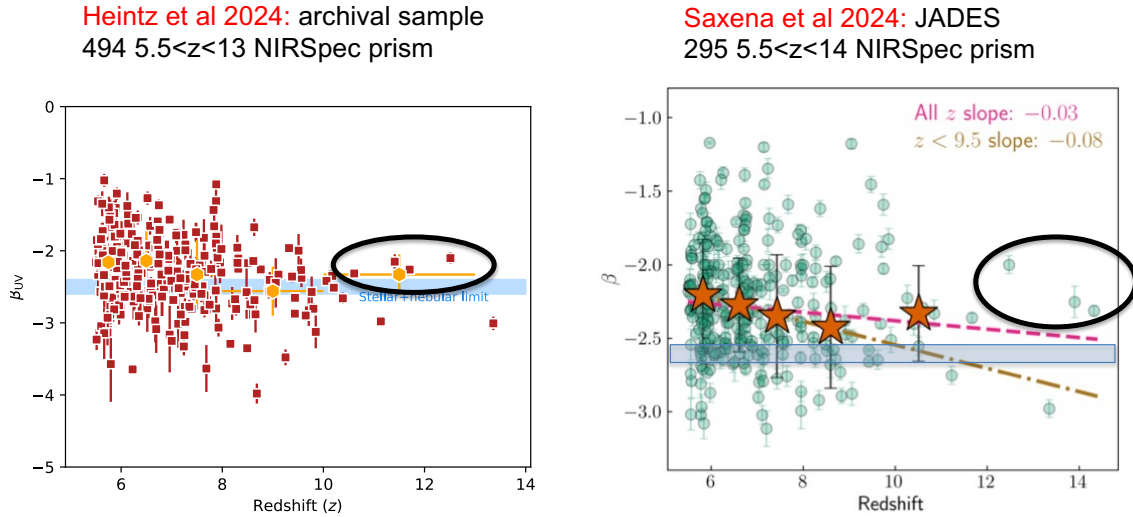


Fig. 32 Spectroscopic measures of the UV continuum slope β from archival data (Heintz et al., 2025a) and the JADES GTO programme (Saxena et al., 2024). The stellar + nebular limit of $\beta < -2.6$ for an instantaneous burst of star formation is indicated by the horizontal blue shaded line. Redshift-binned averages are shown as star symbols. There is a reasonably significant trend for steeper β with increasing redshift and a tentative upturn for $z > 10$ which may arise from an increasing contribution from a redder nebular contributions (highlighted in black).

nebular continuum would temporarily increase the UV luminosity of early galaxies, it will be challenging to identify such signatures at redshifts $z > 10$. Indeed, the downturn signature of two-photon emission is difficult to distinguish from damped Lyman α absorption.

The question of how the UV continuum slope β evolves with redshift has been the focus of much attention in the early years of JWST observations. There have been two basic approaches, each motivated by attempts to chart the effects of decreasing stellar age, metallicity and dust content with increasing redshift. Initially photometric measures had the advantage of large well-controlled samples but individual slope measures can be affected by (unseen) emission lines. Spectroscopic measures are more accurate as any strong emission lines can be masked. However, the spectroscopic samples were initially more modest and could be biased. A common technique is to compile a redshift catalogue from diverse JWST spectroscopic campaigns, each with different selection criteria. Inclusion of a galaxy in such a catalogue may depend on the star-formation rate and/or the presence of emission lines often essential for a robust redshift, possibly rendering the overall sample unrepresentative of the underlying population.

Early photometric studies (Cullen et al., 2023; Topping et al., 2024) found declining values of β over $8 < z < 14$ and steeper values for lower luminosity galaxies as might be expected if they are more metal-poor. However, many high redshift galaxies were found to have unphysically steep values (e.g. $\beta \simeq -4$) raising questions of accuracy or possibly significant Lyman continuum leakage. If the escape fraction f_{esc} (Lecture 1) is very high, clearly the nebular continuum will be weakened, permitting more extreme value of β . Generally speaking the trends are similar for the later spectroscopic studies (Heintz et al., 2025a; Roberts-Borsani et al., 2024; Dottorini et al., 2025), but with the benefit of less scatter and fewer unphysical values (Figure 32). $\beta(z)$ tends to asymptote to the required instantaneous value of -2.6 but it's interesting to note a marginal upturn to redder values for the small sample of $z > 10$ galaxies that may indicate an increased contribution from nebular continuum in young systems with very massive stars.

4 Chemical Evolution

Arguably the most important progress with JWST has been through spectroscopic studies of early galaxies. Although basic redshift measures were possible with the WFC3-IR grism on HST and some diagnostic indicators of ξ_{ion} and potential AGN activity followed ambitious exposures on Keck and VLT, the absence of atmospheric airglow in space and the multiplex gain of JWST's spectrographs has provided a major revolution. Here we focus on what has been learned in tracing the gas-phase chemical composition with increasing redshift (see Curti (2025) for a timely review).

A good example is the spectrum of a $z=7.66$ galaxy released shortly after science operations commenced in July 2022 (Figure 33, Schaerer et al. (2022); Curti et al. (2023)). For the first time in the reionisation era, JWST provides access to the familiar strong nebular emission lines of [O III] 4959 and 5007 Å and Balmer H β , which have underpinned metallicity measures for almost a century. However, of greater significance is the detection of the weak auroral [O III] line at 4363 Å which provides a crucial calibrating measure of the electron temperature T_e . Prior to JWST, observers struggled to calibrate gas phase metallicities derived from the strong [O III] lines and had to rely on local T_e measures which were unlikely to be representative at high redshift. Similar progress with T_e -sensitive auroral lines has been accomplished for other atomic species.

Before discussing the recent JWST progress, let us recap on the likely timescale of enrichment for the various chemical elements we can

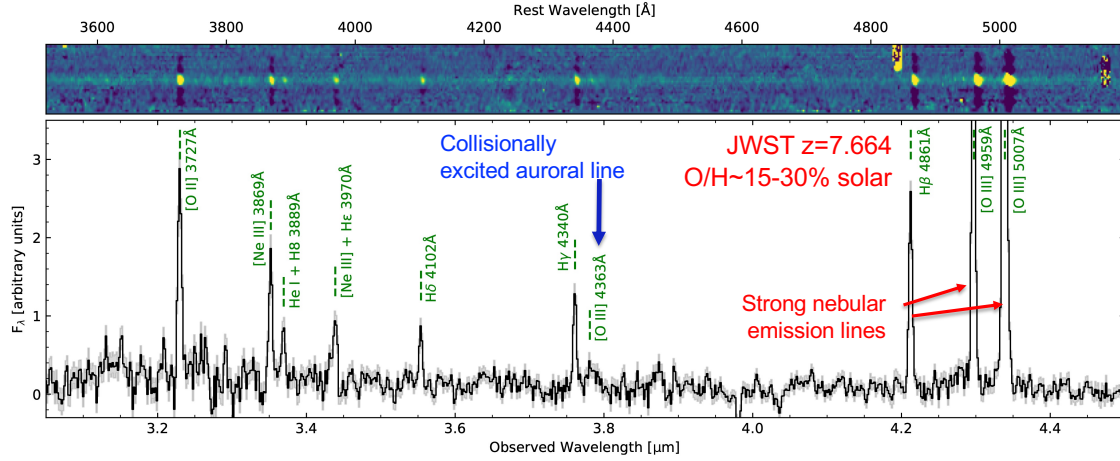


Fig. 33 The rich emission line JWST spectrum of a $z=7.66$ galaxy taken in the early period of operations (Schaerer et al., 2022; Curti et al., 2023). In addition to the familiar rest-frame optical lines of [O II], [O III] and Balmer H β which have formed the basis of metallicity measurements from strong line ratios for decades, the detection of the T_e -sensitive collisionally-excited auroral line of [O III] 4363 Å can be used to calibrate strong-line data in the reionisation era.

detect in JWST spectra. Heavier nuclei are formed continuously via hydrostatic burning in the cores of all stars during their lifetimes. This includes hydrogen to helium while on the main sequence and progressively heavier elements up to iron during various stages of post-main sequence burning depending on the stellar mass. Although mass loss during the asymptotic giant branch (AGB) phase contributes to the enrichment of the interstellar medium, explosive nucleosynthesis that occurs during the final stages of supernovae is the most important mechanism. The so-called α elements (C, O, Mg, Ne, S, Si) are promptly produced in Type II supernovae following the death of short-lived massive stars. In contrast, iron-peak nuclei are produced more slowly in Type Ia supernovae which result from the destruction of a low mass white dwarf whose stellar lifetime is much longer. As we proceed towards stellar systems whose ages are less than a few hundred million years at redshifts $z > 10$, we expect little enrichment from AGB mass loss and Type Ia supernovae (Maiolino and Mannucci, 2019) (Figure 34).

How then do we estimate the chemical abundances from an emission line spectrum? In general an emission line flux $F(\lambda)$ is the product of the ionic abundance Z_{ion} and an emissivity function ϵ

$$F(\lambda) = Z_{ion} * \epsilon(T_e, n_e) \quad (14)$$

the latter of which depends on the physical conditions in the gas, particularly the electron temperature and density. The derived abundance of the element Z follows corrections for the ionic fraction observed and is usually quoted with respect to the hydrogen abundance measured from recombination lines, i.e. Z/H . When quoted on a logarithmic scale with respect to the solar abundance ratio, it is placed in square brackets, e.g. $[O/H] = -1.0$ would indicate an oxygen abundance of 10% solar. Another convention is to quote the abundance on a scale where $H=12$, e.g. $12 + \log(O/H) = 7.6$ would also represent an abundance of oxygen 10% solar given the sun's oxygen abundance is $12 + \log(O/H) \approx 8.6$.

We can estimate the abundances of various species in two ways, via collisionally-excited lines (CEL) or recombination lines (RL). As the collisionally-excited lines are usually much stronger, this is the common method using auroral lines of high principal quantum number n e.g. [O III] 4363 Å to determine T_e and other doublet line ratios e.g. [O II] 3727 Å to determine n_e . Although the RL method is less sensitive to T_e , it is currently only practical for certain species (C, N, O) in nearby galaxies. To illustrate the CEL method, Figure 35 shows the auroral calibration for three popular strong line ratios for SDSS survey galaxies. It can be seen that some of the line ratios are double-valued in terms of the derived abundance (Curti et al., 2017). The real breakthrough with JWST has been the ability to identify such auroral lines at high redshift which has enabled us to bypass assuming such local T_e, n_e calibrations for the various strong emission line ratios. Sanders et al. (2024) first applied this to a sample of 16 galaxies at $z > 6$ which, together with examples in the literature, provided a dataset of 46 galaxies over all redshifts. As expected, there is evidence of a redshift-dependence in the calibration implying T_e changes, although most of the evolution occurs over $0 < z < 2$ (Figure 36, see also Chakraborty et al. (2025)).

Unfortunately, when we compare the CEL and RL abundances for nearby galaxies, they disagree by about 0.25 dex (left panel of Figure 37). Although the origin of this discrepancy is unclear, it may imply there are spatial fluctuations in T_e within the ISM of galaxies and thus when we detect weak [O III] 4363 Å we may be biased to regions of high T_e (García-Rojas and Esteban, 2007; Méndez-Delgado et al., 2023). ALMA may be able to assist, since there are sub-mm emission lines e.g. [O III] 88 μ m and 52 μ m which are much brighter and accessible at high redshift that can be used in combination to control such biases (Jones et al., 2020). Comparing Herschel [O III] 88 μ m and SDSS [O III] 4363 Å calibrations there is a large scatter which might support this explanation (centre panel of Figure 37).

Furthermore, for the small number of $z \approx 6-7$ galaxies for which both JWST [O II] 3727 and 4363 Å and ALMA 88 μ m and 52 μ m

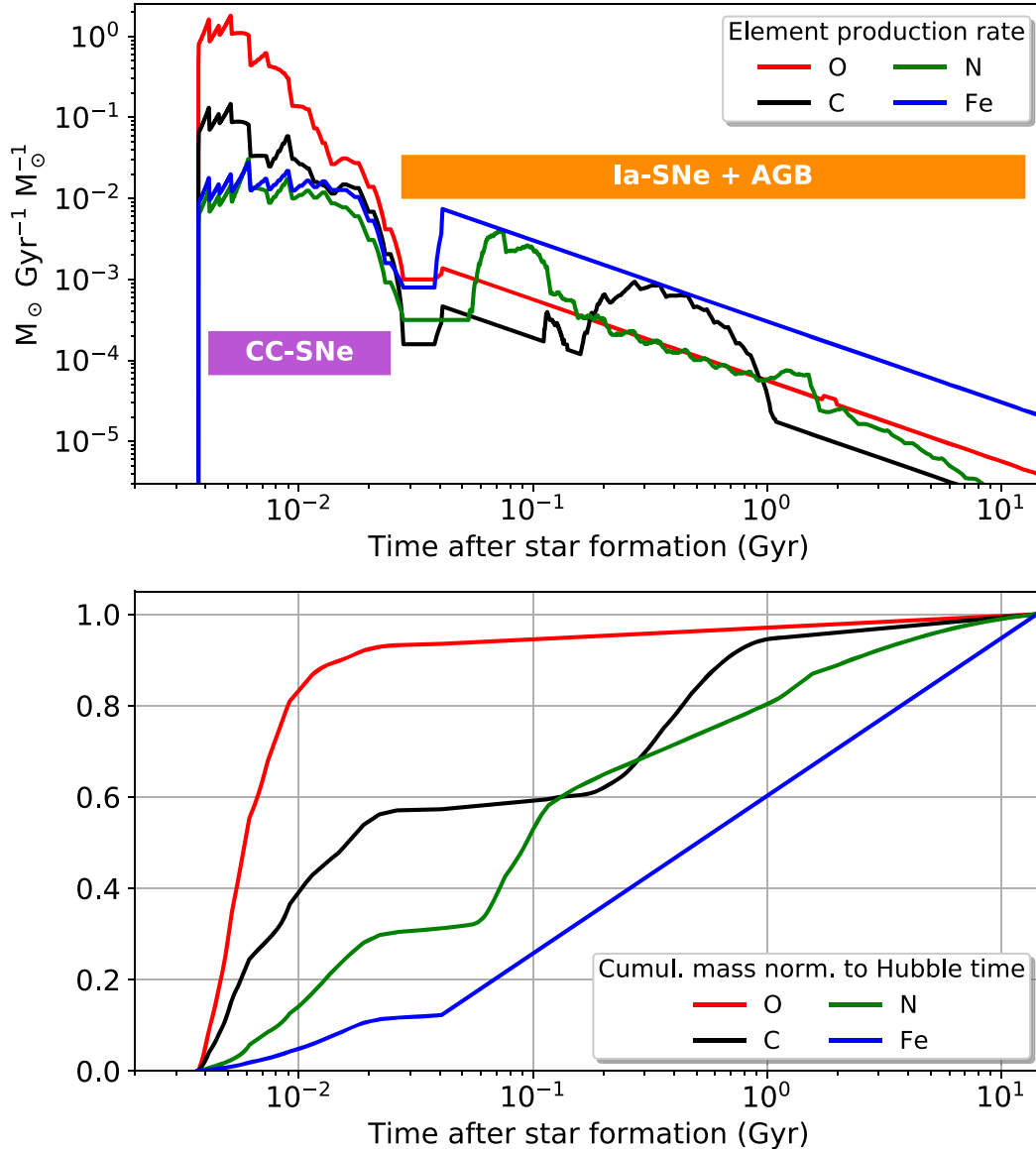


Fig. 34 Chemical enrichment history for various atomic species following a single burst of star formation (Maiolino and Mannucci, 2019). (Top) The mass production rate in solar masses per Gyr normalised to a solar mass of formed stars. (Bottom) The cumulative fraction produced normalised to that produced in a Hubble time. Oxygen forms rapidly from Type II supernovae whereas iron production is dominated by Type Ia supernovae which requires completion of stellar evolution for lower mass stars. Carbon and Nitrogen involve contributions from several processes including mass loss from intermediate age AGB stars.

provide independent measures, there are discrepancies. The far-infrared ALMA data indicates low electron gas measures ($n_e \sim 100 \text{ cm}^{-3}$, $T_e \sim 8000\text{K}$) in contrast to the JWST rest-frame optical lines ($n_e \sim 1000 \text{ cm}^{-3}$, $T_e \sim 13000\text{K}$) thereby suggesting a multi-phase ISM (Harikane et al., 2025). Even within the optical data, there are inconsistencies between electron densities derived from doublets of various ionisation levels. The most commonly-used doublets [O II] 3727/29 and [S II] 6717/31 trace low ionisation gas ($\approx 10 \text{ eV}$) whereas CIII] 1907/09 and [Si III] 18883/92 trace higher ionisation gas ($\approx 16\text{--}24 \text{ eV}$). For a uniphase ISM, the n_e estimates should agree. However, over $1 < z < 7$, the CIII]-derived n_e values are consistently ≈ 30 times larger also suggestive of a highly-structured multi-phase ISM, thereby complicating the interpretation of result based on integrated spectroscopic data (right panel of Figure 37, Topping et al. (2025)).

Perhaps understandably, much early work on chemical evolution has focused on estimating the metallicities of galaxies at the redshift frontier $z > 10$. The remarkable NIRSspec prism and grating spectra of GN-z11 at $z = 10.6$ has yielded many surprises. Although the oxygen abundance is approximately 12% solar, the N/O ratio is 4 times solar (Bunker et al., 2023). This is based on prominent lines of NIV and NIII] which are rarely seen in galaxy spectra (c.f. Figure 26). The origin of this N/O excess is currently unclear. Other N-excess sources

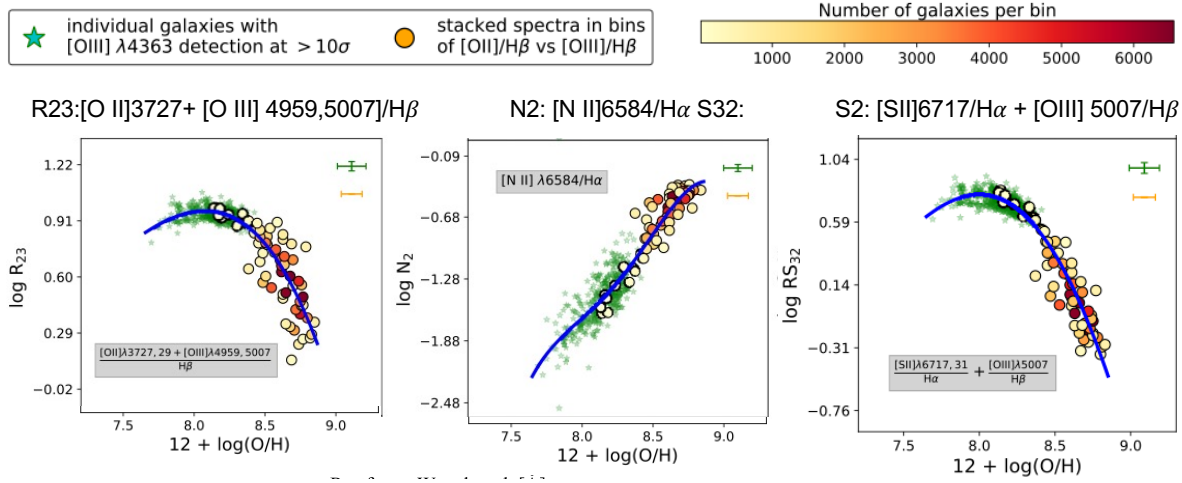


Fig. 35 Calibration of three popular strong line ratios using the collisionally-excited auroral line $[O III] \lambda 4363 \text{ \AA}$ for galaxy spectra in the Sloan Digital Sky Survey (Curti et al., 2017).

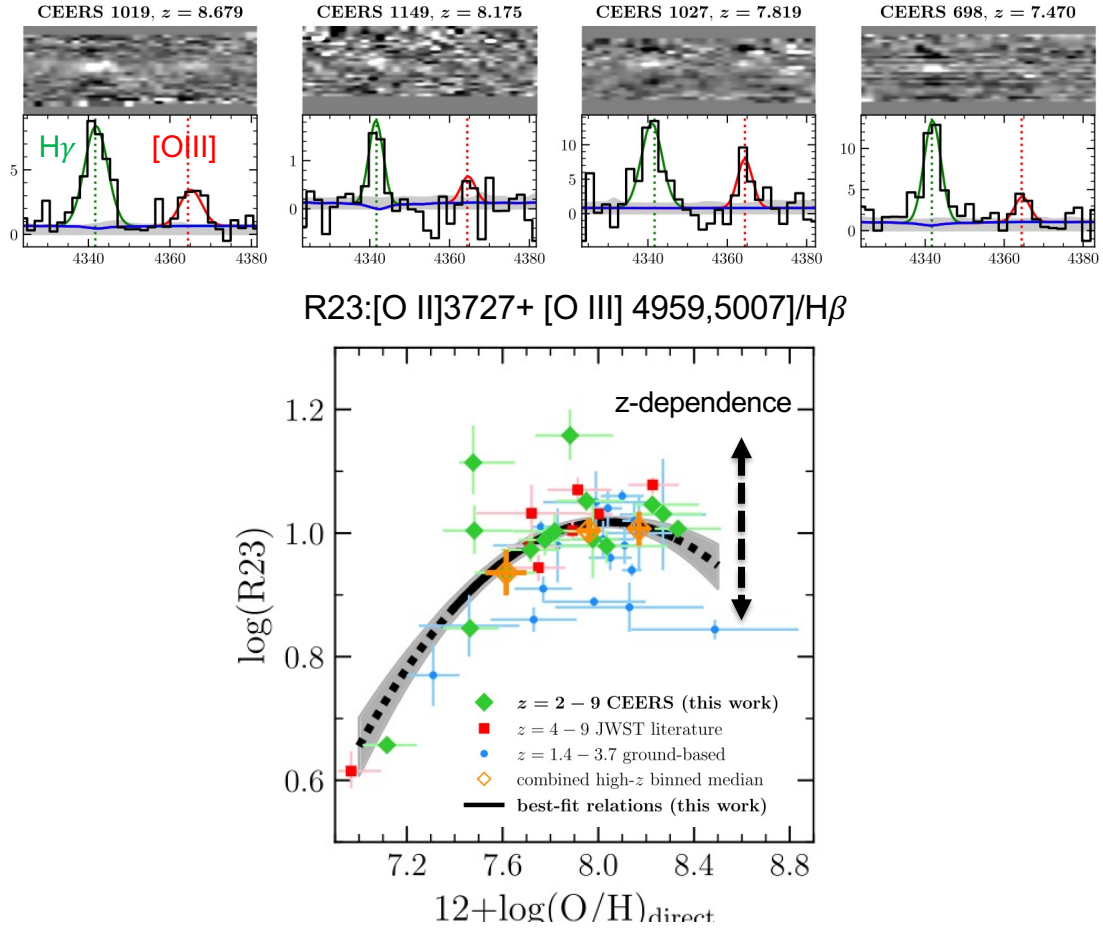


Fig. 36 Application of the collisional excited line method in the reionisation era. (Top) Detection of $[O III] \lambda 4363 \text{ \AA}$ at $z \approx 7-9$. (Bottom) The $R23$ line ratio calibration as seen at various redshifts. The arrow shows the possible redshift dependence which is strongest over $0 < z < 2$ (Sanders et al., 2024).

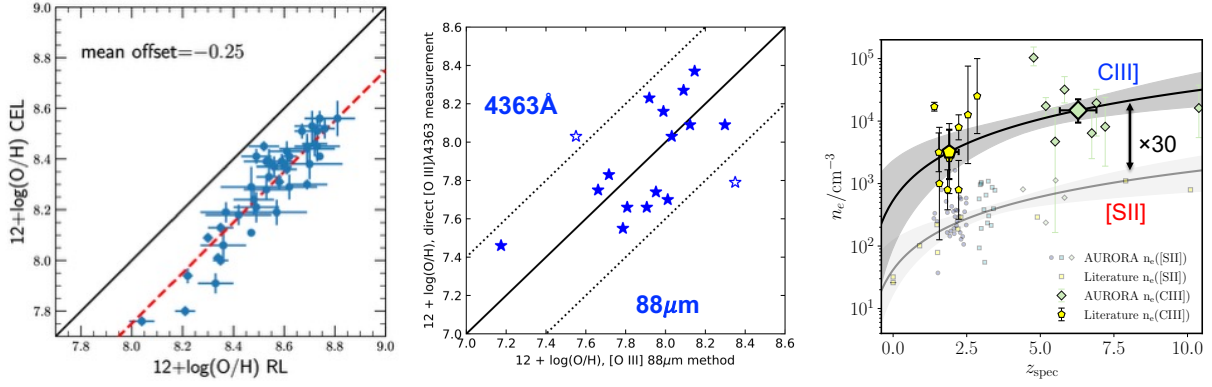


Fig. 37 Cautionary results when considering oxygen abundances derived from the CEL method: (Left) A puzzling discrepancy between the CEL and RL abundances for local galaxies may arise from fluctuations in T_e in the ISM, in which case using weak auroral lines may bias selection to high T_e regions (García-Rojas and Esteban, 2007). (Centre) The scatter seen between complementary calibrations based on far-IR [O III] 88 μ m and optical [O III] 4363 Å lines may support this hypothesis (Jones et al., 2020). (Right) Evidence for a multi-phase ISM is also found from inconsistent n_e values using different doublet lines sensitive to the ionisation state of the gas (Topping et al., 2025).

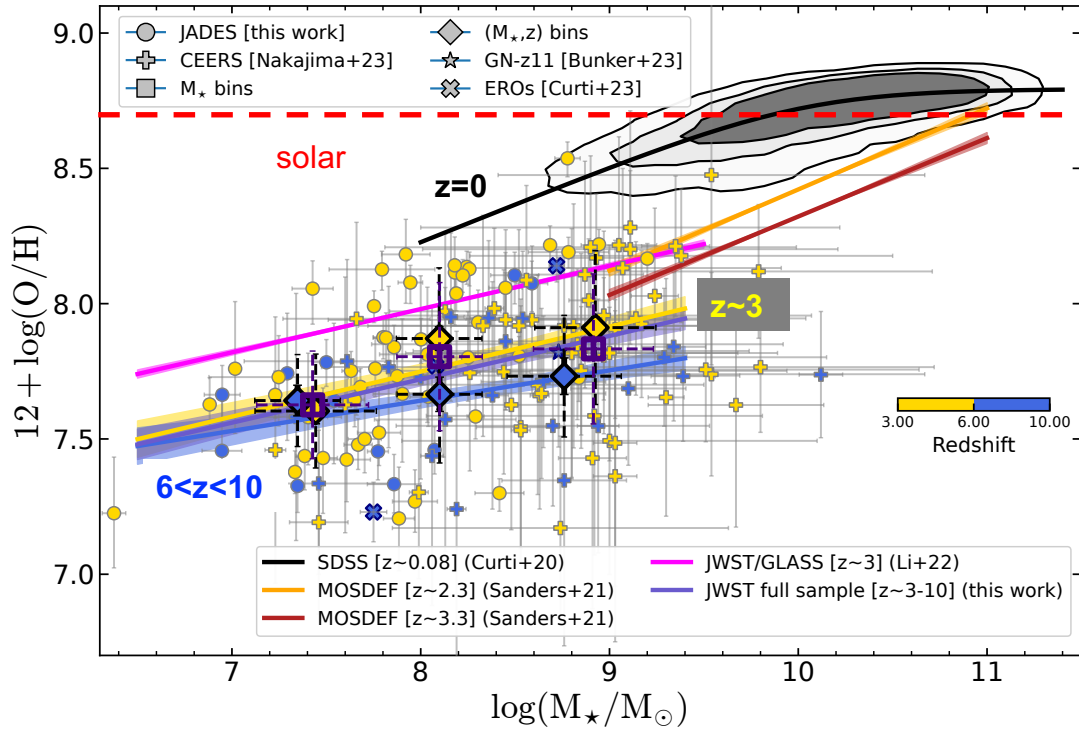


Fig. 38 A compendium of results tracing the evolving mass-metallicity relation in [O/H] for 146 galaxies in the JADES survey over $3 < z < 10$ calibrated using local dwarfs (Curti et al., 2024). The figure includes earlier high redshift results by Nakajima et al. (2023) and Morishita et al. (2024) calibrated using appropriate [O III] 4363 Å data. Various fits to the relation at $z=0$ (SDSS, Curti et al. (2020)), $z=3$ and $6 < z < 10$ are indicated in yellow and blue respectively, and present a convincing evolutionary trend although there is much scatter in the data and differences in various fits to the data at $z=3$. The solar [O/H] abundance is shown by red dashed line.

located by JWST have abundance patterns resembling those seen in the stars in local globular clusters. A possible explanation is preferential N-enrichment following ejecta from super-massive ($> 10^3 M_\odot$) stars that collide in dense hot star-forming regions (Cameron et al., 2023). At the time of writing, oxygen abundances for the first swath of $z > 10$ spectra range from 3-12% solar (Castellano et al., 2024).

In searching for global trends of chemical enrichment over the full redshift baseline, early work exploiting the growing JWST spectroscopic archive has confirmed a declining metallicity trend with redshift. Since luminous/massive galaxies are more enriched than their sub-luminous, less massive cohorts, the results are usually presented in the context of the gas-phase mass-metallicity relation (MMR). This relation has been known at low redshift for decades and can be understood as arising from the increased gravitational potential of massive

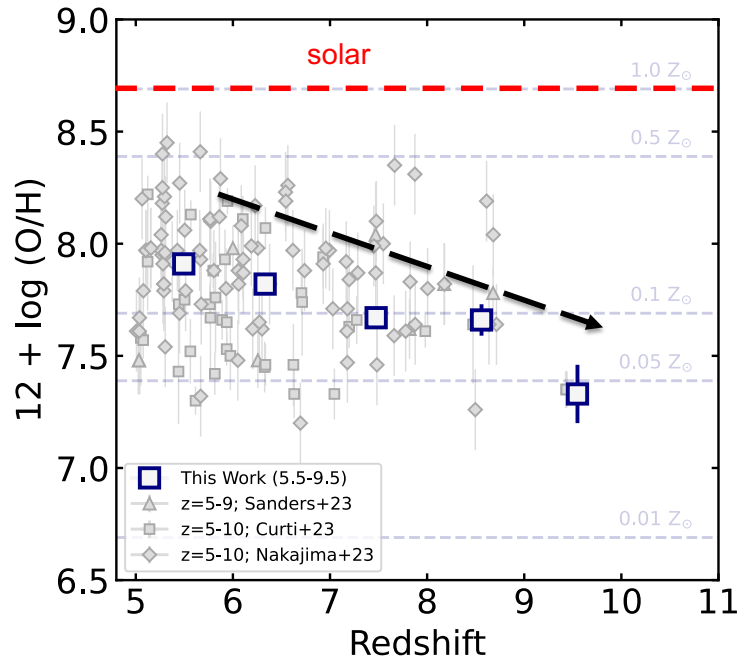


Fig. 39 Redshift-dependent metallicities derived from spectral stacks utilising the $O32$ metallicity diagnostic calibrated by intermediate redshift $[O III] 4363 \text{ \AA}$ measures of T_e from Sanders et al. (2024) (Roberts-Borsani et al., 2024). Similar results have been presented by Heintz et al. (2025a) and Hayes et al. (2025).

galaxies which can retain their enriched supernova products more readily than their less massive counterparts. Campaigns based on the growing amount of archival data show broadly consistent trends in the evolving mass-metallicity relation (MMR), with a mean decline in $[O/H]$ across the relation of 0.8 dex from $z=0$ to $z=3$ and a less marked decline of perhaps 0.2 dex to $z=10$ (Curti et al. (2024); Chakraborty et al. (2025), see Figure 38). The overlap in stellar mass across the full redshift range is not ideal since reionisation era galaxies have stellar masses in the range 10^7 to $10^9 M_\odot$, a range only explored locally with metal-poor systems such as “Green Pea” and “Blueberry” galaxies whose context with respect to normal galaxies is not fully understood. In fact, there is evidence the slope of the MMR flattens at such low masses both at high redshift and locally, a trend that simulations fail to match and maybe suggesting inadequate feedback prescription in the models.

Stacked spectra can also be useful in providing insight into the systematic redshift-dependent trends although compiling samples drawn from inhomogeneous surveys in the data archive risks introducing various biases. The most obvious arises from the need for an accurate spectroscopic redshift which may limit selection to more luminous or line-emitting sources which could, for example, be undergoing bursts. A striking glimpse of a systematic decrease in the oxygen abundance with increasing redshift has nonetheless been provided by Roberts-Borsani et al. (2024), Heintz et al. (2025a) & Hayes et al. (2025) (Figure 39). With care such stacking studies may ultimately be useful in tracing the early enrichment rate and may offer the best statistical estimate of when the first pristine sources emerged (see Lecture 3).

5 Recognising AGN in the Reionisation Era

Although other, more authoritative, lecturers will cover the topic of high redshift quasars and black hole growth, I will finish this second lecture with a purely observational discussion on how we might locate and conduct a census of AGN in the reionisation era. However, I will not address the thorny question of how to estimate their black hole masses and hence the various implications for early black hole growth.

AGN are important to locate at early times for two reasons. Firstly, we need to understand whether their non-thermal radiation provides an important component for cosmic reionisation (Lecture 1). Secondly we need to understand how quasars with black hole masses of $\approx 10^9 M_\odot$ can assemble by redshifts $z \approx 7-7.5$. JWST is pioneering three ways to locate reionisation-era AGN.

1. Rest-frame optical spectra sampling permitted recombination lines whose broad line widths contrast with those of forbidden nebular lines; a key challenge is ruling out stellar-driven winds.
2. X-ray detection and follow-up spectroscopy: individual X-ray detections at high redshift are usually impractical but stacking may be useful and some claims are based on strongly-lensed sources.
3. Time variability: this method has the advantage of probing sub-luminous sources beyond reach of spectroscopy but, due to $(1+z)$ time dilation, an extended time baseline is required.

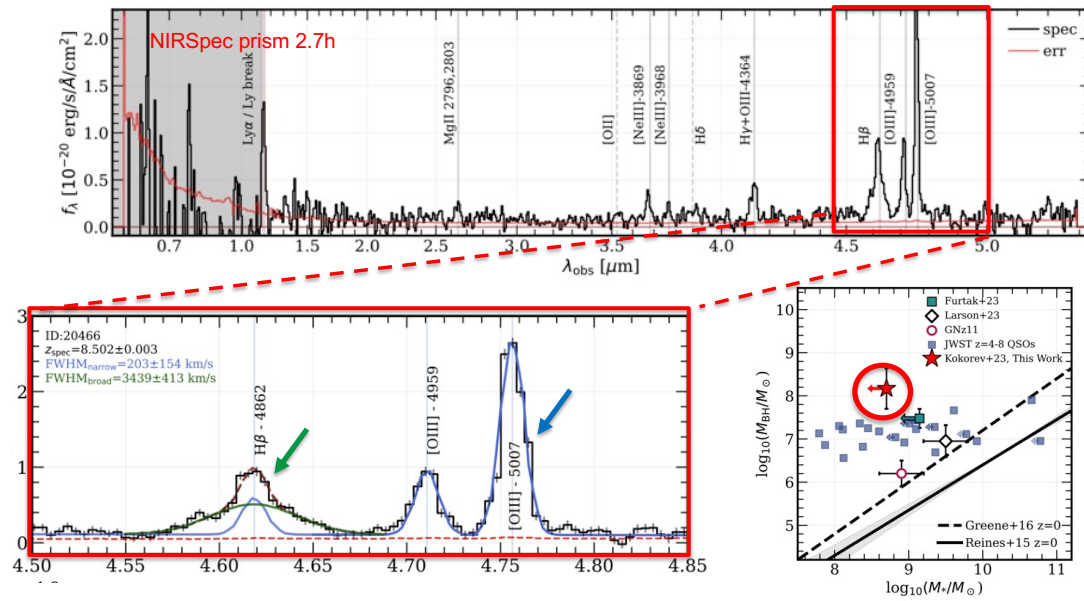


Fig. 40 A convincing case for a high mass black hole in a $z=8.50$ galaxy deep in the reionisation era (Kokorev et al., 2023). The spectrum fulfills the usual AGN criteria with exceptionally broad permitted lines (H β) and narrow forbidden lines ([O III]). A BH mass of $\approx 10^8 M_\odot$ inferred from local reverberation mapping relations assuming virial equilibrium would, if correct, imply $\approx 30\%$ of the stellar mass of the galaxy placing it well above the local $M_{\text{BH}} - M_*$ relation (inset panel).

5.1 Broad-line sources

Figure 40 shows a promising example of a broad-line AGN at a spectroscopic redshift of $z=8.5$ from the UNCOVER survey (Kokorev et al., 2023). Balmer H β has a line width of $\sigma=3400 \text{ km sec}^{-1}$ which contrasts with a much smaller $\sigma=200 \text{ km sec}^{-1}$ for [O III] emission. Such a broad H β line would be difficult to explain solely in terms of gaseous outflows. Using scaling relations adopted from lower redshift reverberation mapping measurements, a compact broad line region in virial equilibrium would imply a black hole mass of $M_{\text{BH}} = 1.5 \times 10^8 M_\odot$ which represents a staggering $\approx 30\%$ of the stellar mass of the galaxy! To reconcile the observations with the local BH - stellar mass relation (see sub-panel in Figure 40) one would have to argue either that the BH mass is overestimated by a factor of 2 dex or the stellar mass similarly underestimated. For most reasonable BH seed masses, one would conclude the BH is assembling more rapidly than the galaxy itself. Early spectroscopic searches locating broad lines in the redshift range $4 < z < 7$ located a significantly higher fraction of low luminosity AGN than pre-JWST studies (Harikane et al., 2023b). As many as 5-10% of the targeted galaxy population showed some evidence of AGN activity with implied BH masses of $10^{6-7} M_\odot$ compared to 1% locally. However, there is much uncertainty regarding the line width threshold that should be adopted as an AGN criterion given outflows may be more energetic in physically smaller galaxies with higher star formation rates at high redshift.

Soon after the high abundance of low luminosity AGN was claimed at $z \sim 5$, a distinct category of broad-line sources termed “little red dots” (LRDs) was discovered from a blind NIRCам grism slitless JWST survey (Matthee et al., 2024). While these do not constitute the entire population of broad line cases (and not all LRDs show broad lines, Greene et al. (2024)), their puzzling nature has led to many studies. Unfortunately, there is no agreed definition of a LRD. Initially located as broad H α emitters in a slitless survey with compact red morphologies, they were considered to be dust-attenuated AGN. Indeed, in many cases the flux observed in the broad H α component is consistent with the fraction of the unresolved flux in the NIRCам images.

Only later was it discovered that many of these so-called LRDs have an unusual V-shaped SED (Figure 41) with a rest-frame UV slope $\beta_{\text{UV}} \approx -2$ (characteristic of star-forming galaxies) and a red rest-frame optical slope $\beta_{\text{opt}} \approx +1$ suggestive of a dust-enshrouded system. However, a dusty AGN hypothesis runs into difficulties in explaining the weak or absent MIRI/ALMA fluxes (Williams et al., 2024; Casey et al., 2025) and no X-ray detection in stacked data (Sacchi and Bogdan, 2025). The presence of a Balmer break in the spectra of several examples led to claims that the optical component of the SED might be more easily explained via an old stellar population (Baggen et al., 2024). However, a stellar-only model would lead to very high stellar densities given the compact nature (Leung et al., 2024). Indeed, the gravitationally-lensed LRD at $z=7.05$ shown in Figure 41 remains unresolved suggesting a physical diameter of less than 60 pc and a low mass host (Furtak et al., 2023). Its Balmer break is inconsistent with a stellar origin (Ji et al., 2025) and variability has been recently detected (D’Eugenio et al., 2025) indicative of an AGN surrounded by dense gas.

At the time of these lectures, the jury was still out on the nature of LRDs. Photometric searches based on the unique V-shaped SEDs has located several hundred examples, mostly beyond $z \approx 4$ (Kocevski et al., 2025). Attempts to explain the complicated SED via a AGN hypothesis require embedding the BH in an extended dust cloud with large grains, thereby enabling little extinction in the UV and a lower dust temperature to satisfy MIRI non-detections (Li et al., 2025). However, a pure stellar non-AGN model requires extraordinary densities

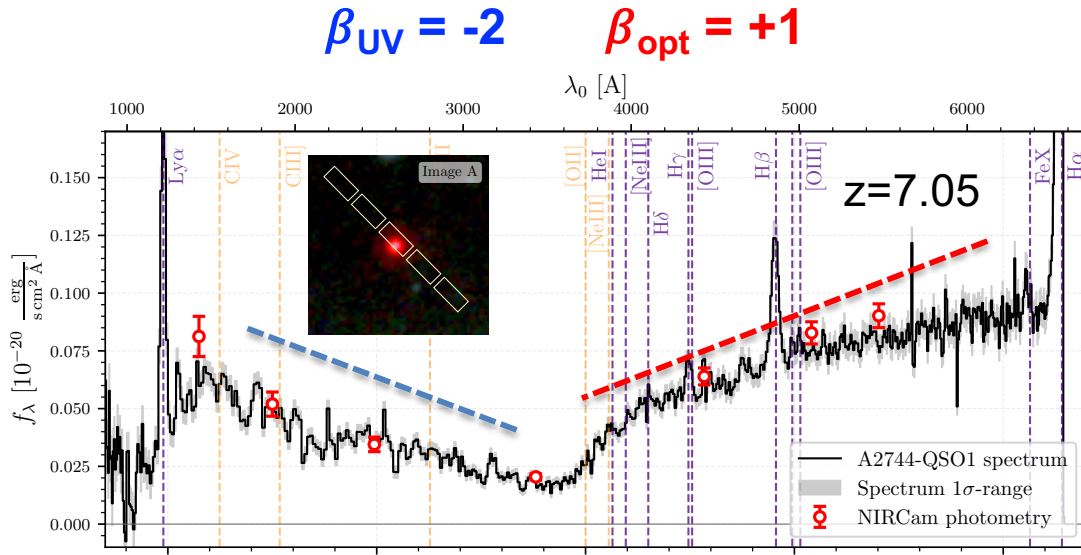


Fig. 41 The puzzling V-shaped spectral energy distribution of the population of compact “Little Red Dots” first identified by Matthee et al. (2024). The steep rest-frame UV continuum slope is characteristic of star-forming galaxies while the red optical slope was originally interpreted either in terms of a dust-enshrouded AGN or an old stellar population. Broad emission lines suggest the AGN hypothesis (Greene et al., 2024) while the occasional detection of a Balmer break suggest a stellar explanation consistent also with weak detections at mid-IR and sub-mm wavelengths (Baggen et al., 2024). This particular example is gravitationally lensed by a foreground cluster indicating that the compact core has a diameter of $< 60\text{pc}$ (Furtak et al., 2023).

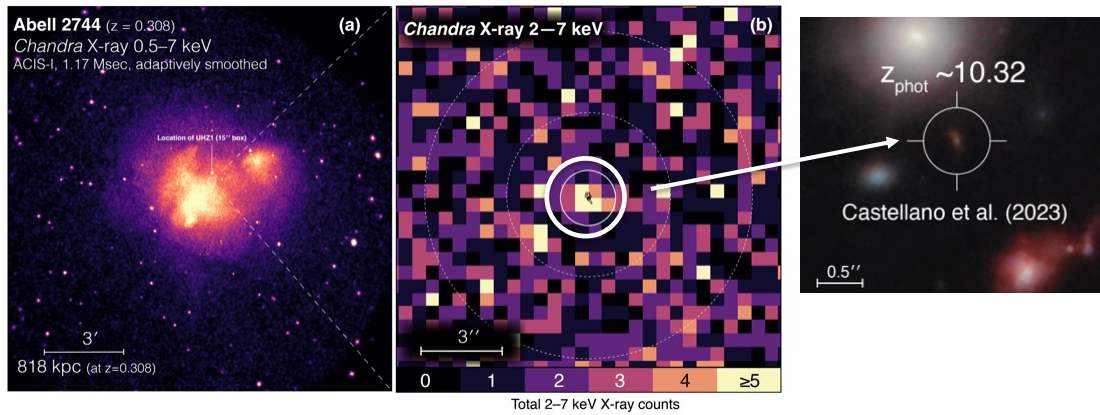


Fig. 42 Evidence for a gravitationally-lensed X-ray emitting AGN at $z > 10$ (Bogdán et al., 2024; Kovács et al., 2024). The massive lensing cluster Abell 2744 has a hot X-ray emitting intracluster medium but a 4σ X-ray feature coincides with the position of a spectroscopically-confirmed background $z=10.07$ galaxy dubbed UHZ-1 (Goulding et al., 2023), although its spectrum shows no evidence of AGN activity. The same authors have located a second lensed X-ray candidate GHZ9 in the same cluster and estimate both black hole masses are in the range 4×10^7 to $2 \times 10^8 M_\odot$ supporting non-stellar BH seeds (Natarajan et al., 2024).

within the compact red core. Since the lectures, it has been proposed that the rest-frame optical continuum may arise from a dense gaseous photosphere that can produce a steep Balmer decrement and also scatter and broaden the recombination lines by various processes thus significantly reducing the implied BH mass (Naidu et al., 2025a; Brazzini et al., 2025). Regardless of the correct interpretation (even if there is only one hypothesis as LRDs show a diversity of properties), they would appear to be a minor contributor to cosmic reionisation.

5.2 X-ray AGN?

Even the powerful Chandra X-ray satellite does not have the sensitivity to detect individual supermassive black holes (SMBH) in the reionisation era and, in the past, only stacked images of $z \approx 6$ Lyman break galaxies have been used to constrain the present of AGN. Nonetheless, two recent claims have been made for X-ray detected AGN at redshifts $z > 10$ which, if correct, would imply the existence of SMBHs at a very early cosmic age (≈ 450 Myr) and hard to reconcile with a stellar BH seed (Figure 42)

In both cases, the detections are point X-ray sources seen through a foreground lensing cluster Abell 2744 which overlap in angular position with a $z > 10$ galaxy (Bogdán et al., 2024; Kovács et al., 2024). Since Abell 2744 is a massive cluster with a hot X-ray emitting intracluster medium, the key question in both cases is whether the X-ray feature is merely a fluctuation in the cluster emission and thus represents a chance alignment with a background galaxy. UHZ-1 is seen in X-rays as a 4σ blip in the cluster emission aligned with a galaxy with a photometric redshift of $z=10.3$. A subsequent JWST spectrum reveals a redshift $z=10.07$ (Goulding et al., 2023) but no broad-line features nor any particularly convincing high ionisation lines. Remarkably, the same authors located a second $4-5\sigma$ X-ray blip in the same cluster. GHZ9 is a $z=10.15$ galaxy which shows some high ionisation lines (CIV, He II, CIII]) (Napolitano et al., 2024) but its angular position is not exactly coincident with the X-ray blip and there is a low redshift galaxy close by. To derive the claimed BH masses of $M_{BH} \approx 4.10^7 M_\odot$ (UHZ-1) and $2.10^8 M_\odot$ (GHZ9) they adopt a bolometric luminosity which, whilst uncertain, is naturally very large when placed at $z \approx 10$. While the potential importance of finding such SMBHs at $z \approx 10$ would undoubtedly be very profound (Natarajan et al., 2024), the absence of convincing spectroscopic features to support the AGN claim is a concern.

Although unrelated to X-ray emission, evidence has also been presented for AGN activity in the spectra of other $z > 10$ galaxies, mostly through high ionisation lines, outflows and high density gas (Maiolino et al., 2024a). However, follow up campaigns with MIRI have not, thus far, provided confirmation via broad H α emission (Álvarez-Márquez et al., 2025).

5.3 Time variable sources

In principle, locating AGN by photometric variability has some distinct advantages over the previously-described methods. Foremost one can penetrate to much fainter luminosities than through methods requiring spectroscopic diagnostics so, whilst not all AGN necessarily display variability, a more complete census is possible even at the highest redshifts. Contaminants such as a Type II supernovae can be readily identified either from multi-epoch observations or, exploiting JWST’s superlative image quality, by location within the host galaxy (if visible). The challenge lies in establishing an appropriate baseline of multi-epoch visits over several years given time dilation scales as $(1+z)$ and typical rest-frame fluctuations of \approx months.

A first attempt at exploiting this method involved revisiting the Hubble Ultra Deep Field (UDF) with WFC3/IR a decade after the original campaigns in 2009 and 2012 (Hayes et al., 2024). 208 (116) sources showed variability at more than 2.5 (3.0) σ down to a luminosity of $M_{UV} \approx -17$, of which 8 (4) have photometric redshifts beyond $z \approx 6$ (Figure 43). By comparing the fraction of $z < 5$ variables found in a UDF catalog of X-ray AGN, volume-based corrections can be made to include non-variable AGN as well as redshift-dependent incompleteness. The resulting integrated number density of BH at $z \approx 6-7$, whilst extremely uncertain as it is only based on a few sources, provides a surprisingly stringent constraint on some models of BH growth exceeding by a large factor the number adopted in current numerical simulations (Cammelli et al., 2025). Given JWST’s extended operational lifetime, extending this method is clearly promising, particularly given its potential to locate sub-luminous AGN beyond reach of spectroscopic surveys.

6 Summary

In this second lecture we have reviewed our physical understanding of galaxies in the reionisation era.

Firstly, we discussed the pros and cons of using spectroscopy and photometry to derive various diagnostics including (i) the UV continuum slope which is sensitive to the stellar age, dust content and nebular continuum and (ii) line emission which gauges the star formation rate and the intrinsic ionisation production rate, and fitting spectral energy distributions for deriving all of the above. JWST’s early photometric samples were larger and more complete whereas early spectroscopic samples have been drawn from different surveys and may be affected by redshift-selection biases. Nonetheless, it seems clear the precision of the spectroscopic data is much greater e.g. for UV continuum slopes and line flux measures, and thus will ultimately represent the way ahead.

Highlights of where JWST has provided new opportunities in the reionisation era include providing access to the Balmer H α and H β line so measures of the star formation rate can be directly compared with UV and other estimates, as well providing measures of the intrinsic Lyman α flux as a guide to the state of the local IGM. Access to MIRI has been shown to be important in deriving robust stellar masses and ages free from the “outshining” effect of a secondary burst of star formation. Spectroscopy has also revealed cases where nebular continuum from a population of supermassive stars may dominate the UV luminosity, although such cases are not common.

However, the most important advance lies in tracing the chemical evolution of the interstellar gas. The temperature-sensitive auroral line [O III]4363 Å has been detected in ≈ 100 $z > 5$ galaxies yielding direct [O/H] abundances and a vital calibration for larger samples. By tracing the mass-metallicity relation and through spectral stacks in redshift bins, we see the first evidence for a declining [O/H] abundance with increasing redshift. Nonetheless, when it comes to precise measurements, we are seeing evidence for a multi-phase ISM in comparing various electron density diagnostics as well as in comparisons of [O III] 4363 Å temperatures with similarly sensitive ALMA lines.

Finally, I touched briefly on searches for AGN activity, focusing primarily on the abundance without commenting in detail on the BH masses and various seed/growth mechanisms. It seems clear that low luminosity AGN are more abundant than pre-JWST estimates and there are many convincing cases of broad-line AGN at $z \approx 7-8$. A new population of compact LRDs appear to be AGN surrounded by dense gaseous photospheres which become rare at $z < 4$. Although there are claims for high mass BHs at $z > 10$, the evidence is not yet compelling in my opinion.

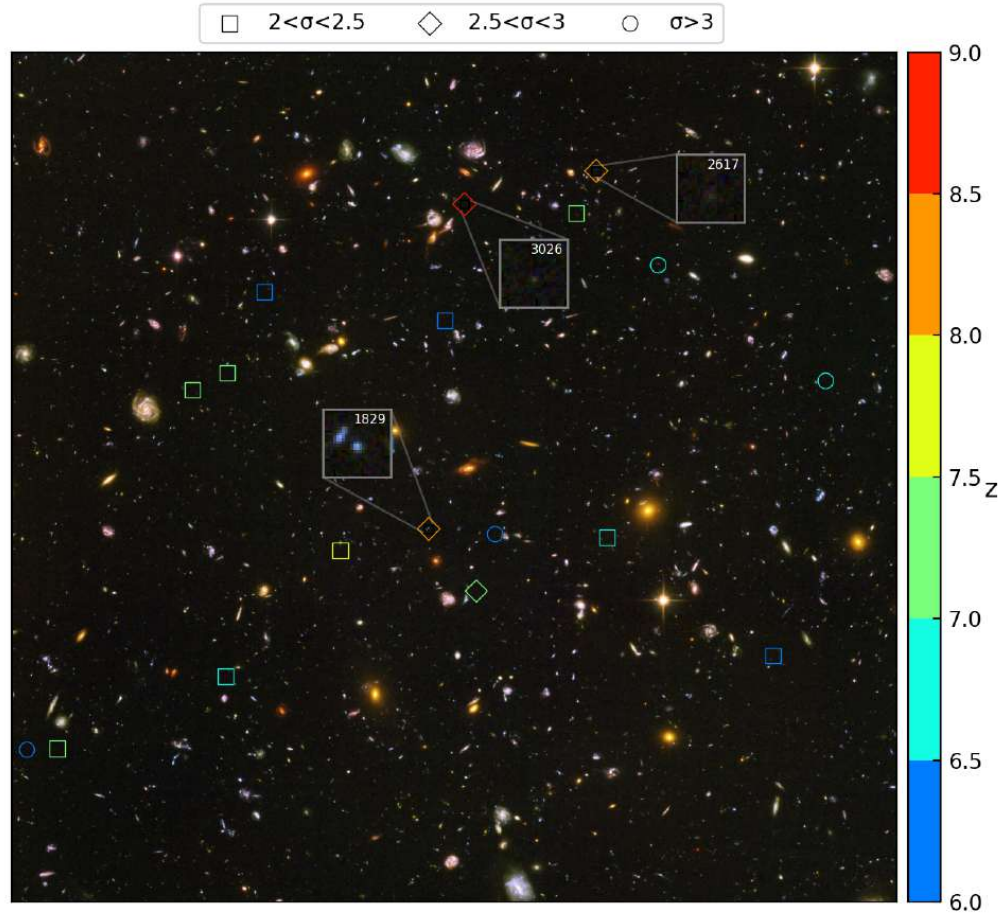


Fig. 43 Time variability as a method for searching for AGN in the reionisation era. The image shows variable sources detected to luminosities of $M_{UV} \approx -17.0$ by comparing HST WFC3/IR images of the Hubble Ultra Deep Field taken with similar filters from 2009, 2012 and 2023 - a rest-frame baseline of ≈ 1 year for $z \approx 7$ sources. Careful photometric comparisons and corrections for non-variable AGN (from intermediate redshift X-ray studies) and luminosity-dependent incompleteness, already suggest a higher volume density of AGN at $z \approx 6-7$ than that adopted in contemporary numerical simulations (Cammelli et al., 2025). Given the extended lifetime of JWST, time variable studies are clearly an important and independent method to probe the presence of AGN at high redshift.

7 Recommended Reading on Galaxies in Reionisation Era

Major Review Articles

1. Conroy (2013) - stellar population synthesis models
2. Madau and Dickinson (2014) - classic paper on cosmic star formation history
3. Stark (2016) - pre-JWST review of galaxies in the first Gigayear
4. Maiolino and Mannucci (2019) - chemical evolution and abundance determination methods
5. Ouchi et al. (2020) - analyses of Lyman alpha emitting galaxies
6. Robertson (2022) - review of early JWST projects and science goals
7. Stark et al. (2025) - a valuable early review of JWST observations of galaxies
8. Curti (2025) - a valuable early review of JWST spectroscopic studies

Pre-JWST articles

1. Ellis et al. (2013) - Hubble Ultra Deep Field galaxies to $z \approx 11$
2. Oesch et al. (2018) - pre-JWST census of star-forming galaxies to $z \approx 11$
3. Stark et al. (2017) - ground-based spectroscopy beyond $z \approx 7$
4. Roberts-Borsani et al. (2016) - Spitzer-excess galaxies with Lyman alpha emission

JWST articles (changing monthly!)

1. Wang et al. (2024b) - MIRI-based stellar masses
2. Topping et al. (2024) - UV continuum slopes at high z

3. Katz et al. (2024) - role of nebular continuum
4. Sanders et al. (2024) - high redshift electron temperature calibrations
5. Cameron et al. (2023) - nitrogen excesses in $z > 10$ galaxies
6. Curti et al. (2024) - evolving mass-metallicity relation
7. Leung et al. (2024) - the puzzling SED of Little Red Dots
8. Naidu et al. (2025a) - the physical nature of Little Red Dots

Lecture 3: The Redshift Frontier and Cosmic Dawn

1 Introduction

In this final lecture we'll explore what has been learned so far from JWST in pushing the redshift frontiers towards 'cosmic dawn' when the first chemically pristine stellar systems emerged from darkness. Something of a 'Holy Grail' in discussing the longer term prospects of JWST observations, we are currently guided largely by numerical simulations in attempting to recognise such first generation galaxies. As in earlier lectures, I wish to emphasise that the topic of searching for *primaeva* galaxies dates back over 50 years. With colleagues I organised a conference at Durham in 1988 entitled *The Epoch of Galaxy Formation*, (Frenk et al. (1989), Figure 44) at the conclusion of which a vote was held on when galaxies formed. The precise definition was the redshift at which a typical (L^*) galaxy had assembled 50% of its stars. Most voted for a redshift within $1 < z < 5$ and only a handful conceived of earlier galaxies. At the time of the 1988 conference, the most distant spectroscopically-confirmed galaxy was 3C326.1 at $z=1.82$ (McCarthy et al., 1987).



Fig. 44 Conference photograph for the *Epoch of Galaxy Formation* meeting at Durham in 1988. (Colour photography hadn't been invented at that time!) Many luminaries, some now sadly departed, were present. See text for the results of a vote as to the redshift of when galaxies formed.

Motivated by observations that supported the view that the oldest stars in the Milky Way had formed during a single monolithic collapse (Eggen et al., 1962), theorists predicted that primordial galaxies would be undergoing energetic initial bursts of star formation and therefore be spectacularly luminous. Partridge and Peebles (1967) estimated that during a brief period of $\approx 10^8$ years, they would attain luminosities ≈ 700 times those of present-day galaxies with gas clouds glowing in Lyman α emission at redshifts $z \approx 10-20$. As such they should be visible at near-infrared wavelengths. Since the concept of hierarchical assembly was not appreciated at the time, a flaw in the calculation was the assumption that galaxies evolved in isolation with constant mass. During 1977 - 1980 Beatrice Tinsley did more than anyone to place the subject on a quantitative basis. A pioneer of stellar population modelling (see Lecture 2), she made detailed galaxy count predictions that motivated observers. As the light of elliptical galaxies is dominated today by old red giants, she predicted their precursors would be blue, luminous and compact, and detectable as an excess signal in number - magnitude counts (Tinsley, 1980b). Faint galaxy counts derived from deep photographic plates taken with the newly-available 4-metre class telescopes failed to see such a strong excess down to blue magnitudes of $B_J \approx 25$ (Peterson et al. (1979), Figure 45).

Nonetheless observers continued to search for luminous *primaeva* galaxies in the redshift range $z \approx 2-5$ and candidates were proposed whose star formation rates deduced from strong Lyman α emission would imply the formation of a massive galaxy on a timescale of less than a Gyr (Djorgovski et al., 1985; McCarthy et al., 1987). Meanwhile deeper galaxy counts and the first faint galaxy redshift surveys enabled by multi-object spectrographs (Lecture 2) suggested only modest evolution in galaxy luminosities with the bulk of galaxies to $B_J = 24$ lying below a redshift $z \approx 1$ with no high redshift tail (Broadhurst et al. (1988); Colless et al. (1993); Glazebrook et al. (1995); Lilly et al. (1995), Figure 46). The resolution of this disagreement was explained by the Cold Dark Matter (CDM) model of structure formation which

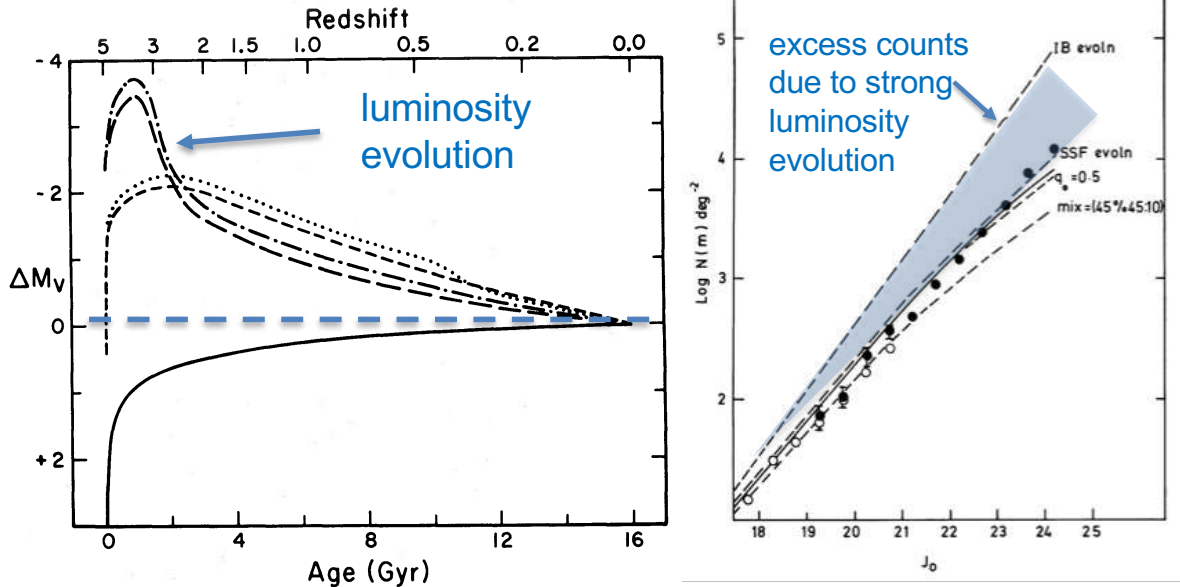


Fig. 45 Evolutionary predictions for *primaeval* galaxies from Beatrice Tinsley (Tinsley, 1980b). (Left) Since early type galaxies presently contain a uniform population of old stars, she conjectured they formed in an “initial burst” at redshift $z=3$ and thus would be spectacularly luminous and detectable as an excess in deep galaxy counts. (Right) Early galaxy counts (Peterson et al., 1979) to 25th magnitude (black dots) found only a modest excess compared to various non-evolving models in a flat ($q_0=0.5$) universe indicating a slow star formation history (SSF) rather than one with an intense initial burst (IB).

postulated a continued hierarchical assembly of galactic mass rather than an intense burst of initial star formation following monolithic collapse. Detailed calculations by Baron and White (1987) were able to reconcile the modest evolution seen in the faintest galaxy counts as well as the absence of a high redshift tail in the early redshift surveys.

2 The JWST Census to $z \approx 14$

As discussed in Lecture 2 (see Figure 22), prior to the launch of JWST, there was a fierce debate in the community as to the rate of decline in the comoving volume density of star forming galaxies beyond a redshift $z \approx 8$. Oesch et al. (2018) argued for a rapid decline consistent with theoretical models based on a constant efficiency of star formation from the baryonic mass associated with growing dark matter halos. McLeod et al. (2016, 2021) argued for a more gradual decline in number density. Part of the discrepancy was simply the paucity of reliable HST candidates beyond $z=8$, of which only 3 had spectroscopic redshifts. Nonetheless, the two decline rates would lead to an order of magnitude difference in the number of candidates beyond $z=11$ expected with JWST. Within only a few weeks following the commencement of JWST science operations, the discrepancy was resolved with numerous groups offering candidates in early release images to redshifts $z \approx 13$ and beyond (Naidu et al. (2022b); Castellano et al. (2023); Finkelstein et al. (2023); Harikane et al. (2023a); Bradley et al. (2023); Donnan et al. (2023); Bouwens et al. (2023); McLeod et al. (2024) Figure 47).

Subsequent to this early glimpse of galaxies seen when the universe was only 300 Myr old, much wider field imaging was undertaken by the PRIMER project sampling 400 arcmin², an area 10 times that of the early release images discussed above. This yielded over 2500 candidates beyond a photometric redshift $z=8.5$ charting a smooth decline to redshift $z=14$ (Donnan et al., 2024). This was complemented by the JADES Origins Field, an ultra-deep exposure in two small fields purposely designed to explore the redshift range $12 < z < 20$ with 14 JWST filters (Robertson et al., 2024). It located 8 new galaxies in the redshift range $11.5 < z < 14.4$. Although no galaxies were detected beyond $z=15$, the absence in the small survey area of 9.05 arcmin² is consistent with the rate of decline seen at lower redshifts (see Figure 48).

Since these early imaging campaigns relied on photometric redshifts, it is interesting to ask how reliable are those redshift estimates now we have extensive spectroscopic data. Figure 49 shows a recent comparison where it can be seen there are very few outliers from a one-to-one relation. Looking more closely, however, it is seen that photometric redshifts are systematically overestimates by $\Delta z = 0.10-0.15$. This can be well-understood by *in situ* hydrogen absorption which damps the blueward edge of the continuum near Ly α (see inset, Heintz et al. (2024)). Indeed, this effect has been used to estimate the redshift-dependent IGM neutral fraction x_{HI} (Mason et al., 2025), although others have expressed concern on the quantitative accuracy of such estimates with low resolution prism spectra (Huberty et al., 2025).

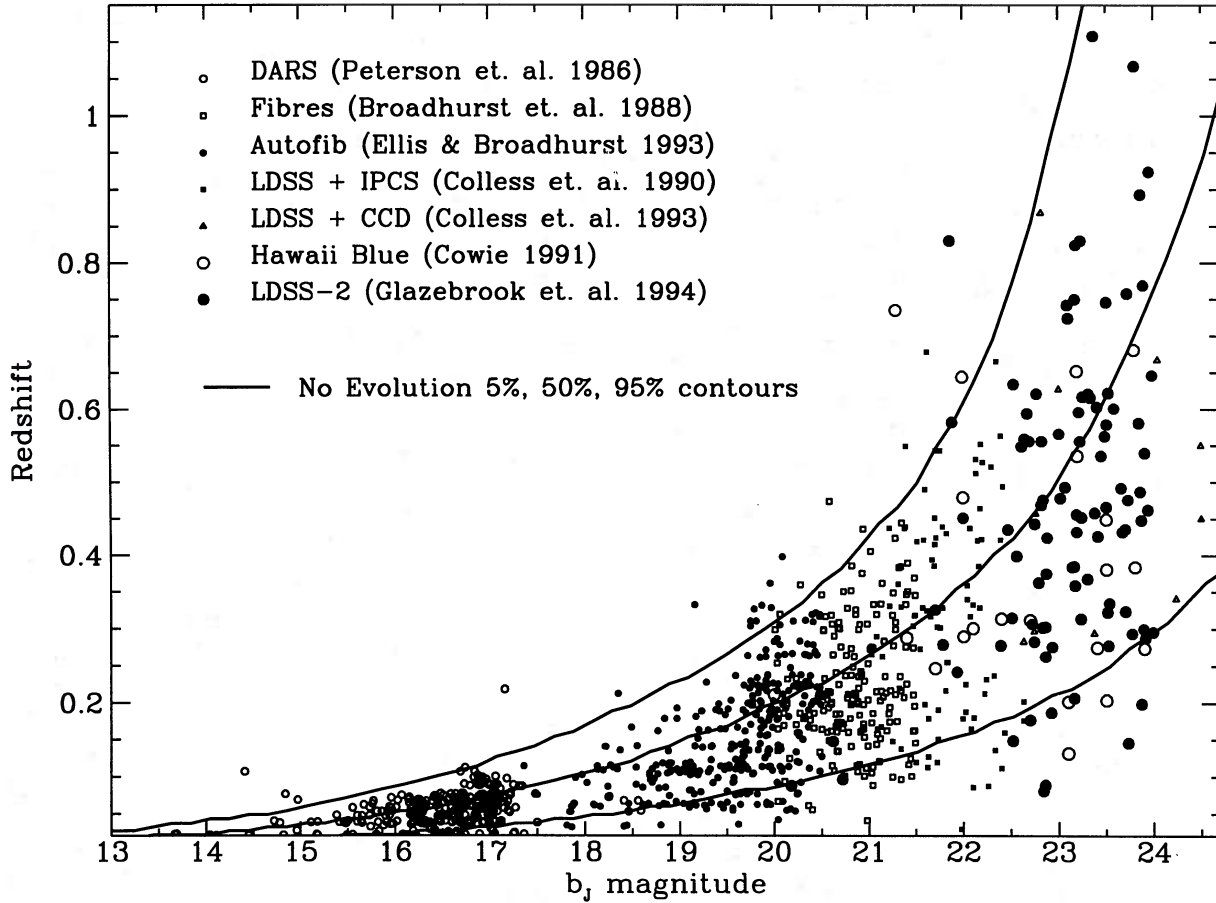


Fig. 46 The status of faint galaxy redshift surveys in the early 1990s, prior to the onset of 8-10 metre class telescopes (Glazebrook et al. (1995) with other campaigns labeled). Despite a significant excess of galaxies to $B_J=24$ over no evolution models, few $z > 1$ galaxies associated with luminous early galaxies were found. The paradox of an excess number but no increased redshift range was explained via a decline in the star formation rate for sub-luminous galaxies (also referred to as ‘downsizing’.) Luminous primaeval galaxies were also shown to be inconsistent with the hierarchical nature of galaxy assembly predicted in cold dark matter models.

One prominent high redshift candidate that did turn out to be a low redshift interloper is instructive to discuss. Donnan et al. (2023) published a fairly convincing $z=16.6$ candidate based on a Lyman break between prominent signals in filters longward of F200W and absent shortward of F150W. However, a spectrum secured by Arrabal Haro et al. (2023) revealed the candidate to be at $z=4.912$ with intense emission lines of [O III] and $H\alpha$ contributing significantly to fluxes at F200W and F277W (see also Naidu et al. (2022a)). This represents an important cautionary tale indicating that the redshift range $16 < z < 18$ is particularly tricky with broad-band photometric selection given the possibility of strong optical emission lines arising from $z \approx 5$ galaxies at $2-4 \mu\text{m}$. Certainly, medium-band photometry will be helpful.

The PRIMER data charted a smooth decline to $z \approx 14$ and hinted a marginal drop in number density beyond (Donnan et al., 2024), so it is natural to ask if any promising candidates have been found beyond. The most recent attempt at the time of writing is that from the GLIMPSE survey (Kokorev et al., 2025) which proposed five $z > 15.9$ candidates based on deep NIRC2 photometry. Several of these candidates lie at the periphery of the imaged areas which may indicate less reliable photometry. The implied comoving number density would also be in significant tension with the upper limit provided by the JADES Origin Field (Robertson et al., 2024). Although the JOF is a small area, this discrepancy is nonetheless a concern. Other $z > 15$ searches since the Lectures include those by Asada et al. (2025) and Weibel et al. (2025).

3 The Mystery of Superluminous $z > 10$ galaxies

Clearly the JWST census beyond $z \approx 8$ is in disagreement with models of constant star formation efficiency based on the baryonic mass associated with growing dark matter halos in ΛCDM . Before attempting to understand this, we will first consider what we can learn from

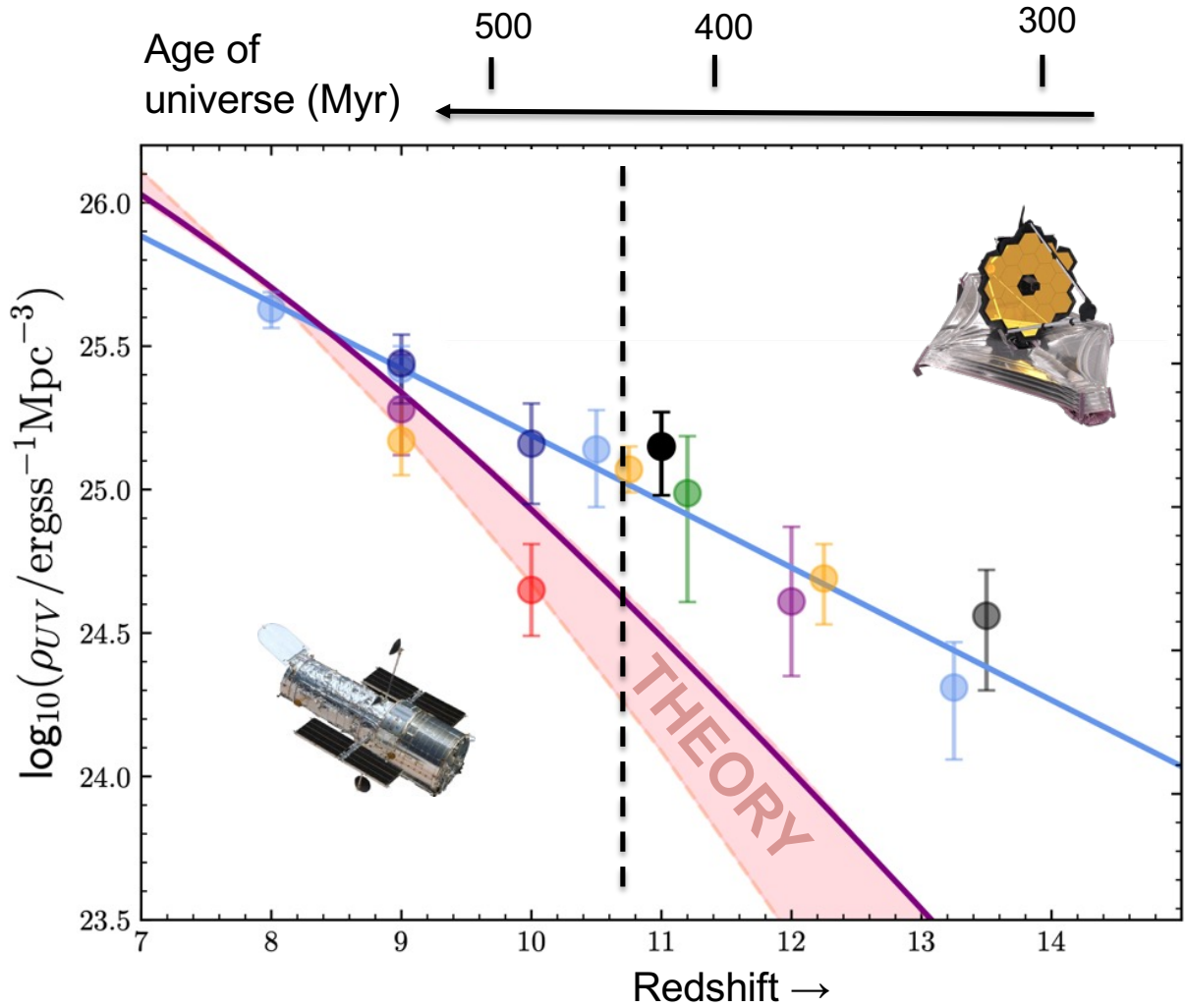


Fig. 47 Early compilation of the rate of decline of the comoving UV luminosity density from star-forming galaxies located in the first public JWST datasets (Donnan et al. (2023), see text for similar articles). The black dashed line indicates the frontier achieved with HST and the band marked "Theory" broadly indicates the prediction for various models assuming a constant star formation efficiency given the cosmological baryon fraction in dark matter halos assembling in standard Λ CDM.

spectroscopy of these luminous sources. Within a few weeks of the start of science operations, the awesome power of JWST's spectrographs became apparent. Figure 50 shows the "poster child" from late 2022, a spectrum of GN-z11 (Bunker et al., 2023) showing an abundance of emission features for the most distant source confirmed with HST by Oesch et al. (2016). The figure also shows the JWST spectrum of JADES-GS-z14.0, the highest redshift object at the time of the Saas-Fee lectures (Carniani et al., 2024), whose precise redshift of $z=14.1$ was later determined using ALMA (Heintz et al., 2025b)³. Both sources are spectacularly luminous ($M_{UV} \approx -21$) with star formation rates of $\approx 20 M_{\odot} \text{ yr}^{-1}$ yet are physically compact with radii of only 100-200 pc. Similar quality spectroscopic data has been presented by Curtis-Lake et al. (2023); Harikane et al. (2023a); Hainline et al. (2024).

Carniani et al. (2024) summarised the surprising luminosities of the spectroscopically confirmed $z > 10$ sources in Figure 51. The two sources shown in Figure 50 are more luminous than most systems down to redshifts $z \approx 8$. Given the small cosmic volumes explored to locate such sources, it is tempting to contemplate we are witnessing some new, time-specific, physical processes responsible for these luminous sources, perhaps even related to the approach to 'cosmic dawn'. Unsurprisingly, many hypotheses have been put forward to explain these extreme luminosities. Broadly speaking they fall into three categories:

1. The absence of dust or processes which regulate star formation in very early sources so that there has been insufficient time for galaxies to assemble a critical mass (Ferrara et al., 2023, 2025; Dekel et al., 2023)

³Unsurprisingly, in a rapidly developing field, since the Lectures the spectroscopic redshift record has been broken and currently stands at $z=14.4$ (Naidu et al., 2025b)

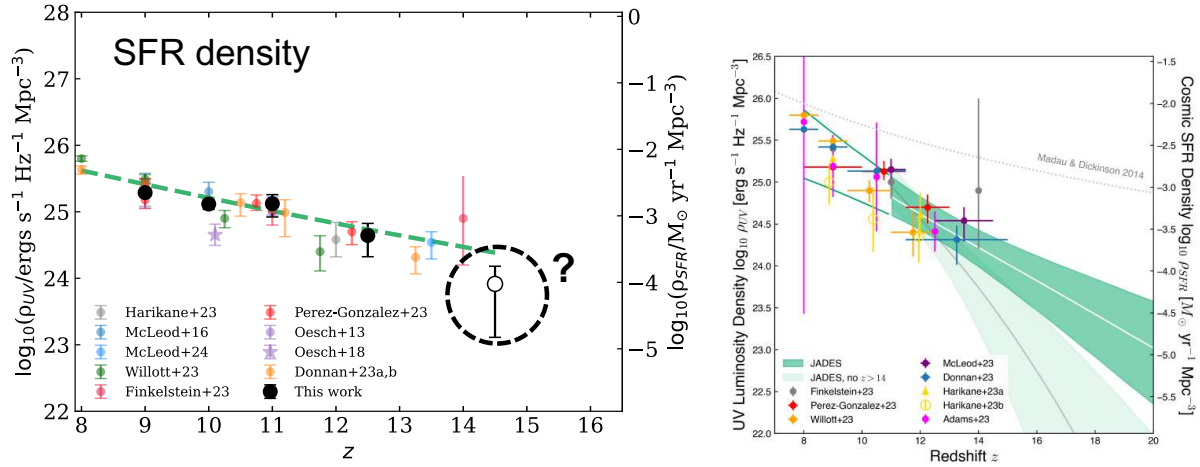


Fig. 48 Wide and deep: (Left) UV luminosity density versus redshift for the panoramic PRIMER survey (incorporating other publicly available datasets) totalling 400 arcmin² with over 2500 galaxies beyond $z=8.5$ (Donnan et al., 2024). The survey demonstrates clear continuity in star-forming galaxies out to $z=14$ with a tantalising 1σ decline thereafter. (Right) Equivalent figure for the ultradeep JADES Origins Field sampling 9.05 arcmin² with the goal of probing the redshift range $12 < z < 20$. Although 8 galaxies were located beyond $z=11.5$, no convincing $z > 15$ galaxies were found (Robertson et al., 2024).

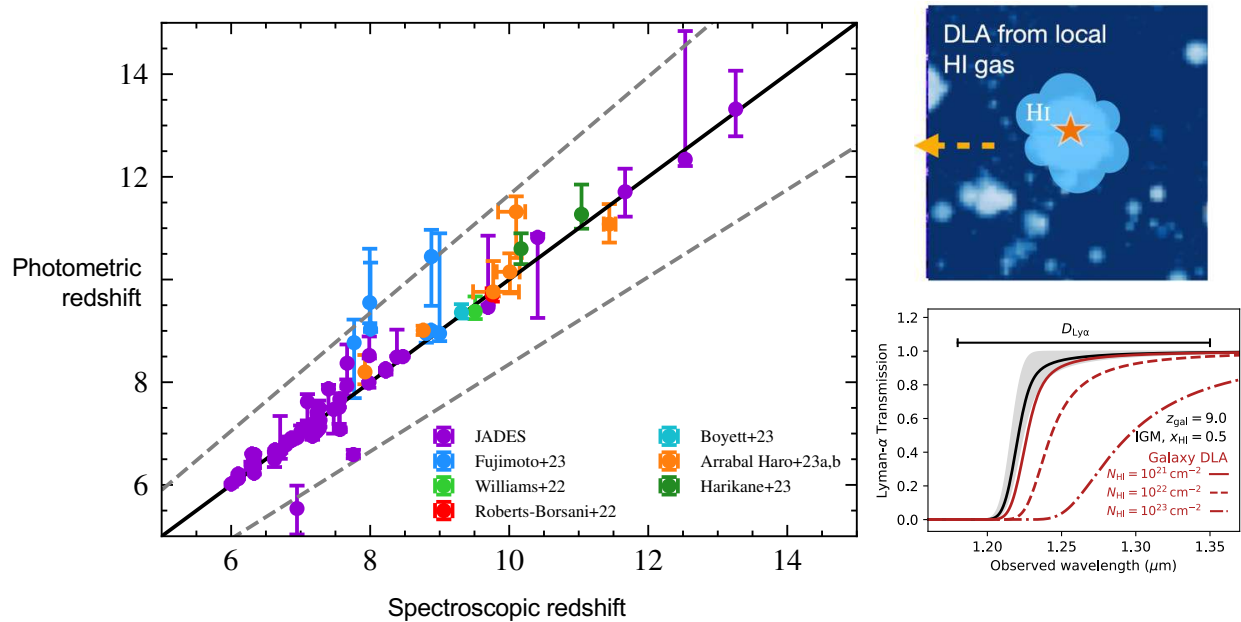


Fig. 49 A recent comparison between JWST photometric and spectroscopic redshifts (Courtesy C. Donnan). In general the agreement is excellent. The small bias of $\Delta z \approx 0.10$ -0.15 arises due to in situ hydrogen absorption (right panels) which damps the Lyman limit, the primarily photometric redshift indicator (Heintz et al., 2024).

- Star formation is burst-like in early systems and thus there is a bias towards finding galaxies at the peak of a duty cycle of activity. The sources are then unlikely to sustain such high star formation rates for very long (Mason et al., 2023; Shen et al., 2023; Gelli et al., 2024; Kravtsov and Belokurov, 2024)
- A top-heavy initial stellar mass function which might arise naturally in low metallicity systems where metal cooling processes whereby gas clouds fragment into smaller masses are less prevalent (Harikane et al., 2023b; Menon et al., 2024; Schaerer et al., 2025).

The no-dust hypothesis proposed by Ferrara et al. (2023) posits that the increasing specific star formation rate (sSFR) at $z > 10$ leads to radiation pressure-driven outflows that expel any dust. By considering the fraction of such critical outflows derived from the sSFRS distribution, it is possible to match the redshift-dependent cosmic star formation rate density in the context of limited data on outflow velocities. However, as we saw in Lecture 2, there is no significant evidence of a steepening in the UV continuum slope β at $z > 10$ (Heintz et al., 2025a; Saxena et al., 2024). Indeed, if anything, there is evidence for redder slopes which may arise from an increased contribution

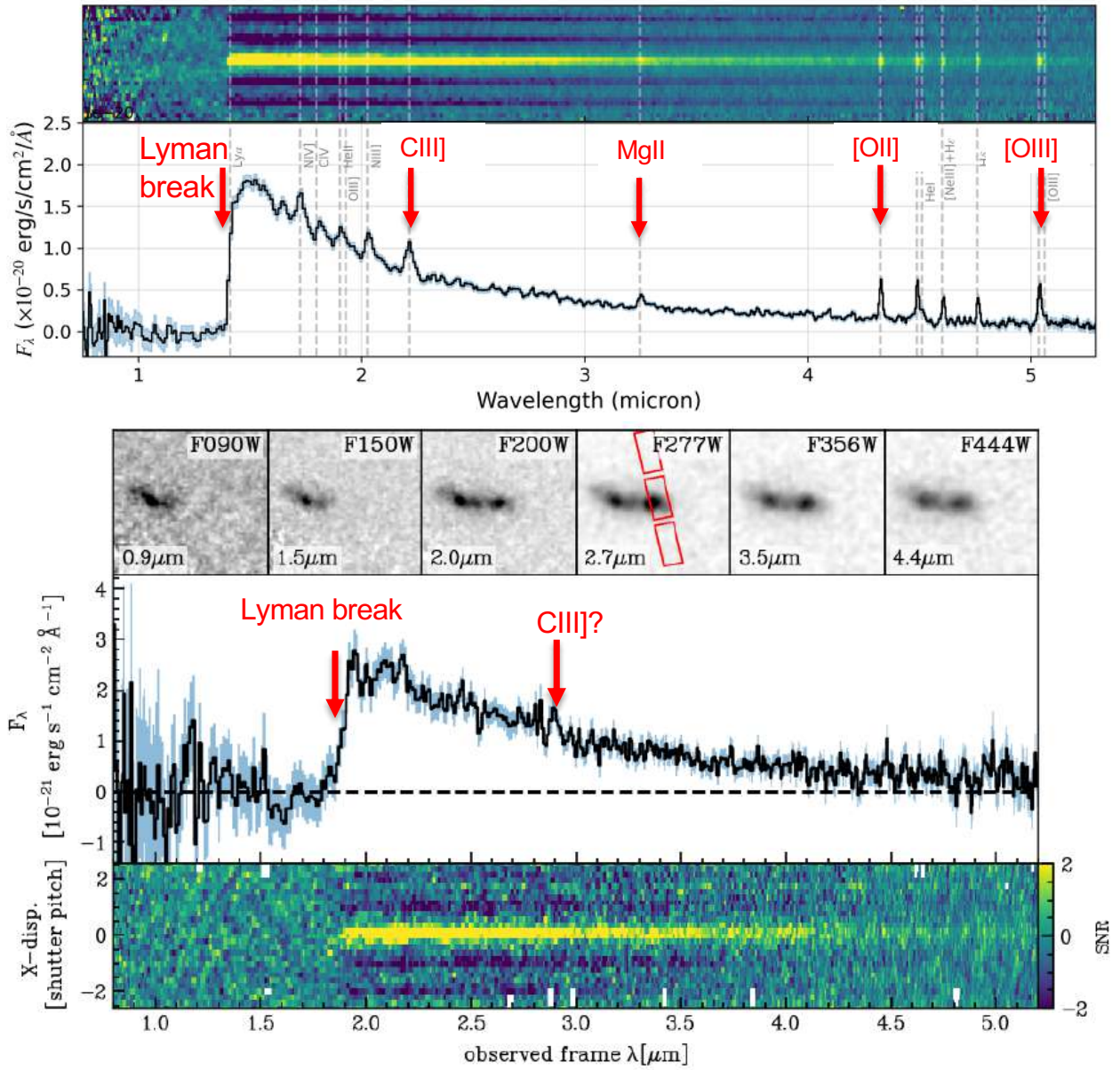


Fig. 50 The remarkable promise of JWST through detailed spectra of two $z > 10$ galaxies. (Top) The “poster child” JWST spectrum of GN-z11 at $z=10.6$ (Bunker et al., 2023), a galaxy whose high redshift was originally claimed via a Lyman break with HST (Oesch et al., 2016). Numerous emission lines are present with only the most prominent highlighted. (Bottom) JWST spectrum of GS-z14 (Carniani et al., 2024). Originally disfavoured as a high redshift candidate by the JADES team as it is 0.4 arcsec from a foreground $z \approx 3.5$ galaxy, perseverance paid off in securing the redshift record holder at the time of the Saas-Fee meeting. Both sources are remarkably luminous and compact, yet forming stars at over $20 M_\odot \text{ yr}^{-1}$.

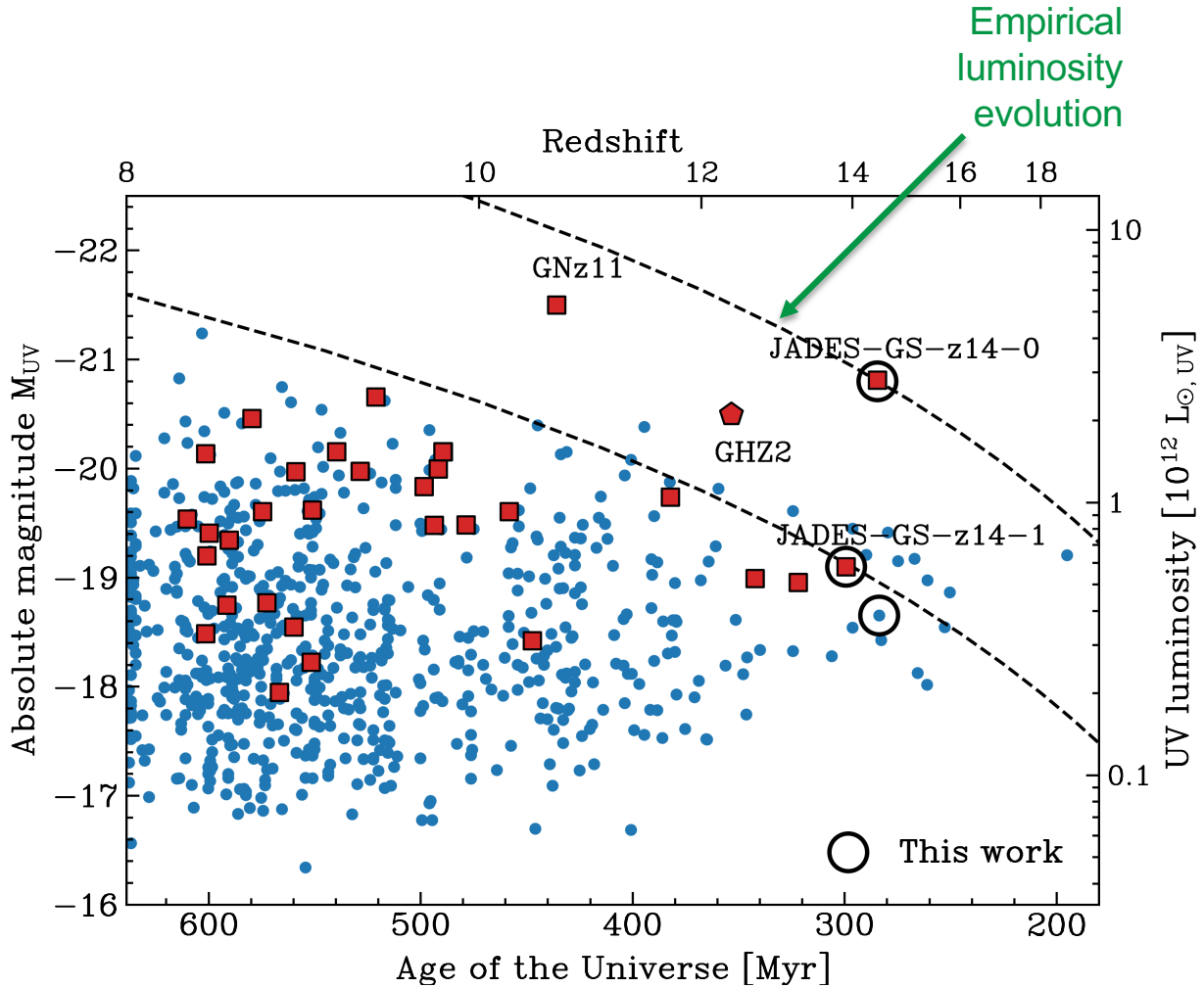


Fig. 51 UV absolute magnitude versus redshift for $z > 8$ galaxies from Carniani et al. (2024). Blue symbols represent sources with photometric redshifts, red squares have spectroscopic confirmation. Selected spectroscopic sources above $z=10$ are highlighted. The dashed curves indicate semi-empirical evolutionary trajectories for halos of a given cosmic abundance. Such analyses have led to numerous explanations for these extraordinarily luminous early galaxies.

from nebular continuum emission.

Many have considered that the young ages inferred for many high redshift galaxies are suggestive of burst-like behaviour that “outshines” older stellar populations (Lecture 2). Endsley et al. (2024) presented a detailed analysis of line emission (albeit inferred from photometric data) that supported the view that low luminosity galaxies show weak spectral features consistent with a downturn in the star formation rate whereas their luminous, stronger line counterparts are “up-scattered” by bursts. Gelli et al. (2024) has developed a predictive bursting model by introducing a scatter σ_{UV} in the UV luminosity - halo mass relation (Figure 52). Incorporating such a scatter increases the visibility of sub-luminous systems and can go some way to reproducing the $z > 10$ observations (see also Mason et al. (2023); Shen et al. (2023); Kravtsov and Belokurov (2024)).

Finally let us consider the impact of a top-heavy stellar initial mass function (IMF). There is some evidence of super-massive ($100-400 M_{\odot}$) stars right on our doorstep in the Large Magellanic cloud. Schaerer et al. (2025) have shown how their presence can provide a huge boost to both the stellar and nebular UV emission for short periods (<10 Myr). Their models predict UV luminosity boosts of $\times 6$ and harder radiation fields with ξ_{ion} increased by $\times 1.5$ (Figure 53). A by-product of super-massive stars would be the presence of high ionisation lines such as He II. While there are some examples of He II line emission, its presence is certainly not ubiquitous in $z > 10$ galaxies.

Some more creative ways to explore the puzzle have also been proposed. Shuntov et al. (2025) have examined the *clustering* of galaxies in the reionisation era since this is linked to their halo masses. Connecting the results with their UV luminosities provides a measure of the star formation efficiency for a given halo mass. They claim no significant evolution in this efficiency during the reionisation era. An independent measure of burstiness can also be gleaned by comparing estimates of star formation rates derived independently from H α and the UV continuum given these diagnostic probe different timescales as discussed in Lecture 2 (Perry et al, in prepn.).

So what are we to make of all these explanations? Whilst theorists often enthusiastically propose a single explanation for a puzzling

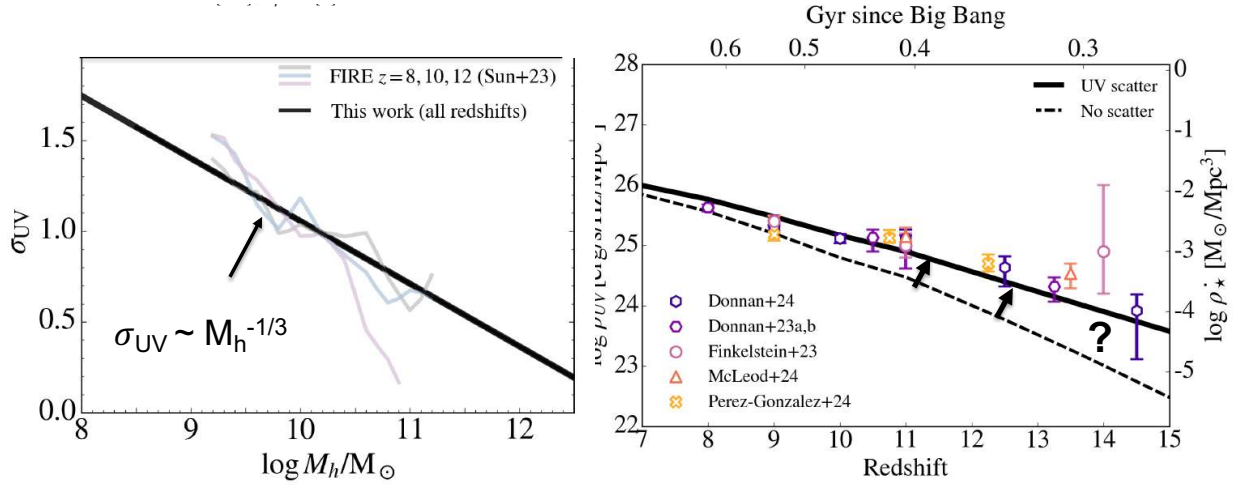


Fig. 52 Modelling how bursty star formation could explain the high luminosities of $z>10$ galaxies as temporarily up-scattered lower luminosity systems (Gelli et al., 2024). (Left) FIRE simulations based on bursty star formation indicate the scatter σ_{UV} in the $M_{UV} - M_{\text{halo}}$ relation is larger for lower mass galaxies. (Right) Incorporating this relation goes some way to explaining the excess luminosity but may be insufficient, on its own, to match the observations at the highest redshifts.

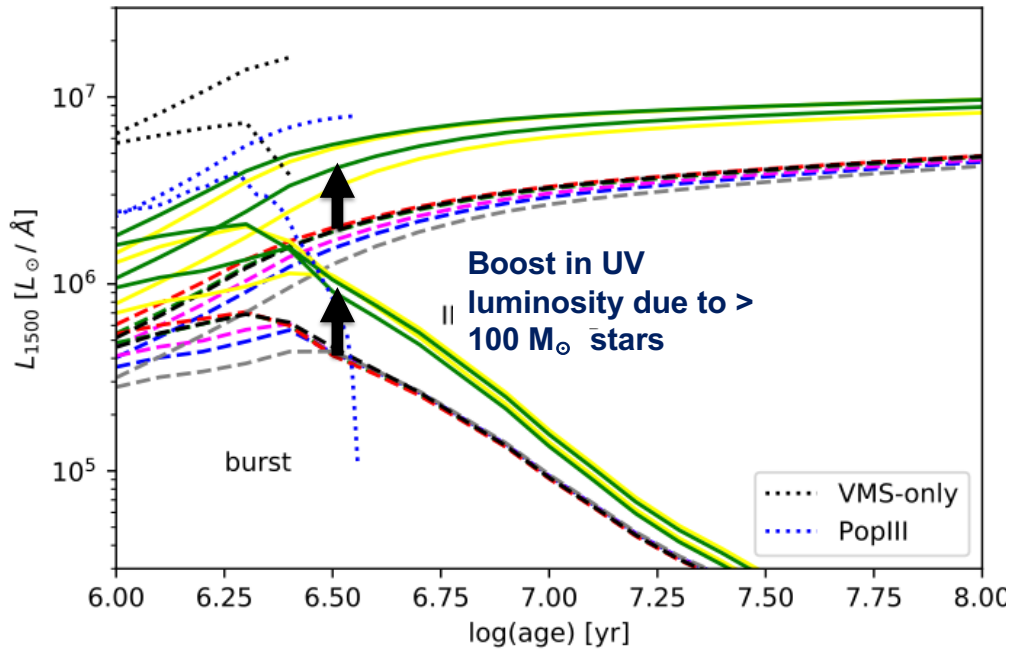


Fig. 53 The dependence of the time-dependent UV 1500 Å monochromatic luminosity on various assumed stellar initial mass functions (Schaerer et al., 2025). Upper curves represent models with constant star formation and the lower ones assume a single burst. The significant boost in luminosity arising from changing the IMF from a classic Salpeter slope of $\alpha_2=-2.35$ above $0.5 M_\odot$ to one with a flatter $\alpha=2.0$ slope that maximises the contribution of massive stars is shown for both star formation histories by vertical arrows for mass functions extending to $150 M_\odot$ (yellow curves) and $300 M_\odot$ (green ones). All models include nebular emission.

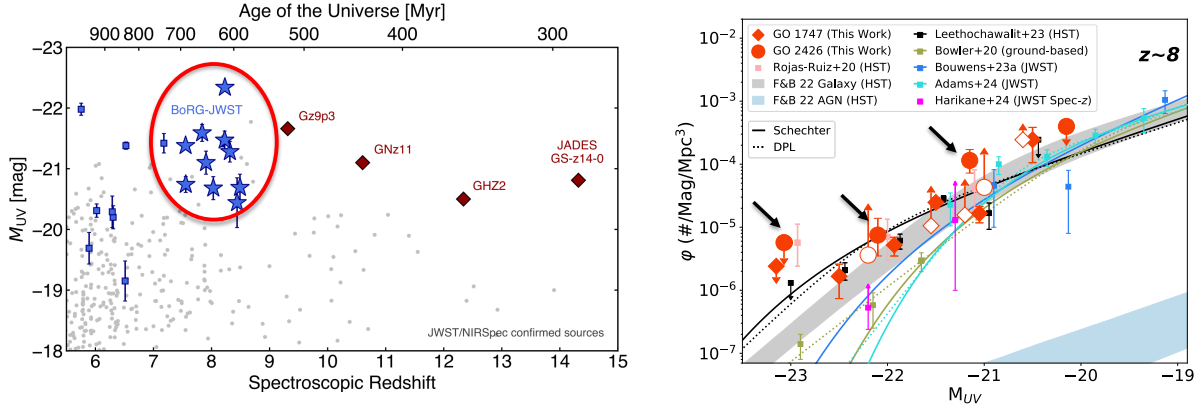


Fig. 54 *Is $z > 10$ the only special era?* (Left) Spectroscopic follow-up of the HST pure parallel BoRG survey is finding similarly super-luminous galaxies at $7.5 < z < 8.5$ (Roberts-Borsani et al., 2025). (Right) The large original survey area ($\approx 10^3$ arcmin²) and numerous sightlines which minimise cosmic variance enables a robust measure of the bright end of the luminosity function at $z \approx 8$ (Rojas-Ruiz et al., 2025).

observational result, experience suggests it's often a combination of physical effects. The dust-free solution is the only one that's readily testable and there seems little correlation between extreme luminosities and steep UV continuum slopes. As an example, the most luminous galaxy of all (GNz-11) has $\beta = -2.36$. Up-scattering from bursty star formation can certainly contribute to an excess star formation rate density at $z > 10$ but models suggest this becomes harder at $z > 12$ (Figure 52). Finally, top heavy IMFs are a good bet given the spectroscopic evidence for very massive stars inferred to explain super-solar N/O abundances (Cameron et al. (2023), Lecture 2).

One final new development might further support the bursting hypothesis. Spectroscopic follow up of candidates located in the HST pure parallel BoRG survey is also finding super-luminous examples at $7.5 < z < 8.5$ (Figure 54, Roberts-Borsani et al. (2022, 2025) suggesting the $z > 10$ era is not so "special". Of course at this later time, finding more massive and energetic sources might not be so surprising. Nonetheless, the wide area covered in the HST survey provides a more representative estimate of the bright end of the luminosity function in the reionisation era (Rojas-Ruiz et al., 2025). Mounting evidence from rest-frame optical spectra in these later examples suggests similar physical conditions to those seen at $z > 10$, including periods of stochastic star-formation. If confirmed with deeper and higher resolution data, this may lead to re-examination of those explanations for the $z > 10$ "blue monsters" that appeal to a brief, very early phase of galaxy assembly.

4 Cosmic Dawn and Population III Stars

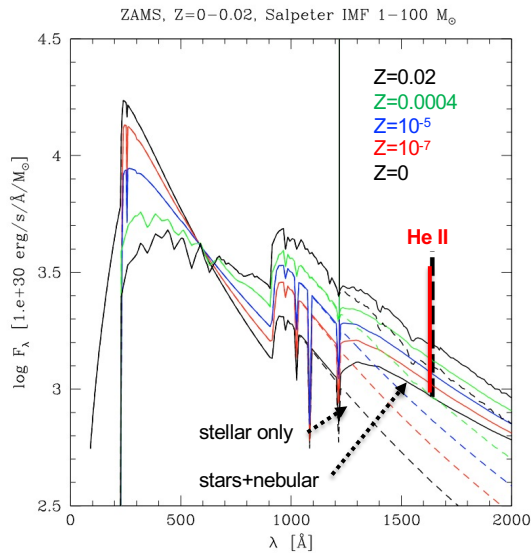
How would we recognise a primordial galaxy? Valuable insight has followed decades of theoretic work predicting spectroscopic signatures for metal-free stellar populations (referred to as Population III stars, Schaerer (2002, 2003)) as well as the nuclear products of pair instability supernovae arising from super-massive stars (Heger and Woosley, 2002).

The formation of a star-forming galaxy requires that the gas cooling timescale is less than the dynamical timescale. Pop III stars would likely form from gas clouds which cooled via molecular hydrogen in halos with virial temperatures of $T_{vir} \sim 10^3$ K. As atomic cooling is ineffective in such situations, the simulations suggest clouds will fragment with scales larger than those seen in present-day galaxies, thereby producing stars with masses $> 100 M_{\odot}$. Such hot stars evolve rapidly in their gaseous environments, producing a dominant nebular continuum which weakens line emission. For these metal-free systems, the most prominent signature expected is an intense He II recombination line at 1640 \AA . Furthermore, stars in the mass range $140 < M/M_{\odot} < 250$ are capable of exploding via a distinct pair instability supernova (PISN) mechanism. For these super-massive stars the core temperature is sufficient to enable pair exchanges between photons and electrons viz:

$$\gamma \rightleftharpoons e^+ + e^- \quad (15)$$

This exchange reduces the core pressure enabling rapid collapse. As the lifetime of such massive stars is very short ($\approx 2\text{-}5$ Myr), the rapid decline in He II visibility represents a major challenge in recognising such primordial systems (Figure 55). However, such PISN may leave characteristic metal signatures such as Fe excess abundance seen in $z > 10$ galaxies (Nakane et al., 2025).

The major factor that governs the transition to enriched Pop II stars is a lower characteristic stellar mass M_c associated with gas cooling with metals and dust as well as the redshift-dependent temperature of the cosmic microwave background $T_{CMB} \approx 2.7(1+z)$ deg K which acts as a temperature floor, e.g. $T = 60$ K at $z \approx 25$. Once M_c is reached, cooling cannot continue and Jeans' instability leads to a single star or cluster of that mass. The timescale of this transition depends on the supernova enrichment history and complexities due to blast wave physics, cosmological accretion, halo mergers and radiative feedback which can suppress H_2 cooling. Clearly hydrodynamical simulations are required to address these many issues. As an early example, Wise et al. (2014) studied the metallicity evolution for $10^6 M_{\odot}$ halos over

Integrated spectrum for $0 < Z/Z_{\odot} < 0.02$ 

Rapid decline in He II visibility

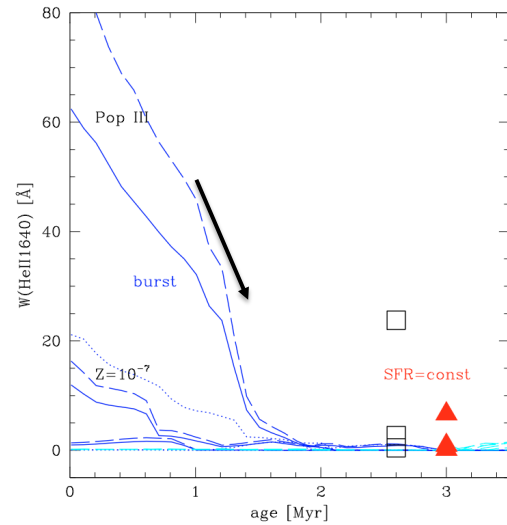


Fig. 55 Pioneering metal-free stellar population synthesis calculations from Schaerer (2003) which have stood the test of time remarkably well. (Left) Integrated spectra for a range of metallicities from zero to 0.02 solar, demonstrating for the metal-free $Z=0$ case the relative contributions of stars and nebular continuum. The prominent emission line of He II 1640 Å emerges as the most likely detectable feature for a Population III system. (Right) The rapid decline in He II visibility over 2 Myr will make it challenging to identify such primordial systems.

$15 < z < 7$ and claimed a critical metallicity of $Z_{crit} \sim 10^{-3}$ for enabling lower mass star formation. The work demonstrated a halo might reach this threshold simply after a single pair instability supernova (PISN). The complete transition from Pop III to Pop II then follows over several hundred Myr. Pockets of Pop III stars can co-exist with Pop II populations throughout the reionisation era and possibly even to lower redshifts. The topic is well reviewed by Bromm and Larson (2004); Bromm and Yoshida (2011) and most recently by Klessen and Glover (2023).

Following the launch of JWST, a number of articles have focused specifically on how to recognise Pop III systems and here I focus on the zoom simulations by Katz et al. (2023) for a $3 \cdot 10^8 M_{\odot}$ halo with sub-parsec resolution using on-the-fly radiative transfer, non-equilibrium chemistry and cooling formalisms (Figure 56, see also Nakajima and Maiolino (2022); Zier et al. (2025); Lecroq et al. (2025); Rusta et al. (2025)). As can be seen, metal enrichment in C, N, O and Fe proceeds almost instantaneously after the first PISN. Pop III star formation can also co-exist with Pop II over several hundred Myr (down to $z \approx 10$ in this particular halo). We can use these simulations to check the credibility of several JWST claims for extremely metal-poor systems.

Figure 57 shows two claimed Pop III candidates that have received widespread discussion at the time of the Lectures. Maiolino et al. (2024b) has located an isolated He II 1640 Å emitter in the vicinity of GNz=11 at $z=10.6$. No other lines are observed and the stellar mass of the associated population is estimated to be $\approx 6 \times 10^5 M_{\odot}$. Vanzella et al. (2023) have used the NIRSpec integral field mode to study a highly-magnified compact source, LAP1-B at $z=6.6$ straddling the critical line of the Frontier Field cluster MACS0416. At this lower redshift, Balmer lines and a tentative He II 1640 Å are detected and the absence of [O III] emission places an impressive upper metallicity limit of $< 0.3\%$ solar. More recent observations of this source are discussed by Nakajima et al. (2025); Visbal et al. (2025). There are several other Pop III claims in the current literature worthy of investigation, including Wang et al. (2024c); Maiolino et al. (2025); Morishita et al. (2025). However, here I focus on the first two claims.

The burden of proof for a Pop III claim is very high! According to the Katz et al. (2023) models, we require He II to be particularly intense in comparison to $H\alpha$ in order to capture the brief lifetime associated with such metal-free massive stars (specifically $\log \text{He II}/H\alpha > -0.5$). Likewise, [O III] 5007 Å, the most prominent metal line accessible at high redshift remains weak initially so any claim for metal-free halos will necessitate exquisitely deep JWST exposures. Katz et al recommend $\log [\text{O III}]/H\beta < -1.5$. Figure 58 shows these constraints as shaded areas in the time evolution of He II/ $H\alpha$ and the [O III]/ $H\beta$ vs metallicity plot. Vanzella’s lensed source LAP1-B certainly fulfills the He II criterion but deeper data would be needed to match the [O III]/ $H\beta$ constraint. At the time of writing the sole detection of He II in the object associated with GNz-11 could be promising in terms of a high He II/Balmer line ratio, but deeper data is required to place a meaningful upper limit on O/H. The candidate proposed by Morishita et al. (2025) is also very promising but at lower redshift.

So what are the prospects for locating ‘cosmic dawn’ with JWST? I’m of the opinion that there may never be an unambiguous discovery of a chemically-pristine galaxy. The time window for metal-free stellar population is < 5 Myr so catching an example would be extremely fortuitous. We may find examples embedded in chemically-enriched regions at lower redshift but I suspect this is not the ‘Holy Grail’ that JWST was hoped to deliver! More likely we may deduce the birth of starlight indirectly from tracing the continued decline of the cosmic star formation rate density and gas phase metallicity from more extensive surveys. Right now the absence of convincing $z > 15$ candidates

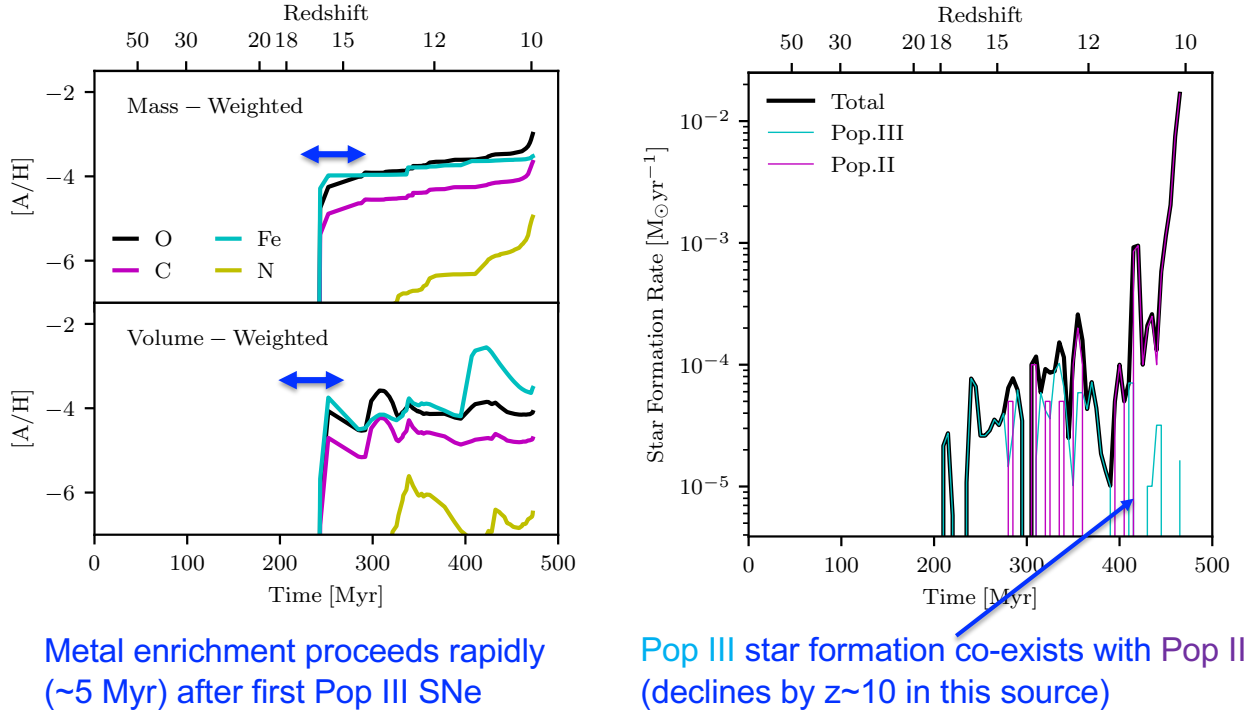


Fig. 56 Hydrodynamical simulation of the Pop III to Pop II transition incorporating radiative transfer, non-equilibrium chemistry and cooling for a $3 \cdot 10^8 M_\odot$ halo (Katz et al., 2023). (Left) Metal-enrichment proceeds extremely rapidly (< 5 Myr) following the first supernovae making any discovery of genuine metal-free populations very challenging observationally. (Right) However Pop III regions can co-exist with enriched stellar populations over many 100 Myr.

might optimistically suggest we can anticipate achieving such a statistical result during the lifetime of JWST.

5 The Promise of 21cm Surveys

Despite considerable technical challenges, charting the redshift-dependent 21 cm signal of neutral hydrogen with radio interferometers offers the exciting prospect of complementing the rapid progress being made in studies of the early universe with JWST. Liu and Shaw (2020) document an exciting array of “pathfinder” facilities prior to the deployment of the Square Kilometre Array (SKA) of which the low frequency component under construction in Western Australia is the most relevant for high redshift surveys. The current facilities of interest include the Giant Metrewave Radio Telescope (GMRT), a 45 metre dish in Pune, India surveying at frequencies above 50 MHz, the Murchison Widefield Array (MWA), a 3km interferometer in Western Australia (> 70 MHz), the Low Frequency Array (LOFAR), a widely distributed European interferometer centered on the Netherlands ($1 - 90$ MHz) and the Hydrogen Epoch of Reionisation Array (HERA), a 3 km interferometer in South Africa (> 50 MHz). At the redshifts of interest for cosmic dawn ($15 < z < 25$ corresponding to 21cm transitions at 100 to 60 MHz), each of these pathfinders is attempting to overcome foreground signals and thereby demonstrate the potential of SKA due to begin science operations later this decade (2028 at the time of writing).

Radio wavelength studies of the 21cm line of neutral hydrogen have a number of advantages over those of Lyman α . The latter is a resonant line and even a small neutral fraction by volume ($x_{HI} \approx 10^{-3}$) renders the IGM opaque to detection. Prior to the onset of reionisation, the temperature of the IGM T_{IGM} is too low to collisionally excite the $n=2$ level of hydrogen so we must use a weaker line. Predicted by van de Hulst (1945) following a suggestion by Jan Oort, the 21cm line was first detected (from the window of a Harvard office!) in 1951 (Ewen and Purcell, 1951). The 21cm transition arises from the spin flip of the electron in the hydrogen atom causing a hyperfine splitting of the ground state with an energy gap of $5.9 \cdot 10^{-6}$ eV. Figure 59 illustrates some of the key characteristics of this remarkable atomic transition.

Radio astronomers have their own nomenclature for studies of this line. The *spin temperature* T_s is defined via

$$n_{F=1}/n_{F=0} \propto \exp(-T_*/T_s) \quad (16)$$

where $T_s = (h\nu_{21}/k) = 68mK$

The associated optical depth τ_{21} is only $\approx 1\%$ so the line can readily be traced even in a fully neutral IGM, a major advantage over Ly α .

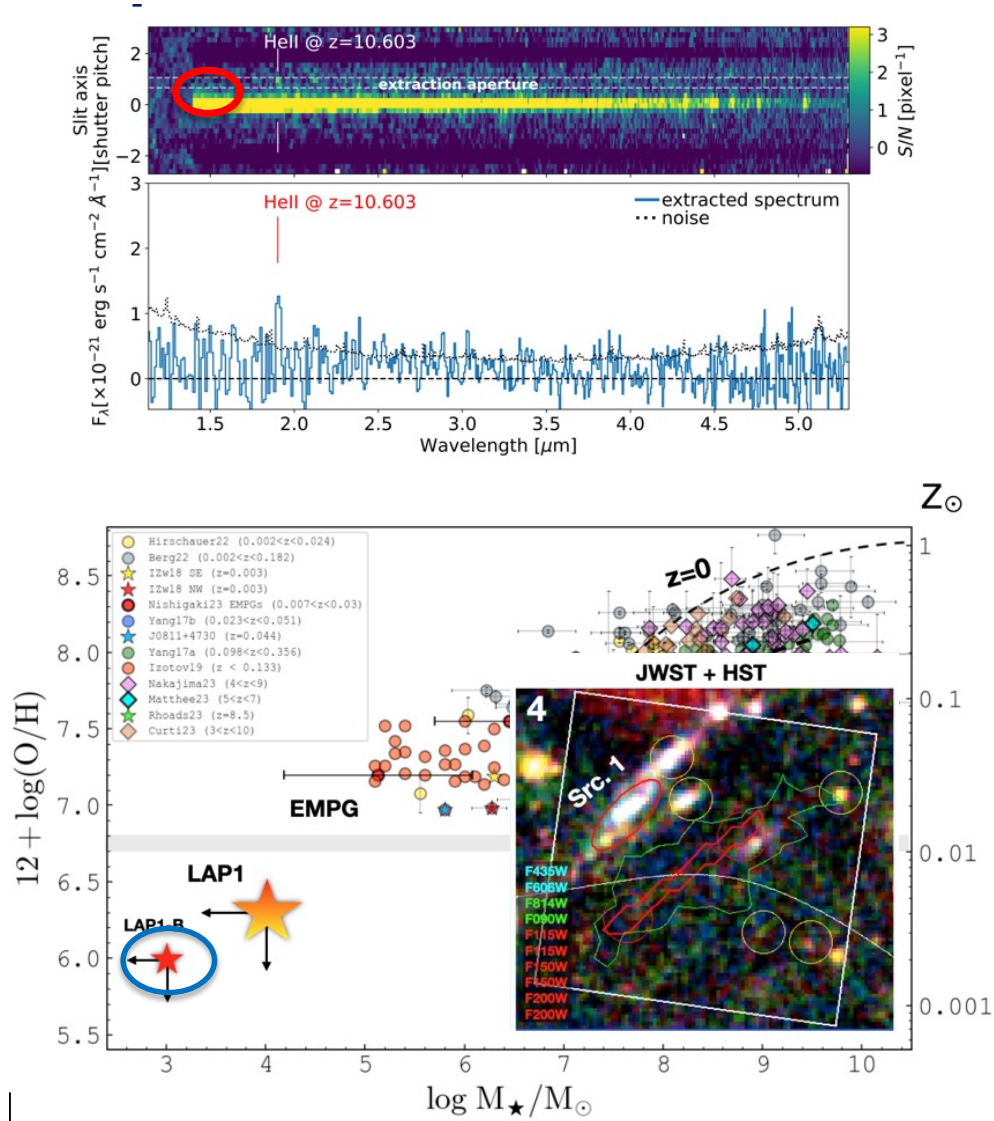


Fig. 57 Two well-discussed recent claims of promising Pop III candidates from JWST observations. (Top) An isolated emission line, ostensibly He II 1640 Å alongside the spectrum of GN-z11 at a redshift $z=10.6$ (Maiolino et al., 2024b). The absence of any continuum suggests a rest-frame equivalent width of 170 Å and no other emission lines are visible. (Bottom) NIRCcam IFS data for a highly-magnified ($\mu > 100$) galaxy (red elongated contour) straddling the critical line of the lensing cluster MACS0416. Lyman and Balmer emission lines are detected and a possible He II but no [O III] leading to an upper limit on the gas-phase metallicity of 0.3% solar (Vanzella et al., 2023; Nakajima et al., 2025).

Radio astronomers also define the *brightness temperature* T_B according to the line intensity I_ν in the Rayleigh-Jeans limit (where the 21cm frequency is less than the peak of the CMB black body emission at that redshift), whence:

$$I_\nu = 2kT_B\nu^3c^{-2} \quad (17)$$

Note that T_S can deviate from the kinetic temperature of the gas due to the presence of radiation.

In the short term, the main utility of SKA 21cm studies will be in tomographic studies of the neutral and ionised regions during the later stages of reionisation. This relates primarily to the topics of Lecture 1 and will not be expanded further here, except to say a particularly promising technique will be the cross-correlation between fluctuations in the 21cm emission and the spatial distribution of various sources (e.g. galaxies and AGN) (Gagnon-Hartman et al., 2025). This will offer a promising causal connection between sources of ionising photons and the nature of the IGM.

However, for the present topic of ‘cosmic dawn’, Figure 60 illustrates how the brightness temperature T_B is expected to evolve during this key era (see Pritchard and Loeb (2012); Koopmans et al. (2021) for details). Starting from the highest redshifts in the dark ages, the cosmic expansion cools the gas at a rate ($T_{\text{gas}} \propto a(t)^{-3}$) faster than the background radiation ($T_{\text{rad}} \propto a(t)^{-1}$), while atomic collisions

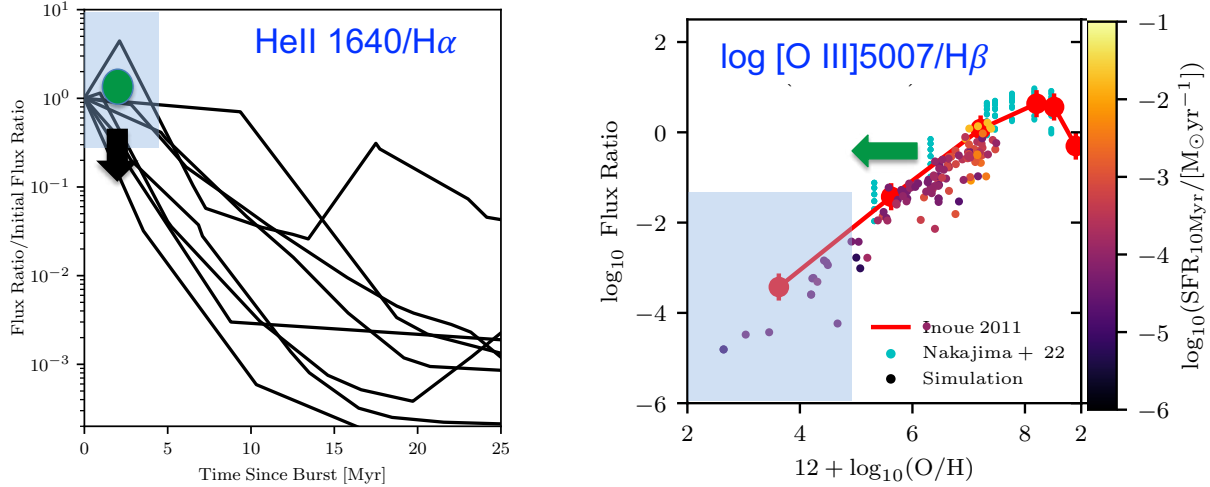


Fig. 58 Comparison of the properties of the two claimed Pop III candidates discussed in Figure 57 in the context of two Pop III criteria proposed by Katz et al. (2023). In both panels these criteria are indicated by the shaded blue region where convincing Pop III candidates should lie. Green symbols refer to the observational data for the lensed source proposed by Vanzella et al. (2023), black symbols to the He II detection of Maiolino et al. (2024b). (Left) The prominence of He II should approximate that of H α as the ratio decays rapidly after an initial metal-free burst. Vanzella et al's He II identification is tentative but would be within range; Maiolino et al see no hydrogen emission so in principle their source is also in range. (Right) [O III] / H β should be lower than 1% for a promising case. Again Vanzella et al are close with such a weak [OIII] but there is no meaningful constraint from Maiolino et al.

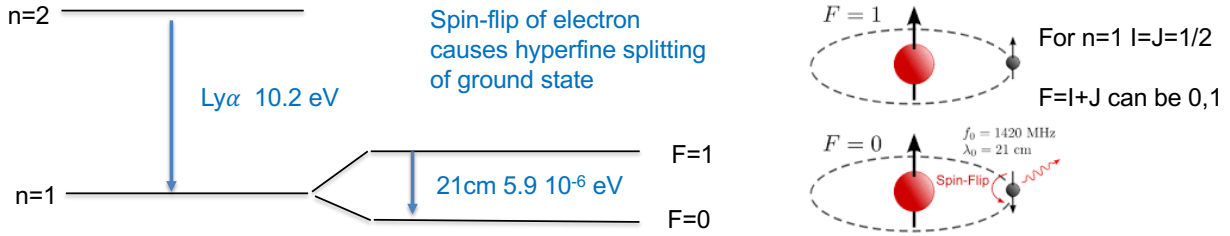


Fig. 59 Physical origin of the 21cm of neutral hydrogen via the hyperfine splitting of the $n=1$ ground state via the two opposing spin states of the electron, corresponding to a total angular momentum quantum number $F=I+J=0$ or 1 . Compared to Ly α , the 21cm line is a sensitive measure of the neutral hydrogen throughout the reionisation era and beyond.

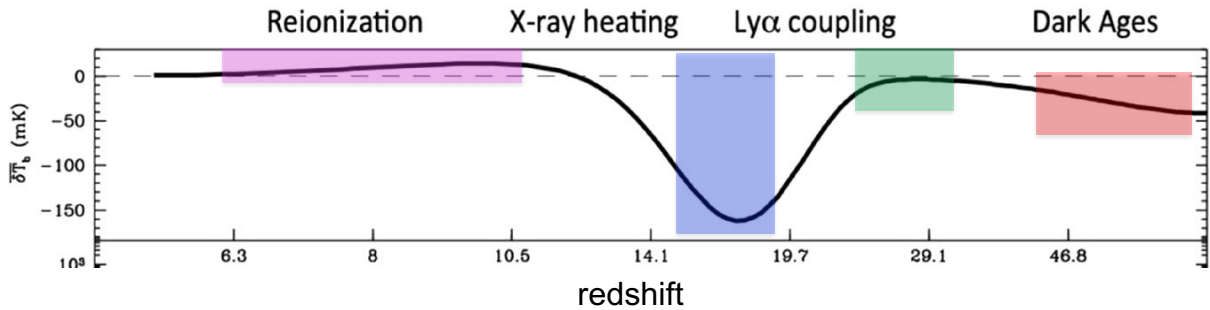


Fig. 60 Evolution of the differential brightness temperature δT_B of the 21cm line of neutral hydrogen with respect to the background microwave background during the transition from the dark ages through cosmic dawn to the reionisation era. A negative differential indicates the line is seen in absorption and a positive one indicates an emission line. Of particular significance is the strong absorption which occurs when Ly α photons propagate from gas clouds heated by young stars (see Figure 61). This offers a promising marker of 'cosmic dawn' (Koopmans et al., 2021).



Fig. 61 Importance of the Wouthuysen-Field effect as a potential 21cm absorption signature of cosmic dawn. (Left) Resonant scattering of Ly α photons from the first stars can excite hydrogen from a hyperfine $n=1$ state to an equivalent $n=2$ state. The selection rule does not permit a transition from $F=0$ to 0 , but from either $n=2$ level a Ly α photon can be emitted and return the atom into the other hyperfine state and thus induce the spin-flip necessary for a 21cm absorption. (Centre and Right) Claimed detection of all-sky 21cm absorption at $z \approx 18$ from the EDGES experiment (Bowman et al., 2018). This potentially exciting result may be consistent with early JWST galaxy data but has not been reproduced by other 21cm experiments.

maintain a spin temperature T_S equal to the gas temperature. In this case the 21cm line is seen in absorption against the CMB. As the universe expands, the decreasing gas density renders atomic collisions ineffective so the spin temperature equals the radiation temperature and there is no 21cm signal. When starlight emerges, the IGM is heated, so the spin temperature matches the gas temperature and the 21cm signal is seen once again in absorption. Eventually T_S exceeds T_{rad} as the radiation continues to cool. This leads to 21cm emission throughout the reionisation era.

Although the spin flip that produces either 21cm emission or absorption is initially produced by collisional processes (e.g. H+H, H+p, H+e), at ‘cosmic dawn’ Lyman α photons can induce an additional process first evaluated independently by Siegfried Wouthuysen (Wouthuysen, 1952) and George Field (Field, 1958). This remarkable effect illustrated in Figure 61 offers a distinct indicator of ‘cosmic dawn’. Resonant scattering of Ly α can excite hydrogen from a hyperfine $n=1$ ground state to a hyperfine $n=2$ state. However, while the dipole selection rule permits quantum changes $\Delta F = 0, 1$ the specific transition $F = 0 \rightarrow 0$ is not permitted. However, from either $n=2$ level a Lyman α photon can be emitted, and by the same selection rule, return the atom into the other hyperfine state. In this way the arrival of Lyman α photons from hydrogen heated by the first stars can induce the spin flip necessary for a 21 cm absorption signal against the CMB.

Since this would be a generic signal at a given redshift across the sky, there have been various attempts to detect it prior to SKA. The most widely-discussed result is a claimed detected at 78 MHz by the EDGES all-sky receiver in Western Australia (Bowman et al. (2018), Figure 61). Skeptics have argued this absorption signal over $15 < z < 20$ is surprisingly deep and may be an artefact of incorrect subtraction of foreground synchrotron and free-free emission (c.f. Hills et al. (2018)). An independent radio telescope, SARAS3 in India, has failed to reproduce the EDGES signal (Singh et al., 2022). Despite these controversies and challenges in removing foregrounds, we can be optimistic that this is a second, independent, probe of the natural of the IGM at early cosmic times which is sensitive to the birth of starlight through a remarkable coupling of Lyman α and the 21 cm transition. It is encouraging that the lifetime of JWST will overlap with almost a decade of SKA observations so synergistic work will hopefully pinpoint cosmic dawn.

6 Summary

In this lecture we discussed the emerging census of galaxies at redshifts $z > 10$. The frontier has been extended from $z=11.1$ with HST (415 Myr after the Big Bang) to $z=14.4$ (290 Myr). Although a mere 125 Myr earlier in cosmic time, both the increased data content and results have been impressive. Specifically

1. Prior to JWST, we only had one spectroscopically confirmed $z > 10$ galaxy (GN-z11 whereas at the time of writing we have over 40. Early exploration of the $15 < z < 20$ redshift range has failed to find credible candidates which may indicate a tantalising downturn in the population towards ‘cosmic dawn’.
2. The abundance and particularly the luminosity of these sources exceeded predictions from models based on the assumption of constant star-formation efficiency in the standard cosmological model. Although the origin of this excess is not yet agreed, some combination of burst-like activity and the presence of super-massive stars in metal-poor halos are promising explanations.

We also discussed the practicality of recognising a primordial galaxy containing purely metal-free Population III stars.

1. Simulations suggest a genuine Pop III stellar system occupies a very brief phase, lasting $< 3-5$ Myr, prior to enrichment from pair instability and Type II supernovae. According to contemporary models, the burden of proof in locating one with the expected ratios of He II, Balmer and oxygen lines will be observationally very challenging. Pop III systems can also be embedded in otherwise enriched galaxies through the reionisation era.
2. The epoch of ‘cosmic dawn’ may more easily be identified statistically via comprehensive measures of the declining gas-phase metallicities or careful ‘age-dating’ of lower redshift systems. We also discussed the Wouthuysen-Field effect whereby Lyman α photons from

gas clouds heated by the first generation of stars can induce an all-sky 21cm absorption signature against the microwave background. SKA-Low and related pathfinders may soon be able to confirm the redshift of this feature.

Finally, as a parting thought, will our work on galaxy formation and reionisation be complete with an estimate of when cosmic dawn occurred? Possibly not if individual super-massive stars could exist at yet higher redshifts leading to an earlier ionised era. Conceivably the universe may then briefly recombine and return to darkness. Such “two-stage” reionisation histories were popular in the early 2000s and may not be ruled out by JWST during its lifetime. Perhaps we can then continue a search for such a brief period of ionised gas with SKA-Low in the redshift range $20 < z < 30$?

7 Recommended Reading on the Redshift Frontier

Classic Articles

1. Partridge and Peebles (1967) - pioneering paper discussing visibility of Ly α in primaeval galaxies (PGs)
2. Baron and White (1987) - primaeval galaxies in CDM cosmology
3. Pritchett (1994) - historic review of attempts to find PGs
4. Bromm and Yoshida (2011) - theory of PGs
5. Klessen and Glover (2023) - theory of Pop III stars
6. Pritchard and Loeb (2012) - prospect of 21cm surveys

JWST-relevant Predictions

1. Schaerer (2003) - visionary article on recognising Pop III stars
2. Inoue (2011) - visibility of metal-free galaxies
3. Wise et al. (2014) - early numerical simulation of PGs
4. Katz et al. (2023) - recent simulations in context of JWST data
5. Koopmans et al. (2021) - 21cm observations at high redshift

Observations

1. Oesch et al. (2016) - pioneering HST redshift measurement for GN-z11
2. Bunker et al. (2023) - JWST spectrum of GN-z11
3. Donnan et al. (2024) - wide-field census of star-forming galaxies beyond $z=10$
4. Robertson et al. (2024) - deep field census of star-forming galaxies beyond $z=11.5$
5. Carniani et al. (2024) - discussion of super-luminous galaxies beyond $z=10$
6. Vanzella et al. (2023) - extremely low metallicity lensing system
7. Maiolino et al. (2024b) - claimed Pop III candidate associated with GN-z11

8 Epilogue

It probably escaped the attention of most Saas-Fee participants that this is the second time I have given a course of lectures at Saas-Fee. I gave a series of nine(!) lectures entitled *Observations of the High Redshift Universe* in 2006. The text of those lectures can be found on the arXiv (Ellis, 2008) and are, of course, published in the relevant Saas-Fee volume 36 entitled *First Light in the Universe*. I thought it would be amusing (and humiliating for me...) to compare what was written about future prospects in 2006 with today's reality!

Here are two examples:

On cosmic reionisation: At the time the most distant galaxy was IOK-1 at $z=6.96$ (Iye et al., 2006) and so observationally we hadn't truly entered the reionisation era. Accordingly I wrote:

It seems an impossible task to give an authoritative observational account of how to probe this era. So many issues are complete imponderables! When did reionisation occur? Was it a gradual event made possible by a complex time sequence of sources, or was there a spectacular synchronised moment? Can we conceive of an initial event, followed by recombination and a second phase? What were the sources responsible? And what is the precise process by which photons escape the sources.

Reading this 19 years later, I think we can all agree we have made remarkable progress with several hundred spectroscopically-studied galaxies in the reionisation era from $7 < z < 14$ (an era completely uncharted in 2006) which has given us a fairly well-defined history of reionisation although the escape fraction challenge remains. We've also encountered new puzzles, including the presence of what appear to be supermassive black holes at early epochs and luminous galaxies at $z > 10$. The difference is the exquisite observational and computational tools we have now to make further progress.

On future prospects: I wrote the following embarrassing prophecy.

I take out my crystal ball and consider the likely progress we can expect with current and near-term facilities including JWST (due to be launched in 2013) and a new generation of extremely large telescopes..due to be operational from 2016. The exciting redshift range $7 < z < 12$ will be the province of improved drop-out searches using the (near-infrared) instrument WFC3 to be installed on HST in 2008-9. A major stumbling block, even at $z=5-6$, is efficient spectroscopic follow-up. Candidates may be found in abundance but how will they be

confirmed? It is quite likely that, by 2013, the redshift range containing the earliest galactic sources, estimated at present to be $10 < z < 20$, will have been refined sufficiently by instruments on our existing 8-10 metre class telescopes. JWST and future ELTs will focus on...the chemical maturity of the most luminous sources found at high redshift.

Although I was pretty good on predicting we'd reach $z=11$ with HST's WFC3, clearly I was over-optimistic by at least a decade with JWST and the US-based ELTs. It may seem depressing to some that what's written about the future in 2006 is almost as apt in some respects today, but I think we have renewed optimism now having seen the spectacular quality of the JWST data and the astonishing progress made in only 2.5 years.

References

- Adamo A, Atek H, Bagley MB, Bañados E, Barrow KSS, Berg DA, Bezanson R, Bradač M, Brammer G, Carnall AC, Chisholm J, Coe D, Dayal P, Eisenstein DJ, Eldridge JJ, Ferrara A, Fujimoto S, de Graaff A, Habouzit M, Hutchison TA, Kartaltepe JS, Kassin SA, Kriek M, Labbé I, Maiolino R, Marques-Chaves R, Maseda MV, Mason C, Matthee J, McQuinn KBW, Meynet G, Naidu RP, Oesch PA, Pentericci L, Pérez-González PG, Rigby JR, Roberts-Borsani G, Schaerer D, Shapley AE, Stark DP, Stiavelli M, Strom AL, Vanzella E, Wang F, Wilkins SM, Williams CC, Willott CJ, Wylezalek D and Nota A (2024), May. The First Billion Years, According to JWST. *arXiv e-prints*, arXiv:2405.21054doi: 10.48550/arXiv.2405.21054. 2405.21054.
- Álvarez-Márquez J, Crespo Gómez A, Colina L, Langeroodi D, Marques-Chaves R, Prieto-Jiménez C, Bik A, Alonso-Herrero A, Boogaard L, Costantin L, García-Marín M, Gillman S, Hjorth J, Iani E, Jermann I, Labiano A, Melinder J, Meyer R, Östlin G, Pérez-González PG, Rinaldi P, Walter F, van der Werf P and Wright G (2025), Mar. Insight into the starburst nature of Galaxy GN-z11 with JWST MIRI spectroscopy. *A&A* 695, A250. doi:10.1051/0004-6361/202451731. 2412.12826.
- Arrabal Haro P, Dickinson M, Finkelstein SL, Kartaltepe JS, Donnan CT, Burgarella D, Carnall AC, Cullen F, Dunlop JS, Fernández V, Fujimoto S, Jung I, Krips M, Larson RL, Papovich C, Pérez-González PG, Amorín RO, Bagley MB, Buat V, Casey CM, Chworowsky K, Cohen SH, Ferguson HC, Gialalisco M, Huertas-Company M, Hutchison TA, Kocovski DD, Koekemoer AM, Lucas RA, McLeod DJ, McLure RJ, Pirzkal N, Seillé LM, Trump JR, Weiner BJ, Wilkins SM and Zavala JA (2023), Oct. Confirmation and refutation of very luminous galaxies in the early Universe. *Nature* 622 (7984): 707–711. doi:10.1038/s41586-023-06521-7. 2303.15431.
- Asada Y, Willott C, Muzzin A, Bradač M, Brammer G, Desprez G, Iyer K, Marchesini D, Martis N, Noirot G, Sarrouh G, Sawicki M, Withers S, Fujimoto S, Felicioni G, Goovaerts I, Judež J, Jagga N, Merchant M, Mérida R and Robbins L (2025), Jul. Earliest Galaxy Evolution in the CANUCS+Technicolor fields: Galaxy Properties at $z \sim 10 - 16$ seen with the Full NIRC2 Medium and Broad Band Filters. *arXiv e-prints*, arXiv:2507.03124doi:10.48550/arXiv.2507.03124. 2507.03124.
- Bacon R (2024), Oct. From TIGER to WST: scientific impact of four decades of developments in integral field spectroscopy. *Astrophysics and Space Science* 369 (10), 111. doi:10.1007/s10509-024-04369-5. 2410.02399.
- Baggen JFW, van Dokkum P, Brammer G, de Graaff A, Franx M, Greene J, Labbé I, Leja J, Maseda MV, Nelson EJ, Rix HW, Wang B and Weibel A (2024), Dec. The Small Sizes and High Implied Densities of "Little Red Dots" with Balmer Breaks Could Explain Their Broad Emission Lines without an Active Galactic Nucleus. *ApJ* 977 (1), L13. doi:10.3847/2041-8213/ad90b8. 2408.07745.
- Baron E and White SDM (1987), Nov. The Appearance of Primeval Galaxies. *ApJ* 322: 585. doi:10.1086/165754.
- Barrow KSS, Robertson BE, Ellis RS, Nakajima K, Saxena A, Stark DP and Tang M (2020), Oct. The Lyman Continuum Escape Survey: Connecting Time-dependent [O III] and [O II] Line Emission with Lyman Continuum Escape Fraction in Simulations of Galaxy Formation. *ApJ* 902 (2), L39. doi:10.3847/2041-8213/abbd8e. 2010.00592.
- Bogdán Á, Goulding AD, Natarajan P, Kovács OE, Tremblay GR, Chadayammuri U, Volonteri M, Kraft RP, Forman WR, Jones C, Churazov E and Zhuravleva I (2024), Jan. Evidence for heavy-seed origin of early supermassive black holes from a $z \approx 10$ X-ray quasar. *Nature Astronomy* 8 (1): 126–133. doi:10.1038/s41550-023-02111-9. 2305.15458.
- Bosman SEI, Fan X, Jiang L, Reed S, Matsuoka Y, Becker G and Haehnelt M (2018), Sep. New constraints on Lyman- α opacity with a sample of 62 quasars at $z \lesssim 5.7$. *MNRAS* 479 (1): 1055–1076. doi:10.1093/mnras/sty1344. 1802.08177.
- Bouwens RJ, Illingworth G, Ellis RS, Oesch P and Stefanon M (2022), Nov. z 2-9 Galaxies Magnified by the Hubble Frontier Field Clusters. II. Luminosity Functions and Constraints on a Faint-end Turnover. *ApJ* 940 (1), 55. doi:10.3847/1538-4357/ac86d1. 2205.11526.
- Bouwens R, Illingworth G, Oesch P, Stefanon M, Naidu R, van Leeuwen I and Magee D (2023), Jul. UV luminosity density results at $z \lesssim 8$ from the first JWST/NIRC2 fields: limitations of early data sets and the need for spectroscopy. *MNRAS* 523 (1): 1009–1035. doi:10.1093/mnras/stad1014. 2212.06683.
- Bowman JD, Rogers AEE, Monsalve RA, Mozdzen TJ and Mahesh N (2018), Mar. An absorption profile centred at 78 megahertz in the sky-averaged spectrum. *Nature* 555 (7694): 67–70. doi:10.1038/nature25792. 1810.05912.
- Bradley LD, Coe D, Brammer G, Furtak LJ, Larson RL, Kokorev V, Andrade-Santos F, Bhatawdekar R, Bradač M, Broadhurst T, Carnall A, Conselice CJ, Diego JM, Frye B, Fujimoto S, Hsiao TYY, Hutchison TA, Jung I, Mahler G, McCandliss S, Oguri M, Postman M, Sharon K, Trenti M, Vanzella E, Welch B, Windhorst RA and Zitron A (2023), Sep. High-redshift Galaxy Candidates at $z = 9-10$ as Revealed by JWST Observations of WHL0137-08. *ApJ* 955 (1), 13. doi:10.3847/1538-4357/acecfe. 2210.01777.
- Brazzini M, D'Eugenio F, Maiolino R, Juodžbalis I, Ji X and Scholtz J (2025), Jul. Ruling out dominant electron scattering in Little Red Dots' Rosetta Stone using multiple hydrogen lines. *arXiv e-prints*, arXiv:2507.08929doi:10.48550/arXiv.2507.08929. 2507.08929.
- Brinchmann J and Ellis RS (2000), Jun. The Mass Assembly and Star Formation Characteristics of Field Galaxies of Known Morphology. *ApJ* 536 (2): L77–L80. doi:10.1086/312738. astro-ph/0005120.
- Broadhurst TJ, Ellis RS and Shanks T (1988), Dec. The Durham/Anglo-Australian telescope faint galaxy redshift survey. *MNRAS* 235: 827–856. doi:10.1093/mnras/235.3.827.
- Bromm V and Larson RB (2004), Sep. The First Stars. *ARA&A* 42 (1): 79–118. doi:10.1146/annurev.astro.42.053102.134034. astro-ph/0311019.
- Bromm V and Yoshida N (2011), Sep. The First Galaxies. *ARA&A* 49 (1): 373–407. doi:10.1146/annurev-astro-081710-102608. 1102.4638.
- Bruzual A. G and Charlot S (1993), Mar. Spectral Evolution of Stellar Populations Using Isochrone Synthesis. *ApJ* 405: 538. doi:10.1086/172385.
- Bunker AJ, Saxena A, Cameron AJ, Willott CJ, Curtis-Lake E, Jakobsen P, Carniani S, Smit R, Maiolino R, Witstok J, Curti M, D'Eugenio F, Jones GC, Ferruit P, Arribas S, Charlot S, Chevallard J, Giardino G, de Graaff A, Looser TJ, Lützgendorf N, Maseda MV, Rawle T, Rix HW, Del Pino BR, Alberts S, Egami E, Eisenstein DJ, Endsley R, Hainline K, Hausen R, Johnson BD, Rieke G, Rieke M, Robertson BE, Shivaee I, Stark DP, Sun F, Tacchella S, Tang M, Williams CC, Willmer CNA, Baker WM, Baum S, Bhatawdekar R, Bowler R, Boyett K, Chen Z, Circosta C, Helton JM, Ji Z, Kumari N, Lyu J, Nelson E, Parlanti E, Perna M, Sandles L, Scholtz J, Suess KA, Topping MW, Übler H, Wallace IEB and Whittier L (2023), Sep. JADES NIRS2 Spectroscopy of GN-z11: Lyman- α emission and possible enhanced nitrogen abundance in a $z =$

- 10.60 luminous galaxy. *A&A* 677, A88. doi:10.1051/0004-6361/202346159. 2302.07256.
- Cameron AJ, Katz H, Rey MP and Saxena A (2023), Aug. Nitrogen enhancements 440 Myr after the big bang: supersolar N/O, a tidal disruption event, or a dense stellar cluster in GN-z11? *MNRAS* 523 (3): 3516–3525. doi:10.1093/mnras/stad1579. 2302.10142.
- Cammelli V, Tan JC, Young AR, Hayes MJ, Singh J, Ellis RS, Saxena A, Laporte N, Monaco P and Keller BW (2025), Jan. Glimmers in the Cosmic Dawn. II. A variability census of supermassive black holes across the Universe. *arXiv e-prints*, arXiv:2501.17675doi:10.48550/arXiv.2501.17675. 2501.17675.
- Carnall AC, McLure RJ, Dunlop JS and Davé R (2018), Nov. Inferring the star formation histories of massive quiescent galaxies with BAGPIPES: evidence for multiple quenching mechanisms. *MNRAS* 480 (4): 4379–4401. doi:10.1093/mnras/sty2169. 1712.04452.
- Carniani S, Hainline K, D'Eugenio F, Eisenstein DJ, Jakobsen P, Witstok J, Johnson BD, Chevallard J, Maiolino R, Helton JM, Willott C, Robertson B, Alberts S, Arribas S, Baker WM, Bhatawdekar R, Boyett K, Bunker AJ, Cameron AJ, Cargile PA, Charlot S, Curti M, Curtis-Lake E, Egami E, Giardino G, Isaak K, Ji Z, Jones GC, Kumari N, Maseda MV, Parlanti E, Pérez-González PG, Rawle T, Rieke G, Rieke M, Del Pino BR, Saxena A, Scholtz J, Smit R, Sun F, Tacchella S, Übler H, Venturi G, Williams CC and Willmer CNA (2024), Sep. Spectroscopic confirmation of two luminous galaxies at a redshift of 14. *Nature* 633 (8029): 318–322. doi:10.1038/s41586-024-07860-9. 2405.18485.
- Casey CM, Akins HB, Finkelstein SL, Franco M, Fujimoto S, Liu D, Long AS, Magdis G, Manning SM, McKinney J, Shuntov M and Tanaka TS (2025), May. An upper limit of $10^6 M_\odot$ in dust from ALMA observations in 60 Little Red Dots. *arXiv e-prints*, arXiv:2505.18873doi:10.48550/arXiv.2505.18873. 2505.18873.
- Castellano M, Fontana A, Treu T, Merlin E, Santini P, Bergamini P, Grillo C, Rosati P, Acebron A, Leethochawalit N, Paris D, Bonchi A, Belfiori D, Calabrò A, Correnti M, Nonino M, Polenta G, Trenti M, Boyett K, Brammer G, Broadhurst T, Caminha GB, Chen W, Filippenko AV, Fortuni F, Glazebrook K, Mascia S, Mason CA, Menci N, Meneghetti M, Mercurio A, Metha B, Morishita T, Nanayakkara T, Pentericci L, Roberts-Borsani G, Roy N, Vanzella E, Vulcani B, Yang L and Wang X (2023), May. Early Results from GLASS-JWST. XIX. A High Density of Bright Galaxies at $z \approx 10$ in the A2744 Region. *ApJ* 948 (2), L14. doi:10.3847/2041-8213/accea5. 2212.06666.
- Castellano M, Napolitano L, Fontana A, Roberts-Borsani G, Treu T, Vanzella E, Zavala JA, Arrabal Haro P, Calabrò A, Llerena M, Mascia S, Merlin E, Paris D, Pentericci L, Santini P, Bakx TJLC, Bergamini P, Cupani G, Dickinson M, Filippenko AV, Glazebrook K, Grillo C, Kelly PL, Malkan MA, Mason CA, Morishita T, Nanayakkara T, Rosati P, Sani E, Wang X and Yoon I (2024), Sep. JWST NIRSpec Spectroscopy of the Remarkable Bright Galaxy GHZ2/GLASS-z12 at Redshift 12.34. *ApJ* 972 (2), 143. doi:10.3847/1538-4357/ad5f88. 2403.10238.
- Chakraborty P, Sarkar A, Smith R, Ferland GJ, McDonald M, Forman W, Vogelsberger M, Torrey P, Garcia AM, Bautz M, Foster A, Miller E and Grant C (2025), May. Unveiling the Cosmic Chemistry. II. “Direct” T_e -based Metallicity of Galaxies at $3 \leq z \leq 10$ with JWST/NIRSpec. *ApJ* 985 (1), 24. doi:10.3847/1538-4357/adc7b5. 2412.15435.
- Chen Z, Stark DP, Mason CA, Tang M, Whittler L, Lu TY and Topping MW (2025), May. The Impact of Galaxy Overdensities and Ionized Bubbles on Ly α Emission at $z \sim 7.0 - 8.5$. *arXiv e-prints*, arXiv:2505.24080doi:10.48550/arXiv.2505.24080. 2505.24080.
- Choustikov N, Katz H, Saxena A, Garel T, Devriendt J, Slyz A, Kimm T, Blaizot J and Rosdahl J (2024), Aug. The great escape: understanding the connection between Ly α emission and LyC escape in simulated JWST analogues. *MNRAS* 532 (2): 2463–2484. doi:10.1093/mnras/stae1586. 2401.09557.
- Colless M, Ellis RS, Broadhurst TJ, Taylor K and Peterson BA (1993), Mar. Faint blue galaxies : high or low redshift ? *MNRAS* 261: 19. doi:10.1093/mnras/261.1.19.
- Conroy C (2013), Aug. Modeling the Panchromatic Spectral Energy Distributions of Galaxies. *ARA&A* 51 (1): 393–455. doi:10.1146/annurev-astro-082812-141017. 1301.7095.
- Conroy C and Gunn JE (2010), Apr. The Propagation of Uncertainties in Stellar Population Synthesis Modeling. III. Model Calibration, Comparison, and Evaluation. *ApJ* 712 (2): 833–857. doi:10.1088/0004-637X/712/2/833. 0911.3151.
- Cullen F, McLure RJ, McLeod DJ, Dunlop JS, Donnan CT, Carnall AC, Bowler RAA, Begley R, Hamadouche ML and Stanton TM (2023), Mar. The ultraviolet continuum slopes (β) of galaxies at $z \approx 8$ –16 from JWST and ground-based near-infrared imaging. *MNRAS* 520 (1): 14–23. doi:10.1093/mnras/stad073. 2208.04914.
- Curti M (2025), Apr. The Chemical Evolution of Galaxies. *arXiv e-prints*, arXiv:2504.08933doi:10.48550/arXiv.2504.08933. 2504.08933.
- Curti M, Cresci G, Mannucci F, Marconi A, Maiolino R and Esposito S (2017), Feb. New fully empirical calibrations of strong-line metallicity indicators in star-forming galaxies. *MNRAS* 465 (2): 1384–1400. doi:10.1093/mnras/stw2766. 1610.06939.
- Curti M, Mannucci F, Cresci G and Maiolino R (2020), Jan. The mass-metallicity and the fundamental metallicity relation revisited on a fully T_e -based abundance scale for galaxies. *MNRAS* 491 (1): 944–964. doi:10.1093/mnras/stz2910. 1910.00597.
- Curti M, D'Eugenio F, Carniani S, Maiolino R, Sandles L, Witstok J, Baker WM, Bennett JS, Piotrowska JM, Tacchella S, Charlot S, Nakajima K, Maheson G, Mannucci F, Amiri A, Arribas S, Belfiore F, Bonaventura NR, Bunker AJ, Chevallard J, Cresci G, Curtis-Lake E, Hayden-Pawson C, Jones GC, Kumari N, Laseter I, Looser TJ, Marconi A, Maseda MV, Scholtz J, Smit R, Übler H and Wallace IEB (2023), Jan. The chemical enrichment in the early Universe as probed by JWST via direct metallicity measurements at $z \sim 8$. *MNRAS* 518 (1): 425–438. doi:10.1093/mnras/stac2737. 2207.12375.
- Curti M, Maiolino R, Curtis-Lake E, Chevallard J, Carniani S, D'Eugenio F, Looser TJ, Scholtz J, Charlot S, Cameron A, Übler H, Witstok J, Boyett K, Laseter I, Sandles L, Arribas S, Bunker A, Giardino G, Maseda MV, Rawle T, Rodríguez Del Pino B, Smit R, Willott CJ, Eisenstein DJ, Hausen R, Johnson B, Rieke M, Robertson B, Tacchella S, Williams CC, Willmer C, Baker WM, Bhatawdekar R, Egami E, Helton JM, Ji Z, Kumari N, Perna M, Shivaee I and Sun F (2024), Apr. JADES: Insights into the low-mass end of the mass-metallicity-SFR relation at $3 \leq z \leq 10$ from deep JWST/NIRSpec spectroscopy. *A&A* 684, A75. doi:10.1051/0004-6361/202346698. 2304.08516.
- Curtis-Lake E, Carniani S, Cameron A, Charlot S, Jakobsen P, Maiolino R, Bunker A, Witstok J, Smit R, Chevallard J, Willott C, Ferruit P, Arribas S, Bonaventura N, Curti M, D'Eugenio F, Franx M, Giardino G, Looser TJ, Lützgendorf N, Maseda MV, Rawle T, Rix HW, Rodríguez del Pino B, Übler H, Sirianni M, Dressler A, Egami E, Eisenstein DJ, Endsley R, Hainline K, Hausen R, Johnson BD, Rieke M, Robertson B, Shivaee I, Stark DP, Tacchella S, Williams CC, Willmer CNA, Bhatawdekar R, Bowler R, Boyett K, Chen Z, de Graaff A, Helton JM, Hviding RE, Jones GC, Kumari N, Lyu J, Nelson E, Perna M, Sandles L, Saxena A, Sues KA, Sun F, Topping MW, Wallace IEB and Whittler L (2023), May. Spectroscopic confirmation of four metal-poor galaxies at $z = 10.3$ – 13.2 . *Nature Astronomy* 7: 622–632. doi:10.1038/s41550-023-01918-w. 2212.04568.
- de Belsunce R, Gratton S, Coulton W and Efstathiou G (2021), Oct. Inference of the optical depth to reionization from low multipole temperature and polarization Planck data. *MNRAS* 507 (1): 1072–1091. doi:10.1093/mnras/stab2215. 2103.14378.
- Dekel A, Sarkar KC, Birnboim Y, Mandelker N and Li Z (2023), Aug. Efficient formation of massive galaxies at cosmic dawn by feedback-free starbursts. *MNRAS* 523 (3): 3201–3218. doi:10.1093/mnras/stad1557. 2303.04827.
- D'Eugenio F, Maiolino R, Perna M, Uebler H, Ji X, McClymont W, Koudmani S, Sijacki D, Juodžbalis I, Scholtz J, Bennett J, Bunker AJ, Carniani S, Charlot S, Cresci G, Curtis-Lake E, Dalla Bontà E, Jones GC, Lyu J, Marconi A, Mazzolari G, Nelson EJ, Parlanti E, Robertson BE, Schneider R, Simmonds C, Tacchella S, Venturi G, Willott C, Witstok J and Witten C (2025), Mar. BlackTHUNDER strikes twice: rest-frame Balmer-line absorption and high Eddington accretion rate in a Little Red Dot at $z = 7.04$. *arXiv e-prints*, arXiv:2503.11752doi:10.48550/arXiv.2503.11752. 2503.11752.

- Dijkstra M (2014), Oct. Ly α Emitting Galaxies as a Probe of Reionisation. *Publications of the Astronomical Society of Australia* 31, e040. doi:10.1017/pasa.2014.33. 1406.7292.
- Djorgovski S, Spinrad H, McCarthy P and Strauss MA (1985), Dec. Discovery of a probable galaxy with a redshift of 3.218. *ApJ* 299: L1–L5. doi:10.1086/184569.
- Donnan CT, McLeod DJ, McLure RJ, Dunlop JS, Carnall AC, Cullen F and Magee D (2023), Apr. The abundance of $z \gtrsim 10$ galaxy candidates in the HUDF using deep JWST NIRC2 medium-band imaging. *MNRAS* 520 (3): 4554–4561. doi:10.1093/mnras/stad471. 2212.10126.
- Donnan CT, McLure RJ, Dunlop JS, McLeod DJ, Magee D, Arellano-Córdova KZ, Barrufet L, Begley R, Bowler RAA, Carnall AC, Cullen F, Ellis RS, Fontana A, Illingworth GD, Grogin NA, Hamadouche ML, Koekemoer AM, Liu FY, Mason C, Santini P and Stanton TM (2024), Sep. JWST PRIMER: a new multifield determination of the evolving galaxy UV luminosity function at redshifts $z = 9 - 15$. *MNRAS* 533 (3): 3222–3237. doi:10.1093/mnras/stae2037. 2403.03171.
- Dottorini D, Calabrò A, Pentericci L, Mascia S, Llerena M, Napolitano L, Santini P, Roberts-Borsani G, Castellano M, Amorin R, Dickinson M, Fontana A, Hathi N, Hirschmann M, Koekemoer AM, Lucas RA, Merlin E, Morales A, Pacucci F, Wilkins S, Arrabal Haro P, Bagley M, Finkelstein SL, Kartaltepe J, Papovich C and Pirzkal N (2025), Jun. Evolution of the UV slope of galaxies at cosmic morning ($z \lesssim 4$): The properties of extremely blue galaxies. *A&A* 698, A234. doi:10.1051/0004-6361/202453267. 2412.01623.
- Ebbels T, Ellis R, Kneib JP, Le Borgne JF, Pello R, Smail I and Sanahuja B (1998), Mar. Spectroscopic confirmation of redshifts predicted by gravitational lensing. *MNRAS* 295 (1): 75–91. doi:10.1046/j.1365-8711.1998.t01-1-29511181.x. astro-ph/9703169.
- Eggen OJ, Lynden-Bell D and Sandage AR (1962), Nov. Evidence from the motions of old stars that the Galaxy collapsed. *ApJ* 136: 748. doi:10.1086/147433.
- Ellis RS (2008), Observations of the High Redshift Universe, Loeb A, Ferrara A and Ellis RS, (Eds.), Saas-Fee Advanced Course 36: Cold Aqueous Planetary Geochemistry with FREZCHEM, 259–364.
- Ellis RS, McLure RJ, Dunlop JS, Robertson BE, Ono Y, Schenker MA, Koekemoer A, Bowler RAA, Ouchi M, Rogers AB, Curtis-Lake E, Schneider E, Charlot S, Stark DP, Furlanetto SR and Cirasuolo M (2013), Jan. The Abundance of Star-forming Galaxies in the Redshift Range 8.5–12: New Results from the 2012 Hubble Ultra Deep Field Campaign. *ApJ* 763 (1), L7. doi:10.1088/2041-8205/763/1/L7. 1211.6804.
- Endsley R, Stark DP, Whittler L, Topping MW, Johnson BD, Robertson B, Tacchella S, Alberts S, Baker WM, Bhatawdekar R, Boyett K, Bunker AJ, Cameron AJ, Carniani S, Charlot S, Chen Z, Chevallard J, Curtis-Lake E, Danhaive AL, Egami E, Eisenstein DJ, Hainline K, Helton JM, Ji Z, Looser TJ, Maiolino R, Nelson E, Puskás D, Rieke G, Rieke M, Rix HW, Sandles L, Saxena A, Simmonds C, Smit R, Sun F, Williams CC, Willmer CNA, Willott C and Witstok J (2024), Sep. The star-forming and ionizing properties of dwarf z 6–9 galaxies in JADES: insights on bursty star formation and ionized bubble growth. *MNRAS* 533 (1): 1111–1142. doi:10.1093/mnras/stae1857. 2306.05295.
- Ewen HJ and Purcell EM (1951), Sep. Observation of a Line in the Galactic Radio Spectrum: Radiation from Galactic Hydrogen at 1,420 Mc./sec. *Nature* 168 (4270): 356. doi:10.1038/168356a0.
- Fan X, Carilli CL and Keating B (2006), Sep. Observational Constraints on Cosmic Reionization. *ARA&A* 44 (1): 415–462. doi:10.1146/annurev.astro.44.051905.092514. astro-ph/0602375.
- Fan X, Bañados E and Simcoe RA (2023), Aug. Quasars and the Intergalactic Medium at Cosmic Dawn. *ARA&A* 61: 373–426. doi:10.1146/annurev-astro-052920-102455. 2212.06907.
- Feltre A, Charlot S and Gutkin J (2016), Mar. Nuclear activity versus star formation: emission-line diagnostics at ultraviolet and optical wavelengths. *MNRAS* 456 (3): 3354–3374. doi:10.1093/mnras/stv2794. 1511.08217.
- Ferland GJ, Chatzikos M, Guzmán F, Lykins ML, van Hooft PAM, Williams RJR, Abel NP, Badnell NR, Keenan FP, Porter RL and Stancil PC (2017), Oct. The 2017 Release Cloudy. *Revista Mexicana de Astronomía y Astrofísica* 53: 385–438. doi:10.48550/arXiv.1705.10877. 1705.10877.
- Ferrara A, Pallottini A and Dayal P (2023), Jul. On the stunning abundance of super-early, luminous galaxies revealed by JWST. *MNRAS* 522 (3): 3986–3991. doi:10.1093/mnras/stad1095. 2208.00720.
- Ferrara A, Gialalisco M, Pentericci L, Vanzella E, Calabrò A and Llerena M (2025), May. Redshift evolution of Lyman continuum escape fraction after JWST. *arXiv e-prints*, arXiv:2505.10619doi:10.48550/arXiv.2505.10619. 2505.10619.
- Field GB (1958), Jan. Excitation of the Hydrogen 21-CM Line. *Proceedings of the IRE* 46: 240–250. doi:10.1109/JRPROC.1958.286741.
- Finkelstein SL, Bagley MB, Ferguson HC, Wilkins SM, Kartaltepe JS, Papovich C, Yung LYA, Arrabal Haro P, Behroozi P, Dickinson M, Kocevski DD, Koekemoer AM, Larson RL, Le Bail A, Morales AM, Pérez-González PG, Burgarella D, Davé R, Hirschmann M, Somerville RS, Wuyts S, Bromm V, Casey CM, Fontana A, Fujimoto S, Gardner JP, Gialalisco M, Grazian A, Grogin NA, Hathi NP, Hutchison TA, Jha SW, Jogee S, Kewley LJ, Kirkpatrick A, Long AS, Lotz JM, Pentericci L, Pierel JDR, Pirzkal N, Ravindranath S, Ryan RE, Trump JR, Yang G, Bhatawdekar R, Bisigello L, Buat V, Calabrò A, Castellano M, Cleri NJ, Cooper MC, Croton D, Daddi E, Dekel A, Elbaz D, Franco M, Gawiser E, Holwerda BW, Huertas-Company M, Jaskot AE, Leung GCK, Lucas RA, Mobasher B, Pandya V, Tacchella S, Weiner BJ and Zavala JA (2023), Mar. CEERS Key Paper. I. An Early Look into the First 500 Myr of Galaxy Formation with JWST. *ApJ* 946 (1), L13. doi:10.3847/2041-8213/acade4. 2211.05792.
- Fletcher TJ, Tang M, Robertson BE, Nakajima K, Ellis RS, Stark DP and Inoue A (2019), Jun. The Lyman Continuum Escape Survey: Ionizing Radiation from [O III]-strong Sources at a Redshift of 3.1. *ApJ* 878 (2), 87. doi:10.3847/1538-4357/ab2045. 1806.01741.
- Flury SR, Jaskot AE, Ferguson HC, Worbeck G, Malkan K, Chisholm J, Saldana-Lopez A, Schaerer D, McCandliss S, Wang B, Ford NM, Heckman T, Ji Z, Gialalisco M, Amorin R, Atek H, Blaizot J, Borthakur S, Carr C, Castellano M, Cristiani S, De Barros S, Dickinson M, Finkelstein SL, Fleming B, Fontanot F, Garel T, Grazian A, Hayes M, Henry A, Mauerhofer V, Micheva G, Oey MS, Ostlin G, Papovich C, Pentericci L, Ravindranath S, Rosdahl J, Rutkowski M, Santini P, Scarlata C, Teplitz H, Thuan T, Trebitsch M, Vanzella E, Verhamme A and Xu X (2022), May. The Low-redshift Lyman Continuum Survey. I. New, Diverse Local Lyman Continuum Emitters. *ApJS* 260 (1), 1. doi:10.3847/1538-4365/ac5331. 2201.11716.
- Frenk CS, Ellis RS, Shanks T, Heavens AF and Peacock JA (1989), Jan., The epoch of galaxy formation. *Proceedings.*, Frenk CS, sEllis RS, Shanks T, Heavens AR and Peacock JA, (Eds.), The Epoch of Galaxy Formation, NATO Advanced Study Institute (ASI) Series C, 264, pp. 257.
- Furtak LJ, Zitrin A, Plat A, Fujimoto S, Wang B, Nelson EJ, Labbé I, Bezanson R, Brammer GB, van Dokkum P, Endsley R, Glazebrook K, Greene JE, Leja J, Price SH, Smit R, Stark DP, Weaver JR, Whitaker KE, Atek H, Chevallard J, Curtis-Lake E, Dayal P, Feltre A, Franx M, Fudamoto Y, Marchesini D, Mowla LA, Pan R, Suess KA, Vidal-García A and Williams CC (2023), Aug. JWST UNCOVER: Extremely Red and Compact Object at $z_{phot} \approx 7.6$ Triply Imaged by A2744. *ApJ* 952 (2), 142. doi:10.3847/1538-4357/acde9d. 2212.10531.
- Gagnon-Hartman S, Davies JE and Mesinger A (2025), Jul. Detecting galaxy – 21-cm cross-correlation during reionization. *A&A* 699, A131. doi:10.1051/0004-6361/202554456. 2502.20447.
- Garaldi E, Kannan R, Smith A, Springel V, Pakmor R, Vogelsberger M and Hernquist L (2022), Jun. The THESAN project: properties of the intergalactic medium and its connection to reionization-era galaxies. *MNRAS* 512 (4): 4909–4933. doi:10.1093/mnras/stac257. 2110.01628.
- García-Rojas J and Esteban C (2007), Nov. On the Abundance Discrepancy Problem in H II Regions. *ApJ* 670 (1): 457–470. doi:10.1086/521871. 0707.3518.
- Gelli V, Mason C and Hayward CC (2024), Nov. The Impact of Mass-dependent Stochasticity at Cosmic Dawn. *ApJ* 975 (2), 192. doi:10.3847/

- 1538-4357/ad7b36. 2405.13108.
- Giovinozzo E, Oesch PA, Weibel A, Meyer RA, Witten C, Bhagwat A, Brammer G, Chisholm J, de Graaff A, Gottumukkala R, Jecmen M, Katz H, Leja J, Marques-Chaves R, Maseda M, Shivaee I, Trebitsch M and Verhamme A (2025), Jul. Breaking Through the Cosmic Fog: JWST/NIRSpec Constraints on Ionizing Photon Escape in Reionization-Era Galaxies. *arXiv e-prints*, arXiv:2507.01096doi:10.48550/arXiv.2507.01096. 2507.01096.
- Glazebrook K, Ellis R, Colless M, Broadhurst T, Allington-Smith J and Tanvir N (1995), Mar. A faint galaxy redshift survey to $B=24$. *MNRAS* 273 (1): 157–168. doi:10.1093/mnras/273.1.157. astro-ph/9503116.
- Goulding AD, Greene JE, Setton DJ, Labbe I, Bezanson R, Miller TB, Atek H, Bogdán Á, Brammer G, Chemerynska I, Cutler SE, Dayal P, Fudamoto Y, Fujimoto S, Furtak LJ, Kokorev V, Khullar G, Leja J, Marchesini D, Natarajan P, Nelson E, Oesch PA, Pan R, Papovich C, Price SH, van Dokkum P, Wang B, Weaver JR, Whitaker KE and Zitrin A (2023), Sep. UNCOVER: The Growth of the First Massive Black Holes from JWST/NIRSpec-Spectroscopic Redshift Confirmation of an X-Ray Luminous AGN at $z = 10.1$. *ApJ* 955 (1), L24. doi:10.3847/2041-8213/ac7c5. 2308.02750.
- Greene JE, Labbe I, Goulding AD, Furtak LJ, Chemerynska I, Kokorev V, Dayal P, Volonteri M, Williams CC, Wang B, Setton DJ, Burgasser AJ, Bezanson R, Atek H, Brammer G, Cutler SE, Feldmann R, Fujimoto S, Glazebrook K, de Graaff A, Khullar G, Leja J, Marchesini D, Maseda MV, Matthee J, Miller TB, Naidu RP, Nanayakkara T, Oesch PA, Pan R, Papovich C, Price SH, van Dokkum P, Weaver JR, Whitaker KE and Zitrin A (2024), Mar. UNCOVER Spectroscopy Confirms the Surprising Ubiquity of Active Galactic Nuclei in Red Sources at $z \lesssim 5$. *ApJ* 964 (1), 39. doi:10.3847/1538-4357/ad1e5f. 2309.05714.
- Greig B and Mesinger A (2017), Mar. The global history of reionization. *MNRAS* 465 (4): 4838–4852. doi:10.1093/mnras/stw3026. 1605.05374.
- Guhathakurta P, Tyson JA and Majewski SR (1990), Jul. A Redshift Limit for the Faint Blue Galaxy Population from Deep U Band Imaging. *ApJ* 357: L9. doi:10.1086/185754.
- Gunn JE and Peterson BA (1965), Nov. On the Density of Neutral Hydrogen in Intergalactic Space. *ApJ* 142: 1633–1636. doi:10.1086/148444.
- Hainline KN, D'Eugenio F, Jakobsen P, Chevallard J, Carniani S, Witstok J, Ji Z, Curtis-Lake E, Johnson BD, Robertson B, Tacchella S, Curti M, Charlot S, Helton JM, Arribas S, Bhatawdekar R, Bunker AJ, Cameron AJ, Egami E, Eisenstein DJ, Hausen R, Kumari N, Maiolino R, Pérez-González PG, Rieke M, Saxena A, Scholtz J, Smit R, Sun F, Williams CC, Willmer CNA and Willott C (2024), Dec. Searching for Emission Lines at $z \lesssim 11$: The Role of Damped Ly α and Hints About the Escape of Ionizing Photons. *ApJ* 976 (2), 160. doi:10.3847/1538-4357/ad8447. 2404.04325.
- Harikane Y, Ouchi M, Oguri M, Ono Y, Nakajima K, Isobe Y, Umeda H, Mawatari K and Zhang Y (2023a), Mar. A Comprehensive Study of Galaxies at $z \sim 9$ –16 Found in the Early JWST Data: Ultraviolet Luminosity Functions and Cosmic Star Formation History at the Pre-reionization Epoch. *ApJS* 265 (1), 5. doi:10.3847/1538-4365/acaa9. 2208.01612.
- Harikane Y, Zhang Y, Nakajima K, Ouchi M, Isobe Y, Ono Y, Hatano S, Xu Y and Umeda H (2023b), Dec. A JWST/NIRSpec First Census of Broad-line AGNs at $z = 4$ –7: Detection of 10 Faint AGNs with $M_{BH} \sim 10^6$ – $10^8 M_{\odot}$ and Their Host Galaxy Properties. *ApJ* 959 (1), 39. doi:10.3847/1538-4357/ad029e. 2303.11946.
- Harikane Y, Sanders RL, Ellis R, Jones T, Ouchi M, Laporte N, Roberts-Borsani G, Katz H, Nakajima K, Ono Y and Gupta M (2025), May. JWST & ALMA Joint Analysis with [OII]??3726,3729, [OIII]??4363, [OIII]88?m, and [OIII]52?m: Multi-Zone Evolution of Electron Densities at $z \sim 0 - 14$ and Its Impact on Metallicity Measurements. *arXiv e-prints*, arXiv:2505.09186doi:10.48550/arXiv.2505.09186. 2505.09186.
- Hayes MJ, Tan JC, Ellis RS, Young AR, Cammelli V, Singh J, Runholm A, Saxena A, Lunnan R, Keller BW, Monaco P, Laporte N and Melinder J (2024), Aug. Glimmers in the Cosmic Dawn: A Census of the Youngest Supermassive Black Holes by Photometric Variability. *ApJ* 971 (1), L16. doi:10.3847/2041-8213/ad63a7. 2403.16138.
- Hayes MJ, Saldana-Lopez A, Citro A, James BL, Mingozi M, Scarlata C, Martinez Z and Berg DA (2025), Mar. On the Average Ultraviolet Emission-line Spectra of High-redshift Galaxies: Hot and Cold, Carbon-poor, Nitrogen Modest, and Oozing Ionizing Photons. *ApJ* 982 (1), 14. doi:10.3847/1538-4357/adaea1. 2411.09262.
- Heger A and Woosley SE (2002), Mar. The Nucleosynthetic Signature of Population III. *ApJ* 567 (1): 532–543. doi:10.1086/338487. astro-ph/0107037.
- Heintz KE, Watson D, Brammer G, Vejlgaard S, Hutter A, Strait VB, Matthee J, Oesch PA, Jakobsson P, Tanvir NR, Laursen P, Naidu RP, Mason CA, Killi M, Jung I, Hsiao TYY, Abdurro'uf, Coe D, Arrabal Haro P, Finkelstein SL and Toft S (2024), May. Strong damped Lyman- α absorption in young star-forming galaxies at redshifts 9 to 11. *Science* 384 (6698): 890–894. doi:10.1126/science.adj0343. 2306.00647.
- Heintz KE, Brammer GB, Watson D, Oesch PA, Keating LC, Hayes MJ, Abdurro'uf, Arellano-Córdova KZ, Carnall AC, Christiansen CR, Cullen F, Davé R, Dayal P, Ferrara A, Finlator K, Fynbo JPU, Flury SR, Gelli V, Gillman S, Gottumukkala R, Gould K, Greve TR, Hardin SE, Hsiao TYY, Hutter A, Jakobsson P, Killi M, Khosravaninezhad N, Laursen P, Lee MM, Magdis GE, Matthee J, Naidu RP, Narayanan D, Pollock C, Prescott MKM, Ruskov V, Shuntov M, Sneppen A, Smit R, Tanvir NR, Terp C, Toft S, Valentino F, Vijayan AP, Weaver JR, Wise JH and Witstok J (2025a), Jan. The JWST-PRIMAL archival survey: A JWST/NIRSpec reference sample for the physical properties and Lyman- α absorption and emission of ~ 600 galaxies at $z = 5.0 - 13.4$. *A&A* 693, A60. doi:10.1051/0004-6361/202450243. 2404.02211.
- Heintz KE, Pollock CL, Witstok J, Carniani S, Hainline KN, D'Eugenio F, Terp C, Saxena A and Watson D (2025b), Jul. Dissecting the Massive Pristine, Neutral Gas Reservoir of a Remarkably Bright Galaxy at $z = 14.179$. *ApJ* 987 (1), L2. doi:10.3847/2041-8213/ade393. 2502.06016.
- Hills R, Kulkarni G, Meerburg PD and Puchwein E (2018), Dec. Concerns about modelling of the EDGES data. *Nature* 564 (7736): E32–E34. doi:10.1038/s41586-018-0796-5. 1805.01421.
- Huberty M, Scarlata C, Hayes MJ and Gazagnes S (2025), Jul. The Pitfalls of Using Ly α Damping Wings in High- z Galaxy Spectra to Measure the Intergalactic Neutral Hydrogen Fraction. *ApJ* 987 (1), 82. doi:10.3847/1538-4357/add5e7. 2501.13899.
- Inoue AK (2011), Aug. Rest-frame ultraviolet-to-optical spectral characteristics of extremely metal-poor and metal-free galaxies. *MNRAS* 415 (3): 2920–2931. doi:10.1111/j.1365-2966.2011.18906.x. 1102.5150.
- Inoue AK, Shimizu I, Iwata I and Tanaka M (2014), Aug. An updated analytic model for attenuation by the intergalactic medium. *MNRAS* 442 (2): 1805–1820. doi:10.1093/mnras/stu936. 1402.0677.
- Iye M, Ota K, Kashikawa N, Furusawa H, Hashimoto T, Hattori T, Matsuda Y, Morokuma T, Ouchi M and Shimasaku K (2006), Sep. A galaxy at a redshift $z = 6.96$. *Nature* 443 (7108): 186–188. doi:10.1038/nature05104. astro-ph/0609393.
- Izotov YI, Schaerer D, Thuan TX, Worseck G, Guseva NG, Orlitová I and Verhamme A (2016), Oct. Detection of high Lyman continuum leakage from four low-redshift compact star-forming galaxies. *MNRAS* 461 (4): 3683–3701. doi:10.1093/mnras/stw1205. 1605.05160.
- Izotov YI, Worseck G, Schaerer D, Guseva NG, Thuan TX, Fricke A. V and Orlitová I (2018), Aug. Low-redshift Lyman continuum leaking galaxies with high [O III]/[O II] ratios. *MNRAS* 478 (4): 4851–4865. doi:10.1093/mnras/sty1378. 1805.09865.
- Izotov YI, Chisholm J, Worseck G, Guseva NG, Schaerer D and Prochaska JX (2022), Sep. Lyman alpha and Lyman continuum emission of Mg II-selected star-forming galaxies. *MNRAS* 515 (2): 2864–2881. doi:10.1093/mnras/stac1899. 2207.04483.
- Ji X, Maiolino R, Übler H, Scholtz J, D'Eugenio F, Sun F, Perna M, Turner H, Arribas S, Bennett JS, Bunker A, Carniani S, Charlot S, Cresci G, Curti M, Egami E, Fabian A, Inayoshi K, Isobe Y, Jones G, Juodžbalis I, Kumari N, Lyu J, Mazzolari G, Parlanti E, Robertson B, Rodríguez Del Pino B, Schneider R, Sijacki D, Tacchella S, Trinca A, Valiante R, Venturi G, Volonteri M, Willott C, Witten C and Witstok J (2025),

- Jan. BlackTHUNDER – A non-stellar Balmer break in a black hole-dominated little red dot at $z = 7.04$. *arXiv e-prints*, arXiv:2501.13082doi:10.48550/arXiv.2501.13082. 2501.13082.
- Jiang L, Kashikawa N, Wang S, Walth G, Ho LC, Cai Z, Egami E, Fan X, Ito K, Liang Y, Schaerer D and Stark DP (2021), Jan. Evidence for GN-z11 as a luminous galaxy at redshift 10.957. *Nature Astronomy* 5: 256–261. doi:10.1038/s41550-020-01275-y. 2012.06936.
- Jones T, Stark DP and Ellis RS (2012), May. Keck Spectroscopy of Faint 3 z \leq 7 Lyman Break Galaxies. III. The Mean Ultraviolet Spectrum at $z \sim 4$. *ApJ* 751 (1), 51. doi:10.1088/0004-637X/751/1/51. 1111.5102.
- Jones TA, Ellis RS, Schenker MA and Stark DP (2013), Dec. Keck Spectroscopy of Gravitationally Lensed $z \sim 4$ Galaxies: Improved Constraints on the Escape Fraction of Ionizing Photons. *ApJ* 779 (1), 52. doi:10.1088/0004-637X/779/1/52. 1304.7015.
- Jones T, Sanders R, Roberts-Borsani G, Ellis RS, Laporte N, Treu T and Harikane Y (2020), Nov. The Mass-Metallicity Relation at $z \sim 8$: Direct-method Metallicity Constraints and Near-future Prospects. *ApJ* 903 (2), 150. doi:10.3847/1538-4357/abb943. 2006.02447.
- Kageura Y, Ouchi M, Nakane M, Umeda H, Harikane Y, Yoshiura S, Nakajima K, Yajima H and Thai TT (2025), Jan. Census of $\text{Ly}\alpha$ Emission from ~ 600 Galaxies at $z = 5 - 14$: Evolution of the $\text{Ly}\alpha$ Luminosity Function and a Late Sharp Cosmic Reionization. *arXiv e-prints*, arXiv:2501.05834doi:10.48550/arXiv.2501.05834. 2501.05834.
- Kakiichi K, Ellis RS, Laporte N, Zitrin A, Eilers AC, Ryan-Weber E, Meyer RA, Robertson B, Stark DP and Bosman SEI (2018), Sep. The role of galaxies and AGN in reionizing the IGM - I. Keck spectroscopy of 5 $z \leq 7$ galaxies in the QSO field J1148+5251. *MNRAS* 479 (1): 43–63. doi:10.1093/mnras/sty1318. 1803.02981.
- Kakiichi K, Jin X, Wang F, Meyer RA, Garaldi E, Bosman SEI, Davies FB, Fan X, Trebitsch M, Yang J, Bañados E, Champagne JB, Eilers AC, Hennawi JF, Sun F, Wu Y, Zou S, Kannan R, Smith A, Becker GD, D’Odorico V, Connor T, Liu W, Protušová K, Walter F and Zhang H (2025), Mar. JWST ASPIRE: How Did Galaxies Complete Reionization? Evidence for Excess IGM Transmission around [O III] Emitters during Reionization. *arXiv e-prints*, arXiv:2503.07074doi:10.48550/arXiv.2503.07074. 2503.07074.
- Kashino D, Lilly SJ, Matthee J, Mackenzie R, Eilers AC, Bordoloi R, Simcoe RA, Naidu RP, Yue M and Liu B (2025), Jun. EIGER VII. The evolving relationship between galaxies and the intergalactic medium in the final stages of reionization. *arXiv e-prints*, arXiv:2506.03121doi:10.48550/arXiv.2506.03121. 2506.03121.
- Katz H, Kimm T, Ellis RS, Devriendt J and Slyz A (2023), Sep. The challenges of identifying Population III stars in the early Universe. *MNRAS* 524 (1): 351–360. doi:10.1093/mnras/stad1903. 2207.04751.
- Katz H, Cameron AJ, Saxena A, Barrufet L, Choustikov N, Cleri NJ, de Graaff A, Ellis RS, Fosbury RAE, Heintz KE, Maseda M, Matthee J, McConchie I and Oesch PA (2024), Aug. 21 Balmer Jump Street: The Nebular Continuum at High Redshift and Implications for the Bright Galaxy Problem, UV Continuum Slopes, and Early Stellar Populations. *arXiv e-prints*, arXiv:2408.03189doi:10.48550/arXiv.2408.03189. 2408.03189.
- Kauffmann G and Charlot S (1998), Jun. The K-band luminosity function at $z=1$: a powerful constraint on galaxy formation theory. *MNRAS* 297 (1): L23–L28. doi:10.1046/j.1365-8711.1998.01708.x. astro-ph/9802233.
- Kennicutt Jr. RC (1998), Jan. Star Formation in Galaxies Along the Hubble Sequence. *ARA&A* 36: 189–232. doi:10.1146/annurev.astro.36.1.189. astro-ph/9807187.
- Klessen RS and Glover SCO (2023), Aug. The First Stars: Formation, Properties, and Impact. *ARA&A* 61: 65–130. doi:10.1146/annurev-astro-071221-053453. 2303.12500.
- Kneib JP, Ellis RS, Smail I, Couch WJ and Sharples RM (1996), Nov. Hubble Space Telescope Observations of the Lensing Cluster Abell 2218. *ApJ* 471: 643. doi:10.1086/177995. astro-ph/9511015.
- Kocevski DD, Finkelstein SL, Barro G, Taylor AJ, Calabrò A, Laloux B, Buchner J, Trump JR, Leung GCK, Yang G, Dickinson M, Pérez-González PG, Pacucci F, Inayoshi K, Somerville RS, McGrath EJ, Akins HB, Bagley MB, Bowler RAA, Bisigello L, Carnall A, Casey CM, Cheng Y, Cleri NJ, Costantin L, Cullen F, Davis K, Donnan CT, Dunlop JS, Ellis RS, Ferguson HC, Fujimoto S, Fontana A, Gialalisco M, Grazian A, Grogin NA, Hathi NP, Hirschmann M, Huertas-Company M, Holwerda BW, Illingworth G, Juneau S, Kartaltepe JS, Koekemoer AM, Li W, Lucas RA, Magee D, Mason C, McLeod DJ, McLure RJ, Napolitano L, Papovich C, Pirzkal N, Rodighiero G, Santini P, Wilkins SM and Yung LYA (2025), Jun. The Rise of Faint, Red Active Galactic Nuclei at $z \lesssim 4$: A Sample of Little Red Dots in the JWST Extragalactic Legacy Fields. *ApJ* 986 (2), 126. doi:10.3847/1538-4357/adbc7d. 2404.03576.
- Kokorev V, Fujimoto S, Labbe I, Greene JE, Bezanson R, Dayal P, Nelson EJ, Atek H, Brammer G, Caputi KI, Chemerynska I, Cutler SE, Feldmann R, Fudamoto Y, Furtak LJ, Goulding AD, de Graaff A, Leja J, Marchesini D, Miller TB, Nanayakkara T, Oesch PA, Pan R, Price SH, Setton DJ, Smit R, Stefanon M, Wang B, Weaver JR, Whitaker KE, Williams CC and Zitrin A (2023), Nov. UNCOVER: A NIRSpec Identification of a Broad-line AGN at $z = 8.50$. *ApJ* 957 (1), L7. doi:10.3847/2041-8213/ad037a. 2308.11610.
- Kokorev V, Atek H, Chisholl J, Endsley R, Chemerynska I, Muñoz JB, Furtak LJ, Pan R, Berg D, Fujimoto S, Oesch PA, Weibel A, Adamo A, Blaizot J, Bouwens R, Dessauges-Zavadsky M, Khullar G, Korber D, Goovaerts I, Jecmen M, Labbé I, Leclercq F, Marques-Chaves R, Mason C, McQuinn KBW, Naidu R, Natarajan P, Nelson E, Rosdahl J, Saldana-Lopez A, Schaerer D, Trebitsch M, Volonteri M and Zitrin A (2025), Apr. A Glimpse of the New Redshift Frontier through AS1063. *ApJ* 983 (1), L22. doi:10.3847/2041-8213/ad458. 2411.13640.
- Koopmans LVE, Barkana R, Bentum M, Bernardi G, Boonstra AJ, Bowman J, Burns J, Chen X, Datta A, Falcke H, Fialkov A, Gehlot B, Gurvits L, Jelić V, Klein-Wolt M, Lazio J, Meerburg D, Mellema G, Mertens F, Mesinger A, Offringa A, Pritchard J, Semelin B, Subrahmanyan R, Silk J, Trott C, Vedantham H, Verde L, Zaroubi S and Zarka P (2021), Jun. Peering into the dark (ages) with low-frequency space interferometers. *Experimental Astronomy* 51 (3): 1641–1676. doi:10.1007/s10686-021-09743-7. 1908.04296.
- Kovács OE, Bogdán Á, Natarajan P, Werner N, Azadi M, Volonteri M, Tremblay GR, Chadayammuri U, Forman WR, Jones C and Kraft RP (2024), Apr. A Candidate Supermassive Black Hole in a Gravitationally Lensed Galaxy at $z \approx 10$. *ApJ* 965 (2), L21. doi:10.3847/2041-8213/ad391f. 2403.14745.
- Kravtsov A and Belokurov V (2024), May. Stochastic star formation and the abundance of $z > 10$ UV-bright galaxies. *arXiv e-prints*, arXiv:2405.04578doi:10.48550/arXiv.2405.04578. 2405.04578.
- Kuruvanthodi A, Schaerer D, Marques-Chaves R, Korber D, Weibel A, Oesch PA and Roberts-Borsani G (2024), Nov. Strong Balmer break objects at $z \sim 7-10$ uncovered with JWST. *A&A* 691, A310. doi:10.1051/0004-6361/202451622. 2407.17410.
- Laporte N, Nakajima K, Ellis RS, Zitrin A, Stark DP, Mainali R and Roberts-Borsani GW (2017), Dec. A Spectroscopic Search for AGN Activity in the Reionization Era. *ApJ* 851 (1), 40. doi:10.3847/1538-4357/aa96a8. 1708.05173.
- Lecroq M, Charlot S, Bressan A, Bruzual G, Costa G, Iorio G, Mapelli M, Santoliquido F, Shepherd K and Spera M (2025), Mar. A new prescription for the spectral properties of population III stellar populations. *A&A* 695, A17. doi:10.1051/0004-6361/202452463. 2502.14028.
- Leethochawalit N, Jones TA, Ellis RS, Stark DP and Zitrin A (2016), Nov. Absorption-line Spectroscopy of Gravitationally Lensed Galaxies: Further Constraints on the Escape Fraction of Ionizing Photons at High Redshift. *ApJ* 831 (2), 152. doi:10.3847/0004-637X/831/2/152. 1606.05309.
- Leung GCK, Finkelstein SL, Pérez-González PG, Morales AM, Taylor AJ, Barro G, Kocevski DD, Akins HB, Carnall AC, Chávez Ortiz ÓA, Cleri NJ, Cullen F, Donnan CT, Dunlop JS, Ellis RS, Grogin NA, Hirschmann M, Koekemoer AM, Kokorev V, Lucas RA, McLeod DJ, Papovich C and Yung LYA (2024), Nov. Exploring the Nature of Little Red Dots: Constraints on AGN and Stellar Contributions from PRIMER MIRI Imaging. *arXiv e-prints*, arXiv:2411.12005doi:10.48550/arXiv.2411.12005. 2411.12005.

- Li Z, Inayoshi K, Chen K, Ichikawa K and Ho LC (2025), Feb. Little Red Dots: Rapidly Growing Black Holes Reddened by Extended Dusty Flows. *ApJ* 980 (1), 36. doi:10.3847/1538-4357/ada5fb. 2407.10760.
- Lilly SJ, Tresse L, Hammer F, Crampton D and Le Fevre O (1995), Dec. The Canada-France Redshift Survey. VI. Evolution of the Galaxy Luminosity Function to z approximately 1. *ApJ* 455: 108. doi:10.1086/176560. astro-ph/9507079.
- Liu A and Shaw JR (2020), Jun. Data Analysis for Precision 21 cm Cosmology. *PASP* 132 (1012), 062001. doi:10.1088/1538-3873/ab5bfd. 1907.08211.
- Llerena M, Pentericci L, Napolitano L, Mascia S, Amorín R, Calabrò A, Castellano M, Cleri NJ, Giallisco M, Grogini NA, Hathi NP, Hirschmann M, Koekemoer AM, Nanayakkara T, Pacucci F, Shen L, Wilkins SM, Yoon I, Yung LYA, Bhatawdekar R, Lucas RA, Wang X, Arrabal Haro P, Bagley MB, Finkelstein SL, Kartaltepe JS, Merlin E, Papovich C and Pirzkal N (2024), Dec. The ionizing photon production efficiency of star-forming galaxies at $z \sim 4 - 10$. *arXiv e-prints*, arXiv:2412.01358doi:10.48550/arXiv.2412.01358. 2412.01358.
- Loeb A and Barkana R (2001), Jan. The Reionization of the Universe by the First Stars and Quasars. *ARA&A* 39: 19–66. doi:10.1146/annurev.astro.39.1.19. astro-ph/0010467.
- Lotz JM, Koekemoer A, Coe D, Grogini N, Capak P, Mack J, Anderson J, Avila R, Barker EA, Borncamp D, Brammer G, Durbin M, Gunning H, Hilbert B, Jenkner H, Khandrika H, Levay Z, Lucas RA, MacKenty J, Ogaz S, Porterfield B, Reid N, Robberto M, Royle P, Smith LJ, Storrie-Lombardi LJ, Sunnquist B, Surace J, Taylor DC, Williams R, Bullock J, Dickinson M, Finkelstein S, Natarajan P, Richard J, Robertson B, Tumlinson J, Zitrin A, Flanagan K, Sembach K, Soifer BT and Mountain M (2017), Mar. The Frontier Fields: Survey Design and Initial Results. *ApJ* 837 (1), 97. doi:10.3847/1538-4357/837/1/97. 1605.06567.
- Madau P (2000), Jul., Cosmological reionization, Astronomy, physics and chemistry of H^+_{γ} , 358, pp. 2021, astro-ph/0003096.
- Madau P and Dickinson M (2014), Aug. Cosmic Star-Formation History. *ARA&A* 52: 415–486. doi:10.1146/annurev-astro-081811-125615. 1403.0007.
- Madau P, Giallongo E, Grazian A and Haardt F (2024), Aug. Cosmic Reionization in the JWST Era: Back to AGNs? *ApJ* 971 (1), 75. doi:10.3847/1538-4357/ad5ce8. 2406.18697.
- Maiolino R and Mannucci F (2019), Feb. De re metallica: the cosmic chemical evolution of galaxies. *A&ARv* 27 (1), 3. doi:10.1007/s00159-018-0112-2. 1811.09642.
- Maiolino R, Scholtz J, Witstok J, Carniani S, D'Eugenio F, de Graaff A, Übler H, Tacchella S, Curtis-Lake E, Arribas S, Bunker A, Charlot S, Chevallard J, Curti M, Looser TJ, Maseda MV, Rawle TD, Rodríguez del Pino B, Willott CJ, Egami E, Eisenstein DJ, Hainline KN, Robertson B, Williams CC, Willmer CNA, Baker WM, Boyett K, DeCoursey C, Fabian AC, Helton JM, Ji Z, Jones GC, Kumari N, Laporte N, Nelson EJ, Perna M, Sandles L, Shivaiei I and Sun F (2024a), Mar. A small and vigorous black hole in the early Universe. *Nature* 627 (8002): 59–63. doi:10.1038/s41586-024-07052-5. 2305.12492.
- Maiolino R, Übler H, Perna M, Scholtz J, D'Eugenio F, Witten C, Laporte N, Witstok J, Carniani S, Tacchella S, Baker WM, Arribas S, Nakajima K, Eisenstein DJ, Bunker AJ, Charlot S, Cresci G, Curti M, Curtis-Lake E, de Graaff A, Egami E, Ji Z, Johnson BD, Kumari N, Looser TJ, Maseda M, Nelson E, Robertson B, Rodríguez Del Pino B, Sandles L, Simmonds C, Smit R, Sun F, Venturi G, Williams CC and Willmer CNA (2024b), Jul. JADES. Possible Population III signatures at $z = 10.6$ in the halo of GN-z11. *A&A* 687, A67. doi:10.1051/0004-6361/202347087. 2306.00953.
- Maiolino R, Uebler H, D'Eugenio F, Scholtz J, Juodzbališ I, Ji X, Perna M, Bromm V, Dayal P, Koudmani S, Liu B, Schneider R, Sijacki D, Valiante R, Trinca A, Zhang S, Volonteri M, Inayoshi K, Carniani S, Nakajima K, Isobe Y, Witstok J, Jones GC, Tacchella S, Arribas S, Bunker A, Cataldi E, Charlot S, Cresci G, Curti M, Fabian AC, Katz H, Kumari N, Laporte N, Mazzolari G, Robertson B, Sun F, Rodríguez Del Pino B and Venturi G (2025), May. A black hole in a near-pristine galaxy 700 million years after the Big Bang. *arXiv e-prints*, arXiv:2505.22567doi:10.48550/arXiv.2505.22567. 2505.22567.
- Mason CA, Treu T, Dijkstra M, Mesinger A, Trenti M, Pentericci L, de Barros S and Vanzella E (2018), Mar. The Universe Is Reionizing at $z \sim 7$: Bayesian Inference of the IGM Neutral Fraction Using $Ly\alpha$ Emission from Galaxies. *ApJ* 856 (1), 2. doi:10.3847/1538-4357/aab0a7. 1709.05356.
- Mason CA, Trenti M and Treu T (2023), May. The brightest galaxies at cosmic dawn. *MNRAS* 521 (1): 497–503. doi:10.1093/mnras/stad035. 2207.14808.
- Mason CA, Chen Z, Stark DP, Lu TY, Topping M and Tang M (2025), Jan. Constraints on the $z \sim 6 - 13$ intergalactic medium from JWST spectroscopy of Lyman-alpha damping wings in galaxies. *arXiv e-prints*, arXiv:2501.11702doi:10.48550/arXiv.2501.11702. 2501.11702.
- Matthee J, Sobral D, Gronke M, Paulino-Afonso A, Stefanon M and Röttgering H (2018), Nov. Confirmation of double peaked $Ly\alpha$ emission at $z = 6.593$. Witnessing a galaxy directly contributing to the reionisation of the Universe. *A&A* 619, A136. doi:10.1051/0004-6361/201833528. 1805.11621.
- Matthee J, Naidu RP, Brammer G, Chisholm J, Eilers AC, Goulding A, Greene J, Kashino D, Labbe I, Lilly SJ, Mackenzie R, Oesch PA, Weibel A, Wuyts S, Xiao M, Bordoloi R, Bouwens R, van Dokkum P, Illingworth G, Kramarenko I, Maseda MV, Mason C, Meyer RA, Nelson EJ, Reddy NA, Shivaiei I, Simcoe RA and Yue M (2024), Mar. Little Red Dots: An Abundant Population of Faint Active Galactic Nuclei at $z \sim 5$ Revealed by the EIGER and FRESCO JWST Surveys. *ApJ* 963 (2), 129. doi:10.3847/1538-4357/ad2345. 2306.05448.
- McCarthy PJ, Spinrad P, Djorgovski S, Strauss MA, van Breugel W and Liebert J (1987), Aug. Extended Lyman- α Emission in 3C 326.1: A 100 Kiloparsec Cloud of Ionized Gas at a Redshift of 1.82. *ApJ* 319: L39. doi:10.1086/184951.
- McLeod DJ, McLure RJ and Dunlop JS (2016), Jul. The $z = 9-10$ galaxy population in the Hubble Frontier Fields and CLASH surveys: the $z = 9$ luminosity function and further evidence for a smooth decline in ultraviolet luminosity density at $z \geq 8$. *MNRAS* 459 (4): 3812–3824. doi:10.1093/mnras/stw904. 1602.05199.
- McLeod DJ, McLure RJ, Dunlop JS, Cullen F, Carnall AC and Duncan K (2021), May. The evolution of the galaxy stellar-mass function over the last 12 billion years from a combination of ground-based and HST surveys. *MNRAS* 503 (3): 4413–4435. doi:10.1093/mnras/stab731. 2009.03176.
- McLeod DJ, Donnan CT, McLure RJ, Dunlop JS, Magee D, Begley R, Carnall AC, Cullen F, Ellis RS, Hamadouche ML and Stanton TM (2024), Jan. The galaxy UV luminosity function at $z \sim 11$ from a suite of public JWST ERS, ERO, and Cycle-1 programs. *MNRAS* 527 (3): 5004–5022. doi:10.1093/mnras/stad3471. 2304.14469.
- Méndez-Delgado JE, Esteban C, García-Rojas J, Kreckel K and Peimbert M (2023), Jun. Temperature inhomogeneities cause the abundance discrepancy in H II regions. *Nature* 618 (7964): 249–251. doi:10.1038/s41586-023-05956-2. 2305.11578.
- Menon SH, Lancaster L, Burkhardt B, Somerville RS, Dekel A and Krumholz MR (2024), Jun. The Interplay between the Initial Mass Function and Star Formation Efficiency through Radiative Feedback at High Stellar Surface Densities. *ApJ* 967 (2), L28. doi:10.3847/2041-8213/ad462d. 2405.00813.
- Meyer RA, Kakiichi K, Bosman SEI, Ellis RS, Laporte N, Robertson BE, Ryan-Weber EV, Mawatari K and Zitrin A (2020), May. The role of galaxies and AGN in reionizing the IGM - III. IGM-galaxy cross-correlations at $z \sim 6$ from eight quasar fields with DEIMOS and MUSE. *MNRAS* 494 (2): 1560–1578. doi:10.1093/mnras/staa746. 1912.04314.
- Meyer RA, Roberts-Borsani G, Oesch P and Ellis RS (2025), Apr. Probing patchy reionisation with JWST: IGM opacity constraints from the Lyman- α forest of galaxies in legacy extragalactic fields. *arXiv e-prints*, arXiv:2504.02683doi:10.48550/arXiv.2504.02683. 2504.02683.

- Michel-Dansac L, Blaizot J, Garel T, Verhamme A, Kimm T and Trebitsch M (2020), Mar. RASCAS: RADIATION SCATTERING in Astrophysical Simulations. *A&A* 635, A154. doi:10.1051/0004-6361/201834961. 2001.11252.
- Miralda-Escudé J, Haehnelt M and Rees MJ (2000), Feb. Reionization of the Inhomogeneous Universe. *ApJ* 530 (1): 1–16. doi:10.1086/308330. astro-ph/9812306.
- Miyazaki S, Komiyama Y, Kawanomoto S, Doi Y, Furusawa H, Hamana T, Hayashi Y, Ikeda H, Kamata Y, Kuroji H, Koike M, Kurakami T, Miyama S, Morokuma T, Nakata F, Namikawa K, Nakaya H, Nariai K, Obuchi Y, Oishi Y, Okada N, Okura Y, Tait P, Takata T, Tanaka Y, Tanaka M, Terai T, Tomono D, Uruguchi F, Usuda T, Utsumi Y, Yamada Y, Yamanoi H, Aihara H, Fujimori H, Mineo S, Miyatake H, Oguri M, Uchida T, Tanaka MM, Yasuda N, Takada M, Murayama H, Nishizawa AJ, Sugiyama N, Chiba M, Futamase T, Wang SY, Chen HY, Ho PTP, Liaw EJY, Chiu CF, Ho CL, Lai TC, Lee YC, Jeng DZ, Iwamura S, Armstrong R, Bickerton S, Bosch J, Gunn JE, Lupton RH, Loomis C, Price P, Smith S, Strauss MA, Turner EL, Suzuki H, Miyazaki Y, Muramatsu M, Yamamoto K, Endo M, Ezaki Y, Ito N, Kawaguchi N, Sofuku S, Taniike T, Akutsu K, Dojo N, Kasumi K, Matsuda T, Imoto K, Miwa Y, Suzuki M, Takeshi K and Yokota H (2018), Jan. Hyper Suprime-Cam: System design and verification of image quality. *PASJ* 70, S1. doi:10.1093/pasj/psx063.
- Morishita T, Stiavelli M, Grillo C, Rosati P, Schudt S, Trenti M, Bergamini P, Boyett K, Chary RR, Leethochawalit N, Roberts-Borsani G, Treu T and Vanzella E (2024), Aug. Diverse Oxygen Abundance in Early Galaxies Unveiled by Auroral Line Analysis with JWST. *ApJ* 971 (1), 43. doi:10.3847/1538-4357/ad5290. 2402.14084.
- Morishita T, Liu Z, Stiavelli M, Treu T, Bergamini P and Zhang Y (2025), Jul. Pristine Massive Star Formation Caught at the Break of Cosmic Dawn. *arXiv e-prints*, arXiv:2507.10521doi:10.48550/arXiv.2507.10521. 2507.10521.
- Mostardi RE, Shapley AE, Steidel CC, Trainor RF, Reddy NA and Siana B (2015), Sep. A High-Resolution Hubble Space Telescope Study of Apparent Lyman Continuum Leakers at $z \sim 3$. *ApJ* 810 (2), 107. doi:10.1088/0004-637X/810/2/107. 1506.08201.
- Naidu RP, Tacchella S, Mason CA, Bose S, Oesch PA and Conroy C (2020), Apr. Rapid Reionization by the Oligarchs: The Case for Massive, UV-bright, Star-forming Galaxies with High Escape Fractions. *ApJ* 892 (2), 109. doi:10.3847/1538-4357/ab7cc9. 1907.13130.
- Naidu RP, Oesch PA, Setton DJ, Matthee J, Conroy C, Johnson BD, Weaver JR, Bouwens RJ, Brammer GB, Dayal P, Illingworth GD, Barrufet L, Belli S, Bezanson R, Bose S, Heintz KE, Leja J, Leonova E, Marques-Chaves R, Stefanon M, Toft S, van der Wel A, van Dokkum P, Weibel A and Whitaker KE (2022a), Aug. Schrodinger's Galaxy Candidate: Puzzlingly Luminous at $z \approx 17$, or Dusty/Quenched at $z \approx 5$? *arXiv e-prints*, arXiv:2208.02794doi:10.48550/arXiv.2208.02794. 2208.02794.
- Naidu RP, Oesch PA, van Dokkum P, Nelson EJ, Suess KA, Brammer G, Whitaker KE, Illingworth G, Bouwens R, Tacchella S, Matthee J, Allen N, Bezanson R, Conroy C, Labbe I, Leja J, Leonova E, Magee D, Price SH, Setton DJ, Strait V, Stefanon M, Toft S, Weaver JR and Weibel A (2022b), Nov. Two Remarkably Luminous Galaxy Candidates at $z \approx 10$ –12 Revealed by JWST. *ApJ* 940 (1), L14. doi:10.3847/2041-8213/ac9b22. 2207.09434.
- Naidu RP, Matthee J, Katz H, de Graaff A, Oesch P, Smith A, Greene JE, Brammer G, Weibel A, Hviding R, Chisholm J, Labbé I, Simcoe RA, Witten C, Atek H, Baggen JFW, Belli S, Bezanson R, Boogaard LA, Bose S, Covelo-Paz A, Dayal P, Fudamoto Y, Furtak LJ, Giovinnazzo E, Goulding A, Gronke M, Heintz KE, Hirschmann M, Illingworth G, Inoue AK, Johnson BD, Leja J, Leonova E, McConachie I, Masada MV, Natarajan P, Nelson E, Setton DJ, Shivaiei I, Sobral D, Stefanon M, Tacchella S, Toft S, Torralba A, van Dokkum P, van der Wel A, Volonteri M, Walter F, Wang B and Watson D (2025a), Mar. A “Black Hole Star” Reveals the Remarkable Gas-Enshrouded Hearts of the Little Red Dots. *arXiv e-prints*, arXiv:2503.16596doi:10.48550/arXiv.2503.16596. 2503.16596.
- Naidu RP, Oesch PA, Brammer G, Weibel A, Li Y, Matthee J, Chisholm J, Pollock CL, Heintz KE, Johnson BD, Shen X, Hviding RE, Leja J, Tacchella S, Ganguly A, Witten C, Atek H, Belli S, Bose S, Bouwens R, Dayal P, Decarli R, de Graaff A, Fudamoto Y, Giovinnazzo E, Greene JE, Illingworth G, Inoue AK, Kane SG, Labbe I, Leonova E, Marques-Chaves R, Meyer RA, Nelson EJ, Roberts-Borsani G, Schaefer D, Simcoe RA, Stefanon M, Sugahara Y, Toft S, van der Wel A, van Dokkum P, Walter F, Watson D, Weaver JR and Whitaker KE (2025b), May. A Cosmic Miracle: A Remarkably Luminous Galaxy at $z_{\text{spec}} = 14.44$ Confirmed with JWST. *arXiv e-prints*, arXiv:2505.11263doi:10.48550/arXiv.2505.11263. 2505.11263.
- Nakajima K and Maiolino R (2022), Jul. Diagnostics for PopIII galaxies and direct collapse black holes in the early universe. *MNRAS* 513 (4): 5134–5147. doi:10.1093/mnras/stac1242. 2204.11870.
- Nakajima K and Ouchi M (2014), Jul. Ionization state of inter-stellar medium in galaxies: evolution, SFR- M_* - Z dependence, and ionizing photon escape. *MNRAS* 442 (1): 900–916. doi:10.1093/mnras/stu902. 1309.0207.
- Nakajima K, Fletcher T, Ellis RS, Robertson BE and Iwata I (2018), Jun. The mean ultraviolet spectrum of a representative sample of faint $z \sim 3$ Lyman alpha emitters. *MNRAS* 477 (2): 2098–2111. doi:10.1093/mnras/sty750. 1801.03085.
- Nakajima K, Ouchi M, Isobe Y, Harikane Y, Zhang Y, Ono Y, Umeda H and Oguri M (2023), Dec. JWST Census for the Mass-Metallicity Star Formation Relations at $z = 4$ –10 with Self-consistent Flux Calibration and Proper Metallicity Calibrators. *ApJS* 269 (2), 33. doi:10.3847/1538-4365/acd556. 2301.12825.
- Nakajima K, Ouchi M, Harikane Y, Vanzella E, Ono Y, Isobe Y, Nishigaki M, Tsujimoto T, Nakamura F, Xu Y, Umeda H and Zhang Y (2025), Jun. An Ultra-Faint, Chemically Primitive Galaxy Forming at the Epoch of Reionization. *arXiv e-prints*, arXiv:2506.11846doi:10.48550/arXiv.2506.11846. 2506.11846.
- Nakane M, Ouchi M, Nakajima K, Ono Y, Harikane Y, Isobe Y, Nomoto K, Ishigaki MN, Yanagisawa H, Kashino D, Tominaga N, Takahashi K, Nishigaki M, Takeda Y and Watanabe K (2025), Mar. Fe Abundances of Early Galaxies at $z = 9$ –12 Derived with Deep JWST Spectra. *arXiv e-prints*, arXiv:2503.11457doi:10.48550/arXiv.2503.11457. 2503.11457.
- Napolitano L, Pentericci L, Calabrò A, Santini P, Castellano M, Cassata P, Fynbo JPU, Jung I, Kashino D, Mascia S and Mignoli M (2023), Sep. Identifying Ly α emitter candidates with Random Forest: Learning from galaxies in the CANDELS survey. *A&A* 677, A138. doi:10.1051/0004-6361/202347026. 2307.11818.
- Napolitano L, Castellano M, Pentericci L, Vignali C, Gilli R, Fontana A, Santini P, Treu T, Calabrò A, Llerena M, Piconcelli E, Zappacosta L, Mascia S, Tripodi R, Arrabal Haro P, Bergamini P, Bakx TJLC, Dickinson M, Glazebrook K, Henry A, Leethochawalit N, Mazzolari G, Merlin E, Morishita T, Nanayakkara T, Paris D, Puccetti S, Roberts-Borsani G, Rojas Ruiz S, Rosati P, Vanzella E, Vito F, Vulcani B, Wang X, Yoon I and Zavala JA (2024), Oct. The dual nature of GHZ9: coexisting AGN and star formation activity in a remote X-ray source at $z=10.145$. *arXiv e-prints*, arXiv:2410.18763doi:10.48550/arXiv.2410.18763. 2410.18763.
- Natarajan P, Pacucci F, Ricarte A, Bogdán Á, Goulding AD and Cappelluti N (2024), Jan. First Detection of an Overmassive Black Hole Galaxy UHZ1: Evidence for Heavy Black Hole Seed Formation from Direct Collapse. *ApJ* 960 (1), L1. doi:10.3847/2041-8213/ad0e76. 2308.02654.
- Oesch PA, Brammer G, van Dokkum PG, Illingworth GD, Bouwens RJ, Labbé I, Franx M, Momcheva I, Ashby MLN, Fazio GG, Gonzalez V, Holden B, Magee D, Skelton RE, Smit R, Spitler LR, Trenti M and Willner SP (2016), Mar. A Remarkably Luminous Galaxy at $z=11.1$ Measured with Hubble Space Telescope Grism Spectroscopy. *ApJ* 819 (2), 129. doi:10.3847/0004-637X/819/2/129. 1603.00461.
- Oesch PA, Bouwens RJ, Illingworth GD, Labbé I and Stefanon M (2018), Mar. The Dearth of $z \sim 10$ Galaxies in All HST Legacy Fields—The Rapid Evolution of the Galaxy Population in the First 500 Myr. *ApJ* 855 (2), 105. doi:10.3847/1538-4357/aab03f. 1710.11131.
- Ouchi M, Ono Y and Shibuya T (2020), Aug. Observations of the Lyman- α Universe. *ARA&A* 58: 617–659. doi:10.1146/annurev-astro-032620-021859. 2012.07960.

- Pahl AJ, Topping MW, Shapley A, Sanders R, Reddy NA, Clarke L, Kehoe E, Bento T and Brammer G (2024), Jul. A spectroscopic analysis of the ionizing photon production efficiency in JADES and CEERS: implications for the ionizing photon budget. *arXiv e-prints*, arXiv:2407.03399doi: 10.48550/arXiv.2407.03399. 2407.03399.
- Partridge RB and Peebles PJE (1967), Mar. Are Young Galaxies Visible? *ApJ* 147: 868. doi:10.1086/149079.
- Pentericci L, Fontana A, Vanzella E, Castellano M, Grazian A, Dijkstra M, Boutsia K, Cristiani S, Dickinson M, Giallongo E, Gialvalisco M, Maiolino R, Moorwood A, Paris D and Santini P (2011), Dec. Spectroscopic Confirmation of $z \sim 7$ Lyman Break Galaxies: Probing the Earliest Galaxies and the Epoch of Reionization. *ApJ* 743 (2), 132. doi:10.1088/0004-637X/743/2/132. 1107.1376.
- Pentericci L, Vanzella E, Fontana A, Castellano M, Treu T, Mesinger A, Dijkstra M, Grazian A, Bradač M, Conselice C, Cristiani S, Dunlop J, Galametz A, Gialvalisco M, Giallongo E, Koekemoer A, McLure R, Maiolino R, Paris D and Santini P (2014), Oct. New Observations of $z \sim 7$ Galaxies: Evidence for a Patchy Reionization. *ApJ* 793 (2), 113. doi:10.1088/0004-637X/793/2/113. 1403.5466.
- Peterson BA, Ellis RS, Kibblewhite EJ, Bridgeland MT, Hooley T and Horne D (1979), Nov. Number magnitude counts of faint galaxies. *ApJ* 233: L109–L113. doi:10.1086/183087.
- Planck Collaboration, Aghanim N, Akrami Y, Ashdown M, Aumont J, Baccigalupi C, Ballardini M, Banday AJ, Barreiro RB, Bartolo N, Basak S, Benabed K, Bernard JP, Bersanelli M, Bielewicz P, Bock JJ, Bond JR, Borrill J, Bouchet FR, Boulanger F, Bucher M, Burigana C, Butler RC, Calabrese E, Cardoso JF, Carron J, Casaponsa B, Challinor A, Chiang HC, Colombo LPL, Combet C, Crill BP, Cuttaia F, de Bernardis P, de Rosa A, de Zotti G, Delabrouille J, Delouis JM, Di Valentino E, Diego JM, Doré O, Douspis M, Ducout A, Dupac X, Dusini S, Efstathiou G, Elsner F, Enßlin H, Eriksen HK, Fantaye Y, Fernandez-Cobos R, Finelli F, Frailis M, Fraisse AA, Franceschi E, Frolov A, Giallioni S, Galli S, Ganga K, Génova-Santos RT, Gerbino M, Ghosh T, Giraud-Héraud Y, González-Nuevo J, Górski KM, Gratton S, Gruppuso A, Gudmundsson JE, Hamann J, Handley W, Hansen FK, Herranz D, Hivon E, Huang Z, Jaffe AH, Jones WC, Keihänen E, Kesikitalo R, Kiviiri K, Kim J, Kisner TS, Krachmalnicoff N, Kunz M, Kurki-Suonio H, Lagache G, Lamarre JM, Lasenby A, Lattanzi M, Lawrence CR, Le Jeune M, Levrier F, Lewis A, Liguori M, Lilje PB, Liddle K, Lindholm V, López-Caniego M, Lubin PM, Ma YZ, Macías-Pérez JF, Maggio G, Maino D, Mandolei N, Mangili A, Marcos-Caballero A, Maris M, Martin PG, Martínez-González E, Matarrese S, Mauri N, McEwen JD, Meinhold PR, Melchiorri A, Mennella A, Migliaccio M, Millea M, Miville-Deschênes MA, Molinari D, Moneti A, Montier L, Morgante G, Moss A, Natoli P, Nørgaard-Nielsen HU, Pagano L, Paoletti D, Partridge B, Patanchon G, Peiris HV, Perrotta F, Pettorino V, Piacentini F, Polenta G, Puget JL, Rachen JP, Reinecke M, Remazeilles M, Renzi A, Rocha G, Rosset C, Roudier G, Roubio-Martin JA, Ruiz-Granados B, Salvati L, Savelainen M, Scott D, Shellard EPS, Sirignano C, Sirri G, Spencer LD, Sunyaev R, Suur-Uski AS, Tauber JA, Tavagnacco D, Tenti M, Toffolatti L, Tomasi M, Trombetti T, Valiviita J, Van Tent B, Vielva P, Villa F, Vittorio N, Wandelt BD, Wehus IK, Zacchei A and Zonca A (2020), Sep. Planck 2018 results. V. CMB power spectra and likelihoods. *A&A* 641, A5. doi:10.1051/0004-6361/201936386. 1907.12875.
- Pritchard JR and Loeb A (2012), Aug. 21 cm cosmology in the 21st century. *Reports on Progress in Physics* 75 (8), 086901. doi:10.1088/0034-4885/75/8/086901. 1109.6012.
- Pritchard CJ (1994), Oct. The Search for Primeval Galaxies. *PASP* 106: 1052. doi:10.1086/133479.
- Roberts-Borsani GW, Bouwens RJ, Oesch PA, Labbe I, Smit R, Illingworth GD, van Dokkum P, Holden B, Gonzalez V, Stefanon M, Holwerda B and Wilkins S (2016), Jun. $z \geq 7$ Galaxies with Red Spitzer/IRAC [3.6]–[4.5] Colors in the Full CANDELS Data Set: The Brightest-Known Galaxies at $z \sim 7$ and a Probable Spectroscopic Confirmation at $z = 7.48$. *ApJ* 823 (2), 143. doi:10.3847/0004-637X/823/2/143. 1506.00854.
- Roberts-Borsani G, Morishita T, Treu T, Leethochawalit N and Trenti M (2022), Mar. The Physical Properties of Luminous $z \geq 8$ Galaxies and Implications for the Cosmic Star Formation Rate Density from 0.35 deg² of (Pure-)Parallel HST Observations. *ApJ* 927 (2), 236. doi:10.3847/1538-4357/ac4803. 2106.06544.
- Roberts-Borsani G, Treu T, Shapley A, Fontana A, Pentericci L, Castellano M, Morishita T, Bergamini P and Rosati P (2024), Dec. Between the Extremes: A JWST Spectroscopic Benchmark for High-redshift Galaxies Using ~ 500 Confirmed Sources at $z \geq 5$. *ApJ* 976 (2), 193. doi:10.3847/1538-4357/ad85d3. 2403.07103.
- Roberts-Borsani G, Bagley M, Rojas-Ruiz S, Treu T, Morishita T, Finkelstein SL, Trenti M, Arrabal Haro P, Bañados E, Chávez Ortiz ÓA, Chworowsky K, Hutchison TA, Larson RL, Leethochawalit N, Leung GCK, Mason C, Somerville RS, Stiavelli M, Yung LYA, Kassin SA and Soto C (2025), Apr. The BoRG-JWST Survey: Program Overview and First Confirmations of Luminous Reionization-era Galaxies from Pure-parallel Observations. *ApJ* 983 (1), 18. doi:10.3847/1538-4357/adba60. 2407.17551.
- Robertson BE (2022), Aug. Galaxy Formation and Reionization: Key Unknowns and Expected Breakthroughs by the James Webb Space Telescope. *ARA&A* 60: 121–158. doi:10.1146/annurev-astro-120221-044656. 2110.13160.
- Robertson BE, Ellis RS, Dunlop JS, McLure RJ and Stark DP (2010), Nov. Early star-forming galaxies and the reionization of the Universe. *Nature* 468 (7320): 49–55. doi:10.1038/nature09527. 1011.0727.
- Robertson BE, Ellis RS, Furlanetto SR and Dunlop JS (2015), Apr. Cosmic Reionization and Early Star-forming Galaxies: A Joint Analysis of New Constraints from Planck and the Hubble Space Telescope. *ApJ* 802 (2), L19. doi:10.1088/2041-8205/802/2/L19. 1502.02024.
- Robertson B, Johnson BD, Tacchella S, Eisenstein DJ, Hainline K, Arribas S, Baker WM, Bunker AJ, Carniani S, Cargile PA, Carreira C, Charlot S, Chevallard J, Curti M, Curtis-Lake E, D'Eugenio F, Egami E, Hausen R, Helton JM, Jakobsen P, Ji Z, Jones GC, Maiolino R, Maseda MV, Nelson E, Pérez-González PG, Puskás D, Rieke M, Smit R, Sun F, Übler H, Whittler L, Williams CC, Willmer CNA, Willott C and Witstok J (2024), Jul. Earliest Galaxies in the JADES Origins Field: Luminosity Function and Cosmic Star Formation Rate Density 300 Myr after the Big Bang. *ApJ* 970 (1), 31. doi:10.3847/1538-4357/ad463d. 2312.10033.
- Rojas-Ruiz S, Roberts-Borsani G, Morishita T, Calabrò A, Bagley MB, Treu T, Finkelstein SL, Stiavelli M, Trenti M and Yung LYA (2025), Jul. The BoRG-JWST Survey: Analogs at $z \sim 8$ to the UV-luminous Galaxy Population at *zsim10*. *arXiv e-prints*, arXiv:2507.01014doi:10.48550/arXiv.2507.01014. 2507.01014.
- Rusta E, Salvadori S, Gelli V, Schaerer D, Marconi A, Koutsouridou I and Carniani S (2025), Jun. Metal-polluted PopIII galaxies and How to Find Them. *arXiv e-prints*, arXiv:2506.17400doi:10.48550/arXiv.2506.17400. 2506.17400.
- Sacchi A and Bogdan A (2025), May. Chandra Rules Out Super-Eddington Accretion Models For Little Red Dots. *arXiv e-prints*, arXiv:2505.09669doi:10.48550/arXiv.2505.09669. 2505.09669.
- Saldana-Lopez A, Hayes MJ, Le Reste A, Scarlata C, Melinder J, Henry A, Leclercq F, Garel T, Amorin R, Atek H, Bait O, Carr CA, Chisholm J, Flury SR, Heckman TM, Jaskot AE, Jung I, Ji Z, Komarova L, Lin YH, Oey MS, Ostlin G, Pentericci L, Runnholm A, Schaerer D, Thuan TX and Xu X (2025), Apr. The Lyman-alpha and Continuum Origins Survey II: the connection between the escape of ionizing radiation and Lyman-alpha halos in star-forming galaxies. *arXiv e-prints*, arXiv:2504.07074doi:10.48550/arXiv.2504.07074. 2504.07074.
- Sanders RL, Shapley AE, Topping MW, Reddy NA and Brammer GB (2024), Feb. Direct T_e-based Metallicities of $z = 2$ – 9 Galaxies with JWST/NIRSpec: Empirical Metallicity Calibrations Applicable from Reionization to Cosmic Noon. *ApJ* 962 (1), 24. doi:10.3847/1538-4357/ad15fc. 2303.08149.
- Saxena A, Bunker AJ, Jones GC, Stark DP, Cameron AJ, Witstok J, Arribas S, Baker WM, Baum S, Bhatawdekar R, Bowler R, Boyett K, Carniani S, Charlot S, Chevallard J, Curti M, Curtis-Lake E, Eisenstein DJ, Endsley R, Hainline K, Helton JM, Johnson BD, Kumari N, Looser TJ, Maiolino R, Rieke M, Rix HW, Robertson BE, Sandles L, Simmonds C, Smit R, Tacchella S, Williams CC, Willmer CNA and Willott C (2024), Apr. JADES: The production and escape of ionizing photons from faint Lyman-alpha emitters in the epoch of reionization. *A&A* 684,

- A84. doi:10.1051/0004-6361/202347132. 2306.04536.
- Schaerer D (2002), Jan. On the properties of massive Population III stars and metal-free stellar populations. *A&A* 382: 28–42. doi:10.1051/0004-6361:20011619. astro-ph/0110697.
- Schaerer D (2003), Jan. The transition from Population III to normal galaxies: Ly α and He II emission and the ionising properties of high redshift starburst galaxies. *A&A* 397: 527–538. doi:10.1051/0004-6361:20021525. astro-ph/0210462.
- Schaerer D, Marques-Chaves R, Barrufet L, Oesch P, Izotov YI, Naidu R, Guseva NG and Brammer G (2022), Sep. First look with JWST spectroscopy: Resemblance among $z \sim 8$ galaxies and local analogs. *A&A* 665, L4. doi:10.1051/0004-6361/202244556. 2207.10034.
- Schaerer D, Guibert J, Marques-Chaves R and Martins F (2025), Jan. Observable and ionizing properties of star-forming galaxies with very massive stars and different initial mass functions. *A&A* 693, A271. doi:10.1051/0004-6361/202451454. 2407.12122.
- Schechter P (1976), Jan. An analytic expression for the luminosity function for galaxies. *ApJ* 203: 297–306. doi:10.1086/154079.
- Schenker MA, Ellis RS, Konidaris NP and Stark DP (2014), Nov. Line-emitting Galaxies beyond a Redshift of 7: An Improved Method for Estimating the Evolving Neutrality of the Intergalactic Medium. *ApJ* 795 (1), 20. doi:10.1088/0004-637X/795/1/20. 1404.4632.
- Shen X, Vogelsberger M, Boylan-Kolchin M, Tacchella S and Kannan R (2023), Nov. The impact of UV variability on the abundance of bright galaxies at $z \geq 9$. *MNRAS* 525 (3): 3254–3261. doi:10.1093/mnras/stad2508. 2305.05679.
- Shivaei I, Reddy NA, Siana B, Shapley AE, Kriek M, Mobasher B, Freeman WR, Sanders RL, Coil AL, Price SH, Fetherolf T, Azadi M, Leung G and Zick T (2018), Mar. The MOSDEF Survey: Direct Observational Constraints on the Ionizing Photon Production Efficiency, ξ_{ion} , at $z \sim 2$. *ApJ* 855 (1), 42. doi:10.3847/1538-4357/aaad62. 1711.00013.
- Shuntov M, Oesch PA, Toft S, Meyer RA, Covelo-Paz A, Paquereau L, Bouwens R, Brammer G, Gelli V, Giovinozzo E, Herard-Demanche T, Illingworth GD, Mason C, Naidu RP, Weibel A and Xiao M (2025), Jul. Constraints on the early Universe star formation efficiency from galaxy clustering and halo modeling of H α and [O III] emitters. *A&A* 699, A231. doi:10.1051/0004-6361/202554618. 2503.14280.
- Simmonds C, Tacchella S, Hainline K, Johnson BD, Puskás D, Robertson B, Baker WM, Bhatawdekar R, Boyett K, Bunker AJ, Cargile PA, Carniani S, Chevallard J, Curti M, Curtis-Lake E, Ji Z, Jones GC, Kumari N, Laseter I, Maiolino R, Maseda MV, Rinaldi P, Stoffers A, Übler H, Villanueva NC, Williams CC, Willott C, Witstok J and Zhu Y (2024), Dec. Ionizing properties of galaxies in JADES for a stellar mass complete sample: resolving the cosmic ionizing photon budget crisis at the Epoch of Reionization. *MNRAS* 535 (4): 2998–3019. doi:10.1093/mnras/stae2537. 2409.01286.
- Sims PH, Bevins HTJ, Fialkov A, Anstey D, Handley WJ, Heimersheim S, de Lera Acedo E, Mondal R and Barkana R (2025), Apr. Rapid and Late Cosmic Reionization Driven by Massive Galaxies: a Joint Analysis of Constraints from 21-cm, Lyman Line & CMB Data Sets. *arXiv e-prints*, arXiv:2504.09725doi:10.48550/arXiv.2504.09725. 2504.09725.
- Singh S, Jishnu NT, Subrahmanyan R, Udaya Shankar N, Girish BS, Raghunathan A, Somashekar R, Srivani KS and Sathyanarayana Rao M (2022), Feb. On the detection of a cosmic dawn signal in the radio background. *Nature Astronomy* 6: 607–617. doi:10.1038/s41550-022-01610-5. 2112.06778.
- Soucaill G, Mellier Y, Fort B, Mathez G and Cailloux M (1988), Feb. The giant arc in A 370 : spectroscopic evidence for gravitational lensing from a source at $Z=0.724$. *A&A* 191: L19–L21.
- Stark DP (2016), Sep. Galaxies in the First Billion Years After the Big Bang. *ARA&A* 54: 761–803. doi:10.1146/annurev-astro-081915-023417.
- Stark DP, Ellis RS and Ouchi M (2011), Feb. Keck Spectroscopy of Faint $3\leq z \leq 7$ Lyman Break Galaxies: A High Fraction of Line Emitters at Redshift Six. *ApJ* 728 (1), L2. doi:10.1088/2041-8205/728/1/L2. 1009.5471.
- Stark DP, Walth G, Charlot S, Clément B, Feltre A, Gutkin J, Richard J, Mainali R, Robertson B, Siana B, Tang M and Schenker M (2015), Dec. Spectroscopic detection of C IV $\lambda 1548$ in a galaxy at $z = 7.045$: implications for the ionizing spectra of reionization-era galaxies. *MNRAS* 454 (2): 1393–1403. doi:10.1093/mnras/stv1907. 1504.06881.
- Stark DP, Ellis RS, Charlot S, Chevallard J, Tang M, Belli S, Zittrn A, Mainali R, Gutkin J, Vidal-García A, Bouwens R and Oesch P (2017), Jan. Ly α and C III] emission in $z = 7-9$ Galaxies: accelerated reionization around luminous star-forming systems? *MNRAS* 464 (1): 469–479. doi:10.1093/mnras/stw2233. 1606.01304.
- Stark DP, Topping MW, Endsley R and Tang M (2025), Jan. Observations of the First Galaxies in the Era of JWST. *arXiv e-prints*, arXiv:2501.17078doi:10.48550/arXiv.2501.17078. 2501.17078.
- Steidel CC, Pettini M and Hamilton D (1995), Dec. Lyman Imaging of High-Redshift Galaxies.III.New Observations of Four QSO Fields. *AJ* 110: 2519. doi:10.1086/117709. astro-ph/9509089.
- Steidel CC, Giallisco M, Pettini M, Dickinson M and Adelberger KL (1996), May. Spectroscopic Confirmation of a Population of Normal Star-forming Galaxies at Redshifts $Z \leq 3$. *ApJ* 462: L17. doi:10.1086/310029. astro-ph/9602024.
- Steidel CC, Bogosavljević M, Shapley AE, Reddy NA, Rudie GC, Pettini M, Trainor RF and Strom AL (2018), Dec. The Keck Lyman Continuum Spectroscopic Survey (KLCS): The Emergent Ionizing Spectrum of Galaxies at $z \sim 3$. *ApJ* 869 (2), 123. doi:10.3847/1538-4357/aad28. 1805.06071.
- Sullivan M, Mobasher B, Chan B, Cram L, Ellis R, Treyer M and Hopkins A (2001), Sep. A Comparison of Independent Star Formation Diagnostics for an Ultraviolet-selected Sample of Nearby Galaxies. *ApJ* 558 (1): 72–80. doi:10.1086/322451. astro-ph/0104425.
- Tang M, Stark DP, Topping MW, Mason C and Ellis RS (2024), Nov. JWST/NIRSpec Observations of Lyman α Emission in Star-forming Galaxies at $6.5 \leq z \leq 13$. *ApJ* 975 (2), 208. doi:10.3847/1538-4357/ad7eb7. 2408.01507.
- Tinsley BM (1980a), Jan. Evolution of the Stars and Gas in Galaxies. *Fundamental Cosmic Physics* 5: 287–388. doi:10.48550/arXiv.2203.02041. 2203.02041.
- Tinsley BM (1980b), Oct. On the interpretation of galaxy counts. *ApJ* 241: 41–53. doi:10.1086/158315.
- Topping MW, Stark DP, Endsley R, Whittler L, Hainline K, Johnson BD, Robertson B, Tacchella S, Chen Z, Alberts S, Baker WM, Bunker AJ, Carniani S, Charlot S, Chevallard J, Curtis-Lake E, DeCoursey C, Egami E, Eisenstein DJ, Ji Z, Maiolino R, Williams CC, Willmer CNA, Willott C and Witstok J (2024), Apr. The UV continuum slopes of early star-forming galaxies in JADES. *MNRAS* 529 (4): 4087–4103. doi:10.1093/mnras/stae800. 2307.08835.
- Topping MW, Sanders RL, Shapley AE, Pahl AJ, Reddy NA, Stark DP, Berg DA, Clarke L, Cullen F, Dunlop JS, Ellis RS, Förster Schreiber NM, Illingworth GD, Jones T, Narayanan D, Pettini M and Schaerer D (2025), Feb. The AURORA Survey: The Evolution of Multi-phase Electron Densities at High Redshift. *arXiv e-prints*, arXiv:2502.08712doi:10.48550/arXiv.2502.08712. 2502.08712.
- Trebtsch M, Blaizot J, Rosdahl J, Devriendt J and Slyz A (2017), Sep. Fluctuating feedback-regulated escape fraction of ionizing radiation in low-mass, high-redshift galaxies. *MNRAS* 470 (1): 224–239. doi:10.1093/mnras/stx1060. 1705.00941.
- Treu T and Ellis RS (2015), Jan. Gravitational Lensing: Einstein’s unfinished symphony. *Contemporary Physics* 56 (1): 17–34. doi:10.1080/00107514.2015.1006001. 1412.6916.
- Treu T, Schmidt KB, Trenti M, Bradley LD and Stiavelli M (2013), Sep. The Changing Ly α Optical Depth in the Range $6 \leq z \leq 9$ from the MOSFIRE Spectroscopy of Y-dropouts. *ApJ* 775 (1), L29. doi:10.1088/2041-8205/775/1/L29. 1308.5985.
- Treu T, Roberts-Borsani G, Bradac M, Brammer G, Fontana A, Henry A, Mason C, Morishita T, Pentericci L, Wang X, Acebron A, Bagley M, Bergamini P, Belfiori D, Bonchi A, Boyett K, Boutsia K, Calabró A, Caminha GB, Castellano M, Dressler A, Glazebrook K, Grillo C, Jacobs C,

- Jones T, Kelly PL, Leethochawalit N, Malkan MA, Marchesini D, Mascia S, Mercurio A, Merlin E, Nanayakkara T, Nonino M, Paris D, Poggianti B, Rosati P, Santini P, Scarlata C, Shipley HV, Strait V, Trenti M, Tubthong C, Vanzella E, Vulcani B and Yang L (2022), Aug. The GLASS-JWST Early Release Science Program. I. Survey Design and Release Plans. *ApJ* 935 (2), 110. doi:10.3847/1538-4357/ac8158. 2206.07978.
- Umeda H, Ouchi M, Kageura Y, Harikane Y, Nakane M, Thai TT and Nakajima K (2025), Apr. Probing the Cosmic Reionization History with JWST: Gunn-Peterson and Ly α Damping Wing Absorption at $4.5 < z < 13$. *arXiv e-prints*, arXiv:2504.04683doi:10.48550/arXiv.2504.04683. 2504.04683.
- van de Hulst HC (1945), Jan. Radiogolven uit het wereldruim: II. Herkomst der radiogolvenRadiogolven uit het wereldruim: II. Herkomst der radiogolvenRadio waves from space. *Nederlandsch Tijdschrift voor Natuurkunde* 11: 210–221.
- Vanzella E, Loiacono F, Bergamini P, Meštrić U, Castellano M, Rosati P, Meneghetti M, Grillo C, Calura F, Mignoli M, Bradač M, Adamo A, Rihtaršič G, Dickinson M, Gronke M, Zanella A, Annibali F, Willott C, Messa M, Sani E, Acebron A, Bolamperti A, Comastri A, Gilli R, Caputi KI, Ricotti M, Gruppioni C, Ravindranath S, Mercurio A, Strait V, Martis N, Pascale R, Caminha GB, Annunziatella M and Nonino M (2023), Oct. An extremely metal-poor star complex in the reionization era: Approaching Population III stars with JWST. *A&A* 678, A173. doi:10.1051/0004-6361/202346981. 2305.14413.
- Verhamme A, Orlitová I, Schaerer D and Hayes M (2015), Jun. Using Lyman- α to detect galaxies that leak Lyman continuum. *A&A* 578, A7. doi:10.1051/0004-6361/201423978. 1404.2958.
- Visbal E, Hazlett R and Bryan GL (2025), Aug. LAP1-B is the First Observed System Consistent with Theoretical Predictions for Population III Stars. *arXiv e-prints*, arXiv:2508.03842doi:10.48550/arXiv.2508.03842. 2508.03842.
- Wang B, Leja J, de Graaff A, Brammer GB, Weibel A, van Dokkum P, Baggen JFW, Suess KA, Greene JE, Bezanson R, Cleri NJ, Hirschmann M, Labbé I, Matthee J, McConachie I, Naidu RP, Nelson E, Oesch PA, Setton DJ and Williams CC (2024a), Jul. RUBIES: Evolved Stellar Populations with Extended Formation Histories at $z \sim 7\text{--}8$ in Candidate Massive Galaxies Identified with JWST/NIRSpec. *ApJ* 969 (1), L13. doi:10.3847/2041-8213/ad55f7. 2405.01473.
- Wang T, Sun H, Zhou L, Xu K, Cheng C, Li Z, Chen Y, Mo HJ, Dekel A, Yang T, Wang Y, Zheng X, Cai Z, Elbaz D, Dai YS and Huang JS (2024b), Mar. JWST/MIRI reveals the true number density of massive galaxies in the early Universe. *arXiv e-prints*, arXiv:2403.02399doi:10.48550/arXiv.2403.02399. 2403.02399.
- Wang X, Cheng C, Ge J, Meng XL, Daddi E, Yan H, Ji Z, Jin Y, Jones T, Malkan MA, Arrabal Haro P, Brammer G, Oguri M, Hou M and Zhang S (2024c), Jun. A Strong He II $\lambda 1640$ Emitter with an Extremely Blue UV Spectral Slope at $z = 8.16$: Presence of Population III Stars? *ApJ* 967 (2), L42. doi:10.3847/2041-8213/ad4ced. 2212.04476.
- Wang B, Leja J, Atek H, Bezanson R, Burnham E, Dayal P, Feldmann R, Greene JE, Johnson BD, Labbé I, Maseda MV, Nanayakkara T, Price SH, Suess KA, Weaver JR and Whitaker KE (2025), Jul. Population Models for Star Formation Timescales in Early Galaxies: The First Step toward Solving Outshining in Star Formation History Inference. *ApJ* 987 (2), 184. doi:10.3847/1538-4357/adddb8. 2504.15255.
- Weibel A, Oesch PA, Williams CC, Jaspersen CK, Shuntov M, Whitaker KE, Atek H, Bezanson R, Brammer G, Chemerynska I, Cloonan AP, Dayal P, Furtak LJ, Hutter A, Ji Z, Maseda MV and Xiao M (2025), Jul. Exploring Cosmic Dawn with PANORAMIC I: The Bright End of the UVLF at $z \sim 9\text{--}17$. *arXiv e-prints*, arXiv:2507.06292doi:10.48550/arXiv.2507.06292. 2507.06292.
- Whitler L, Stark DP, Endsley R, Leja J, Charlot S and Chevallard J (2023), Mar. Star formation histories of UV-luminous galaxies at $z \sim 6\text{--}8$: implications for stellar mass assembly at early cosmic times. *MNRAS* 519 (4): 5859–5881. doi:10.1093/mnras/stad004. 2206.05315.
- Williams CC, Alberts S, Ji Z, Hainline KN, Lyu J, Rieke G, Endsley R, Suess KA, Sun F, Johnson BD, Florian M, Shivaee I, Rujopakarn W, Baker WM, Bhatawdekar R, Boyett K, Bunker AJ, Cameron AJ, Carniani S, Charlot S, Curtis-Lake E, DeCoursey C, de Graaff A, Egami E, Eisenstein DJ, Gibson JL, Hausen R, Helton JM, Maiolino R, Maseda MV, Nelson EJ, Pérez-González PG, Rieke MJ, Robertson BE, Saxena A, Tacchella S, Willmer CNA and Willott CJ (2024), Jun. The Galaxies Missed by Hubble and ALMA: The Contribution of Extremely Red Galaxies to the Cosmic Census at $3 < z < 8$. *ApJ* 968 (1), 34. doi:10.3847/1538-4357/ad3f17. 2311.07483.
- Wise JH, Demchenko VG, Halicek MT, Norman ML, Turk MJ, Abel T and Smith BD (2014), Aug. The birth of a galaxy - III. Propelling reionization with the faintest galaxies. *MNRAS* 442 (3): 2560–2579. doi:10.1093/mnras/stu979. 1403.6123.
- Witstok J, Jakobsen P, Maiolino R, Helton JM, Johnson BD, Robertson BE, Tacchella S, Cameron AJ, Smit R, Bunker AJ, Saxena A, Sun F, Alberts S, Arribas S, Baker WM, Bhatawdekar R, Boyett K, Cargile PA, Carniani S, Charlot S, Chevallard J, Curti M, Curtis-Lake E, D'Eugenio F, Eisenstein DJ, Hainline KN, Jones GC, Kumari N, Maseda MV, Pérez-González PG, Rinaldi P, Scholtz J, Übler H, Williams CC, Willmer CNA, Willott C and Zhu Y (2024), Aug. Witnessing the onset of reionisation via Lyman- α emission at redshift 13. *arXiv e-prints*, arXiv:2408.16608doi:10.48550/arXiv.2408.16608. 2408.16608.
- Wouthuysen SA (1952), Jan. On the excitation mechanism of the 21-cm (radio-frequency) interstellar hydrogen emission line. *AJ* 57: 31–32. doi:10.1086/106661.
- Yue M, Eilers AC, Matthee J, Naidu RP, Bordoloi R, Davies FB, Hennawi JF, Kashino D, Mackenzie R and Simcoe RA (2025), Jul. Escape fractions from unattenuated Ly α emitters around luminous $z > 6$ quasars. *arXiv e-prints*, arXiv:2507.05381doi:10.48550/arXiv.2507.05381. 2507.05381.
- Zier O, Kannan R, Smith A, Puchwein E, Vogelsberger M, Borrow J, Garaldi E, Keating L, McClymont W, Shen X and Hernquist L (2025), Mar. The THESAN-ZOOM project: Population III star formation continues until the end of reionization. *arXiv e-prints*, arXiv:2503.03806doi:10.48550/arXiv.2503.03806. 2503.03806.